HIGHWAY RESEARCH **RECORD**

Number 400	Bridge Design, Construction, and Repair
	10 reports prepared for the 51st Annual Meeting

HIGHWAY RESEARCH BOARD

NOTICE

The studies reported herein were not undertaken under the aegis of the National Academy of Sciences or the National Research Council. The papers report research work of the authors done at the institution named by the authors. The papers were offered to the Highway Research Board of the National Research Council for publication and are published herein in the interest of the dissemination of information from research, one of the major functions of the HRB.

Before publication, each paper was reviewed by members of the HRB committee named as its sponsor and was accepted as objective, useful, and suitable for publication by NRC. The members of the committee were selected for their individual scholarly competence and judgment, with due consideration for the balance and breadth of disciplines. Responsibility for the publication of these reports rests with the sponsoring committee; however, the opinions and conclusions expressed in the reports are those of the individual authors and not necessarily those of the sponsoring committee, the HRB, or the NRC.

Although these reports are not submitted for approval to the Academy membership or to the Council of the Academy, each report is reviewed and processed according to procedures established and monitored by the Academy's Report Review Committee.

CONTENTS

FOREWORD

THE 10 papers contained in this RECORD describe the results of bridge research on a variety of projects ranging from cost optimization of girders to deck repairs. Included is analytical and experimental information of particular value in expanding the state of knowledge regarding properties and performance of structural materials and members under test conditions. Also included is information related to problems encountered during construction and operation.

The advent of computer technology has provided the designer with the capability to optimize the cost of highway bridges. Busek, Gaunt, and Lewis describe programs that use the exhaustive-search technique to solve the design of composite or noncomposite steel girders. The programs will optimize the design of either simple-span or continuous girders up to four spans based on either total weight or total cost.

Fracture-mechanics concepts of stable crack growth are evaluated and judged by Hirt and Fisher to be a rational way to analyze and characterize the behavior of welded steel beams. Porosity caused by entrapped gas was found to be the most common defect in plain welded beams, and the initial crack size was concluded to be the controlling factor for determining fatigue life. A fracture-mechanics model for cracks originating from pores in the web-to-flange fillet weld is presented.

Buth and Furr report on the testing to failure of two full-scale concrete bridge beams under torsional load. Experimental values of torsional stiffness of the beams compared favorably with predicted values computed by using elastic theory. A comparison between theoretical and experimental values using splitting tensile strength in the maximum tensile-strength failure theory also yielded favorable results.

The report by Sozen and Siess provides a valuable summary of work accomplished from 1951 to 1969 in the course of an extensive research project on the use of prestressed concrete for highway bridges. The project covered various topics related to flexural strength, shear strength, time-dependent deformations, anchorage-zone stresses, and bond characteristics of prestressed concrete beams.

The results of experimental studies on creep and shrinkage behavior of concrete made with Hawaiian aggregates is the subject of the paper by Hamada, Zundelevich, and Chiu. Both lightweight and normal-weight concretes were studied and compared with data from published literature. Although creep coefficients of all concretes tested agreed with published data, ultimate shrinkage strains of Hawaiian aggregate concretes were larger. Concretes made with lightweight Hawaiian aggregates exhibited smaller ultimate shrinkage strains than did concretes made with normal-weight Hawaiian aggregates.

When span-length longitudinal screeding is used in bridge deck construction, the finished grade elevations are set on the screeding edge of the machine and remain independent of girder deflections during concrete placement. Consequently, any factors affecting girder deflections during deck placement, and thus the forming elevations, will in turn cause the deck thickness to deviate from the plan thickness. The study reported by Hilton identified several significant factors that contribute to the problem of obtaining desired deck thickness.

The paper by Kozlov reports on research aimed at providing engineers with procedures for the design and construction of adequately sealed bridge joints. The author suggests that armored joints sealed with preformed elastomeric sealers are the most satisfactory solution to the problem.

Motorists passing under structures are endangered by objects either thrown from above or from objects balanced on bridge railings that drop some time after vandals have deposited them. Harley provides data that concern the installation of protective fences on such structures.

Development of a corrosion detector by the staff of the California Division of Highways, coupled with identification of salt as an important factor in bridge deck deterioration, led the Federal Highway Administration to include a program to encourage use of the instrument as a project in the FHWA demonstration projects activity. Kliethermes presents suggested guidelines for determining whether or not a bridge deck is likely to deteriorate from corrosion and whether or not a bridge deck should be repaired or replaced. Although the author's findings are still controversial, there seems little reason to doubt that the value of the instrument has been well demonstrated.

Furr and Ingram confirm previous research and field practice by showing in laboratory studies that concrete overlays can be bonded to concrete bridge decks without using special adhesives.

PRACTICAL OPTIMIZATION OF
STEEL HIGHWAY BRIDGE BEAMS

R. H. Busek, N. H. Bettigole Company; and
J. T. Gaunt and A. D. M. Lewis, Purdue University

ABRIDGMENT

•THE objective of highway bridge design is to specify the most economical structure
for a given situation. The loads that the structure must be capable of supporting, re-
quired clearances and other details, acceptable material stresses, and acceptable pro-
portions are given in the AASHO specification (1). The engineer must select from
available structural arrangements the arrangement that meets the design criteria and
minimizes the function by which the cost of the structure is evaluated.

By using hand methods of calculation, the consideration of only a few structural con-
figurations has been practical in attempting to design economical structures. With
digital computers, the number of structural configurations that can be investigated has
been greatly increased, and the development of optimum designs has become practical.

A computer program referred to as Girder Automated Design-I or GAD-I (4, 5) is
available for the design of noncomposite welded plate girder bridges. There exists the
possibility, particularly in the case of relatively short spans, that a more economical
structure could be constructed by using rolled steel beams with cover plates, if re-
quired, in composite or noncomposite construction. The computer program described
in this paper was developed for designing such rolled-beam bridges for required static
and fatigue highway loads. The fatigue conditions are based on 500,000 cycles of stress.
If the design is composite, $\frac{7}{8}$-in. diameter shear connector studs are provided at proper
spacing. Only W36 and W33 sections are investigated by this program because shallower
sections are not likely to prove economical for these bridges.

The objective of the program is to produce the rolled-beam bridge design with mini-
mum estimated cost. Wherever possible, cost estimation follows the pattern of GAD-I
in order to facilitate comparison of costs of rolled-beam bridges with welded plate
girder bridges.

GIRDER ANALYSIS

The program will handle either simple-span girders or continuous structures up to
four spans. The analysis is carried out by calculating influence coefficients at a speci-
fied number of analysis points, equally spaced in each span. Initially, a constant mo-
ment of inertia throughout the length of the bridge is assumed. Loadings considered
include AASHO truck and lane loadings, Interstate military load, pedestrian walkways
if provided, and dead-load conditions. Dead loads include the weight of the steel beams,
deck slab, bridge railings, and light fixtures. In the case of composite design, the dead
loads are separated into two groups: one for the steel beam only and the other for the
composite section. Influence coefficients are used for computing the shear and moment
at each analysis point.

ROLLED-SECTION DESIGN

The shears and moments at the analysis points are used for determining the govern-
ing shear and moment for the elements of the member between each pair of adjacent
analysis points. Initially, stresses are computed for each element by using the heaviest

available rolled section. If the stresses do not violate the AASHO specification, the next lighter rolled section is tried. If the stresses violate the AASHO specification, an attempt is made to eliminate these violations by the addition of cover plates.

In the addition of cover plates, requirements on extension beyond theoretical cutoff points and minimum cover-plate length requirements are considered. After cover-plate thicknesses required in different sections of the member have been determined, optimum locations for plate thickness changes are determined by dynamic programming using the procedures developed by Goble and DeSantis (3, 4, 5) and Razani (6, 7).

After final locations of cover-plate splices have been determined, details such as cover-plate welds, bearing stiffeners, and shear connectors for composite construction are designed.

COMPUTER PROGRAM

The computer program for the design of rolled-section beam bridges consists of a main program and 34 subroutines. The main program calls the subroutines in the correct sequence for reading data, performing an initial analysis, and selecting the most economical section.

Beam selection is started by checking the bending stress in the heaviest rolled section at the critical moment location and proceeds in descending weight order until the lightest acceptable rolled section without cover plates is determined. If the assumption is made that the cost of shear connectors and stiffeners is independent of the section used for beams without cover plates, all heavier sections can be eliminated from further consideration with a consequent reduction in computations. The design of this lightest acceptable section without cover plates is then completed, and the cost is estimated.

Cover-plate requirements for the lighter rolled sections are then determined, and cost estimates are made to see if a more economical structure is possible than the best determined previously. When cover plates are added, the girder is reanalyzed to consider the changes in moment of inertia along the length of the girder.

After the final design is obtained, deflections are calculated, and design details are printed along with the estimated cost. An option is available to design on the basis of either least cost or least weight. A complete listing of the program is available elsewhere (2).
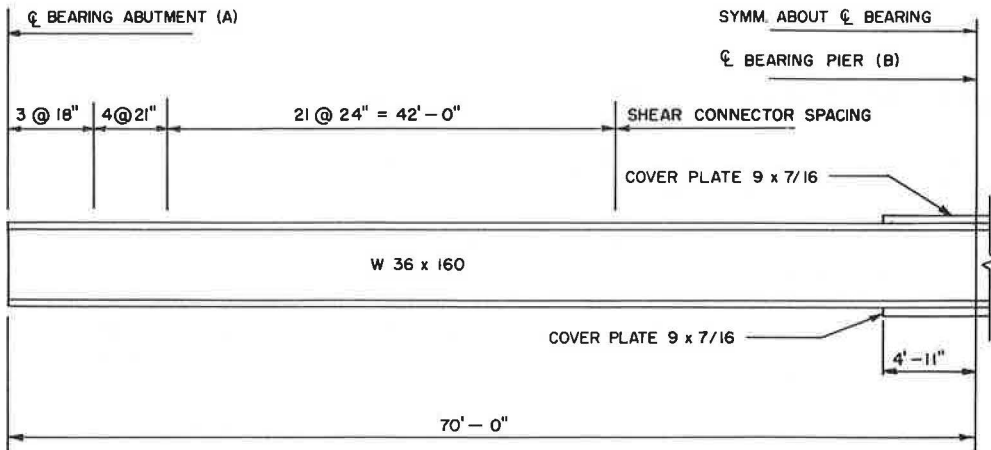
SAMPLE PROBLEM

As an example of the application of the program, a structure for the problem originally presented elsewhere (8) has been designed. The problem is a two-span girder with span lengths of 70 ft. The design is based on a composite section having the following properties: (a) slab width, 84 in.; (b) slab thickness, 7 in; (c) f_c', 3,000 psi; (d) modular ratio, 8; and (e) haunch, 1.875 in. The design loading is AASHO HS20. The unit costs used in design optimizations are as follows: (a) rolled section, $0.15 per lb; (b) cover plates, $0.12 per lb; (c) stiffeners, $0.12 per lb; (d) connector installation, $0.75 each; (e) fixed weld cost, $20.00 each; and (f) weld material cost, $2.00 per cu in. The final design is shown in Figure 1. The costs and weights of the computer program solution and the solution given in the manual are compared in Table 1. The design produced by the computer will be noted to be approximately 6.4 percent heavier than the published design, but the estimated cost is 4.3 percent less. The total cost of the plates, including both material and fabrication costs, for the computer design is $238.48 compared with a cost of $911.69 in the published solution. This cost difference offsets the increased cost of the rolled section.

The computer program is approximately 4,000 cards in length and was developed and executed on a CDC 6500 computer. The compilation time for the program was about 48 sec, and the execution time for the preceding sample problem was about 40 sec.

CONCLUSIONS

The computer program is another step in the automation of steel-beam bridge design. The previous sample problem shows that cost savings are possible by using the total-

Figure 1. Computer optimum design for sample problem.

Table 1. Itemized costs and weights for two-span sample problem.

Item	U.S. Steel Manual Weight (lb)	Cost ($)	Computer Program Weight (lb)	Cost ($)
Rolled section	18,900.0	2,835.00	22,400.0	3,360.00
Cover plates	2,361.6	283.40	360.1	31.22
Stiffeners	—	—	—	—
Connectors	202.2	193.50	179.8	174.00
Welds	—	628.29	—	207.26
Total	21,463.8	3,940.19	22,839.9	3,772.48

cost concept in design. The digital computer makes possible the use of optimum-seeking methods in practical problems such as highway bridge design. However, many problems remain to be solved before the optimization of an entire bridge design project will be possible.

ACKNOWLEDGMENTS

REFERENCES

1. American Association of State Highway Officials. Standard Specifications for Highway Bridges. Tenth Edition, 1969.
2. Busek, R. H. Practical Optimization of Steel Highway Bridge Beams. Purdue University and Indiana State Highway Commission, Joint Highway Res. Proj., Rept. 8, May 1971.
3. Goble, G., and DeSantis, P. V. Optimum Design of Mixed Steel Composite Girders. ASCE Jour. Struct. Div., Vol. 92, No. 12, Dec. 1966.
4. Goble, G., and DeSantis, P. V. Girder Automated Design—I. User's Manual, Vol. 1, Oct. 1968.
5. Goble, G., and DeSantis, P. V. Girder Automated Design—I. Manintenance Manual, Vol. 2, Oct. 1968.
6. Razani, R. The Iterative Smoothing Method and Its Application to Minimum Cost Design of Highway Bridge Girders. Case Institute of Technology, PhD dissertation, 1965.
7. Razani, R., and Goble, G. Optimum Design of Constant Depth Plate Girders. ASCE Jour. Struct. Div., Vol. 92, Apr. 1966.
8. United States Steel Company. Highway Structures and Design Handbook, Vols. 1 and 2, 1965.

FATIGUE BEHAVIOR OF WELDED BEAMS

Manfred A. Hirt, Howard, Needles, Tammen and Bergendoff; and
John W. Fisher, Lehigh University

The fatigue behavior of welded steel beams is evaluated by using the
fracture-mechanics concepts of stable crack growth. A fracture-mechanics
model for cracks originating from the pores in the web-to-flange fillet weld
is developed. Estimates of the stress-intensity factor are made that nu-
merically describe the initial flaw condition. With the final crack size
known, a theoretical crack-growth equation was derived from the fatigue
test data of the welded beams. The derived relationship compares well
with actual crack-growth measurements on a welded beam and available
data from crack-growth specimens. The regime of crack growth, where
most of the time is spent growing a fatigue crack in a structural element,
is shown to correspond to growth rates below 10^{-6} in. per cycle. Few ex-
perimental crack-growth data are available at this level. It is concluded
that the fracture-mechanics concepts can be used to analyze fatigue be-
havior and to rationally evaluate the major variables that influence the fa-
tigue life of welded beams.

•THIS paper evaluates the fatigue behavior of welded steel beams without attachments
by using the fracture-mechanics concepts of stable crack growth. Earlier studies had
indicated that various flaw conditions existed in welded beams. Both internal and ex-
ternal weld defects in the web-to-flange fillet weld were evaluated and discussed in
detail elsewhere (4, 9, 10). Internal pores caused by entrapped gas in the weldment
are known to form a common defect. The gas pores and their effect on the fatigue be-
havior of welded beams are discussed in this paper.

A fracture-mechanics model for cracks originating from the pores in the web-to-
flange fillet weld is developed. Estimates of the stress-intensity factor are made that
numerically describe the initial flaw condition. With the initial and final crack size
known, a theoretical crack-growth equation was derived from the fatigue test data of the
welded beams. The experimental data of 56 plain-welded beams covering three grades
of steel—ASTM A 36, A 441, and A 514—are presented elsewhere (4, 9) together with an
analysis of the test variables.

Fracture toughness was not a significant factor in the determination of crack propa-
gation and the fatigue life of the beams tested. Net-section yielding generally termi-
nated fatigue testing. Hence, no emphasis was placed on this aspect of failure be-
cause it was not relevant to the study. Fracture toughness can become a problem
when steel with low toughness is used and adverse environmental and load conditions
exist. These limitations were not the subject of this investigation.

The main objective of this paper is to demonstrate the validity and applicability of
fracture-mechanics concepts of fatigue crack growth to the fatigue behavior of actual
structural elements containing real flaws. It is also shown that the ΔK-values respon-
sible for crack growth in these beams are well below the ΔK-values normally obtained
during crack-growth testing. A theoretical crack-growth equation was derived from
the fatigue life data of welded beams and compared with available crack-growth data.

The following notation is used in this paper:

C = a material related constant in crack-growth equation;
K = elastic stress-intensity factor for a crack (ksi√in.);
N = number of applied stress cycles;
N_{ij} = number of cycles required for a crack to grow from size a_i to size a_j;
S = nominal applied stress in the extreme fiber of the tension flange;
S_r = stress range;
a = crack size, crack radius for penny-shaped crack, half-crack width for tunnel crack or through-the-thickness crack, crack depth for surface crack, crack radius for corner crack, minor half axis for elliptical crack;
a_e = equivalent radius of a penny-shaped crack that provides the same K-factor estimated for the arbitrarily shaped crack;
a_f = final crack size;
a_i = initial crack size (for integration interval);
a_j = final crack size (for integration interval);
b = major half axis for an elliptical crack;
f(a) = nondimensional geometry correction factor for stress-intensity factor K;
n = exponent of crack-growth equation; slope of equation in log-log transformation;
α = (n/2) - (1);
ΔK = stress-intensity factor range;
$\Delta\sigma$ = stress range relevant for the determination of the stress-intensity factor range; and
σ = stress applied sufficiently away from the crack tip.

FATIGUE STRENGTH OF WELDED BEAMS WITH INTERNAL WELD DISCONTINUITIES

It was observed that cracks in the welded beams always originated from a discontinuity (flaw) in the web-flange fillet weld unless a severe notch existed at the flame-cut flange tip. More than 180 cracks were found in the plain-welded beams reported on elsewhere (4, 9). Seventy-five of these cracks were cut open for fractographic examination. It was found that about 80 percent of the cracks had originated from porosity caused by the entrapment of gas. In general, these cavities were completely inside the weld. The gas pores appeared on the fracture surface as rounded cavities with a smooth and shiny surface as shown in Figure 1. A few pipe or blow holes extended to the surface of the weld.

All test data for beams failing from porosity in the longitudinal fillet weld are plotted by the solid circles shown in Figure 2. The equation of the mean line resulting from a least squares fit to these test data is

$$\log N = 10.3528 - 2.9844 \log S_r \qquad (1)$$

Previous analyses (4, 9) had indicated that stress range was the dominant variable and that grade of steel did not significantly affect the fatigue strength.

The open symbols shown in Figure 2 represent plain-welded beams that failed from defects other than porosity. This included beams failing from weld repairs, stop-start positions, other weld defects, and severe notches in the flame-cut flange tips. Generally, these beams yielded shorter lives than did beams failing from porosity.

When weld repairs were absent in the fillet weld of beams with stiffeners or attachments, failure occurred at these welded details because they were more critical than was porosity. These beam data are also included because they revealed no visible crack growth in the longitudinal fillet weld at lower stress ranges. An indication of a run out level is seen at the 18-ksi stress-range level. Only three data points from plain-welded beams failing from porosity were observed at that stress range.

CRACK-GROWTH OBSERVATION ON A PLAIN-WELDED BEAM

One plain-welded beam was closely observed in order to investigate crack formation and growth on the surfaces of the fillet weld, web, and flange. Measurements of crack

length and load were made so that crack-growth rates could be determined for the structural element and compared with the crack-growth relationship analytically derived from the S-N data of the welded beams. Beam PWB-341 (4) was selected for this study because it had failed prematurely after 192,000 cycles of stress from a flange-tip crack. Replicate beams tested at the same stress range of 36 ksi indicated that a crack from a gas pore could be expected to become visible within an additional 200,000 cycles. The flange-tip crack was carefully repaired, and testing was resumed under the same stress conditions. The fillet welds on both sides of the web in the constant moment region were searched for cracks by using a regular hand magnifying glass while testing at 250 cycles per minute. Testing was interrupted periodically so that the weld could be examined under static load. Suspicious locations were further examined with a 50-power microscope.

A hairline crack was first detected on the weld surface after a total of 351,700 applied stress cycles. The apparent total crack size visible on the weld surface was found to measure about 0.05 in. when the load was removed from the beam. This increased to 0.25 in. under maximum stress of 50 ksi in the extreme fiber. Only the linear dimension of the crack on the fillet weld could be observed during continued testing until the crack reached the extreme fiber.

After about 435,000 cycles, the crack was first detected on the bottom surface of the flange. It was only then observed with certainty that the crack had also penetrated through the other fillet weld. The increase in crack size was very rapid after the crack had penetrated the bottom flange surface. The cross section of the flange fractured at 467,000 cycles as one crack tip reached the flange tip. The advancement of the crack is shown in Figure 3, which indicates a transition from a penny-shaped crack with a continuous crack front in the flange-web junction to a three-ended crack with two crack tips in the flange and one in the web.

Hence, two basic stages of growth were observed for cracks originating from pores in the longitudinal fillet weld of welded beams. The first stage of growth was in the flange-to-web junction from the initial crack size (flaw) up to the point where the crack reached the extreme fiber of the flange. After penetration of the extreme flange fiber, the crack changed its shape rapidly to become a three-ended crack.

A PENNY-SHAPED CRACK MODEL

Fractographic examination of small cracks that had originated from pores in the fillet weld showed that many were almost perfectly circular in shape. This circular shape was found at various stages of growth up to the point where the crack had reached the extreme fiber of the flange, as shown in Figures 4, 5, and 6.

One of the smallest cracks was discovered during an examination of a crack in the fillet weld. A tiny crack about 0.07 in. in diameter had originated from a very small pore in the left weld as shown in Figure 4. The extent of the circular crack is seen from the smooth crack surface surrounding the pore, as compared to the rough appearance caused by static tearing when the cross section was opened for inspection. The small crack on the left was completely inside the flange-to-web junction and could not be detected by inspection of the weld surface.

A small crack discovered by the magnetic particle inspection method is shown in Figure 5. The crack had initiated from the elongated pore and grown to the surface of the fillet weld. Almost no deviation from a circular shape is visible. This crack is about 0.26 in. in diameter and could not be detected on the weld surface with the aid of a magnifying glass even under favorable circumstances and under sustained loading.

A crack that has nearly penetrated the extreme fiber of the tension flange is shown in Figure 6. Again, no significant disturbance of the circular shape is apparent at either side of the web or at the front approaching the surface of the flange. This crack, although quite sizable, is not easily detected on a structural element under applied loading. The linear dimension of the crack visible on the surface of the flange-to-web junction is somewhat less than 1 in.

The phenomenon of a circular crack shape, seemingly not influenced by the free surfaces, is believed to be a result of the compatibility condition of the basically

Figure 1. Examples of porosity from the root of the longitudinal fillet weld.
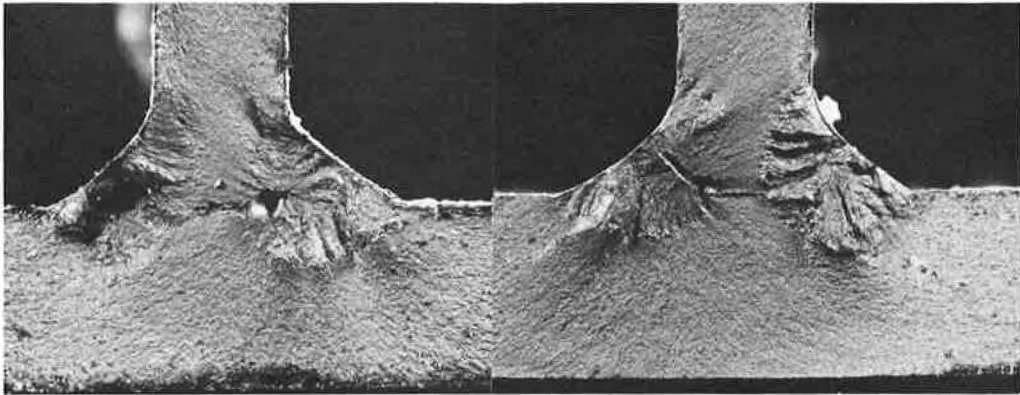
(a) Typical gas pore (x2.5)

(b) Pore elongated and perpendicular to the weld surface (x2.5)

Figure 2. Comparison of welded beams failing from porosity in the fillet weld with beams failing from other defects.

Log N = 10.3528 - 2.9844 Log S_r

Crack Initiation

• From Porosity
○ From Other Defects
ℓ At Stiffener or Attachment, no Visible Cracks in Longitudinal Weld
○— No Cracks

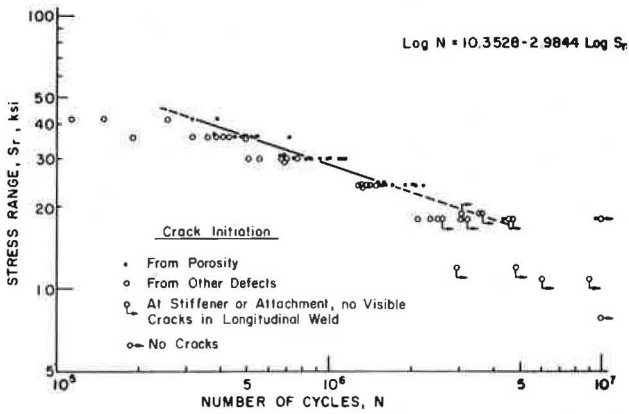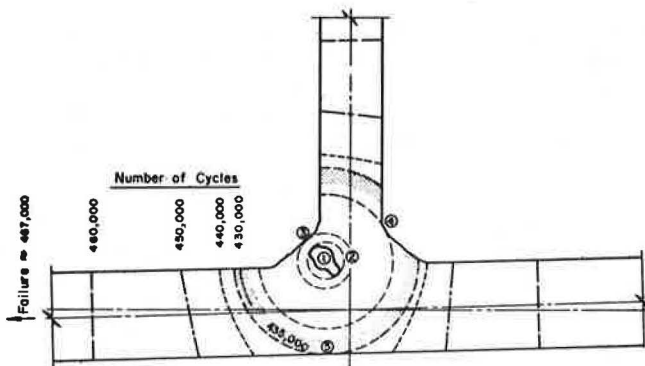STRESS RANGE, S_r, ksi

NUMBER OF CYCLES, N

Figure 3. Stages of crack growth from a pore in the fillet weld.

Number of Cycles

elastic cross section. Based on this photographic evidence, a circular disc-like crack was assumed to model the actual crack during growth inside the flange-web connection (Fig. 3).

EVALUATION OF FATIGUE BEHAVIOR USING FRACTURE-MECHANICS CONCEPTS

The fatigue test data and fractographic observations of small fatigue cracks suggested that fracture mechanics of stable crack growth might be useful in evaluating the observed behavior of the test beams. The stress intensity factor K introduced by Irwin ([11]) describes in convenient form the influence of the stress, applied sufficiently away from the crack tip, and the crack size, a. The relative size is usually expressed in terms of a correction function, f(a), where the linear dimensions of the plate, or the distance to a free edge or surface, are introduced.

$$K = \sigma\sqrt{\pi^a}\ f(a)\ (ksi\sqrt{in.}) \tag{2}$$

Paris ([15]) has suggested the following relation between the rate of crack propagation and the change in the stress-intensity factor:

$$da/dN = C\Delta K^n \tag{3}$$

This model expresses crack growth per cycle, da/dN, in terms of the variation of the stress intensity factor, ΔK, and two material constants, C and n.

For the case of a crack with constant correction factor, f(a), which is subjected to constant amplitude stress, integration of Eq. 3 yields

$$N_{1j} = (1/C)\ [(1/\alpha f(a)^n\ \pi^{n/2}\ \Delta\sigma^n)\ (a_1{}^{-\alpha} - a_j{}^{-\alpha})] \tag{4}$$

where $\alpha = (n/2) - (1)$. For specimens with equal initial crack size, a_1, final crack size, a_j, and identical boundary conditions, a theoretical value for the prediction of the life interval, N_{1j}, can be expressed in terms of a new constant, C', times the applied stress range, $\Delta\sigma$, as

$$N_{1j} = C'\ \Delta\sigma^{-n} \tag{5}$$

where

$$C' = (1/C)\ [(1/\alpha f(a)\ \pi^{n/2})\ (a_1{}^{-\alpha} - a_j{}^{-\alpha})] \tag{6}$$

The log-log transformation of Eq. 5 yields a straight line in the form

$$\log N_{1j} = \log C' - n\ \log(\Delta\sigma) \tag{7}$$

APPLICATION TO THE PLAIN-WELDED BEAM

For the application of the outlined concepts of fracture mechanics, a reasonable characterization of the flaws was needed. A large number of cracks that originated from porosity in the fillet weld were examined closely to establish the initial flaw condition. Flaws were photographed and enlarged to at least four times, as shown in Figure 1. The dimensions of the defects were measured on the photographs under 10-power magnification.

Pores were examined in beams fabricated from three different grades of steel (A 36, A 441, and A 514). K-values were estimated to numerically describe the measured flaw dimensions. The estimated K-values describing the pores were obtained by using a circumscribed ellipse for flaws similar to the shapes shown in Figure 1a and Figure 6. For elongated flaws comparable to those shown in Figure 1b and Figure 5, the K-estimate at the narrow transition from the circular void to the elongated pore was generally used.

It was previously concluded from fractographic inspection of very small fatigue cracks (Figs. 4 and 5) that a penny-shaped crack model described the shape of cracks during crack growth. However, the estimated K-values for the initial flaws represent

elliptical shapes with various a-b ratios. Hence, each individual defect was trans-
formed into a penny-shaped crack with an "equivalent crack-radius, a_e," correspond-
ing to the estimated K-value. An average equivalent crack radius, a_e = 0.04 in., was
selected from the sample to represent the collection of measured pores. The initial
crack radius, a_i, was then assumed equal to this average value.

Derivation of Crack-Growth Constants

The coefficients of the crack-growth equation can now be established from the
equivalence of the coefficients in Eqs. 1 and 7. Equation 7 is the theoretical prediction
of the fatigue life using fracture-mechanics concepts, and Eq. 1 expresses the statistical
mean line of the relevant fatigue test data shown by the solid circles in Figure 2. The
following assumptions were made to assist with the evaluation of the crack-growth
constants, C and n.

1. The crack was assumed to be described by a disc-like penny-shaped crack with
a constant correction factor, f(a), over the interval of integration. The correction
factor, f(a), for a penny-shaped crack is $2/\pi$.

2. The estimates of the initial and final crack radii, a_i and a_j, were available
from visual observations. The average initial crack radius, a_i, was assumed to equal
the estimate of the equivalent crack radius, a_e = 0.04 in., which represents the sample
of measured pores. The final crack radius, a_j, was assumed to be reached when the
crack had penetrated the extreme fiber of the flange. The life remaining after this
occurred was at most 10 percent of the total fatigue life of the beam as was shown by
the measurements given in Figure 3. The final crack radius was assumed to be equal
to the nominal flange thickness. Experimental observations indicated this to be
reasonable.

3. It was assumed that all three grades of steel could be represented by the same
crack-growth equation. This assumption was based on results of tests on the welded
beams. It was shown elsewhere (4) that grade of steel did not significantly influence
the fatigue life of the beams.

If we equate the values of the coefficients for the mean regression curve (Eq. 1) to
the coefficients n and C' (Eq. 7) and substitute the crack radii, a_i and a_j, and the
correction factor, f(a), into Eq. 6, the growth constants, $n \simeq 3$ and $\bar{C} = 2.05 \times 10^{-10}$, are
derived. Substitution of these constants into Eq. 3 numerically describes the crack
growth rate in terms of ΔK:

$$da/dN = 2.05 \times 10^{-10} \ \Delta K^3 \qquad (8)$$

The measurement used for crack-growth rates, da/dN, was inch/cycle; and for the
stress-intensity factor range, ΔK, it was $ksi\sqrt{in.}$

COMPARISON OF DERIVED CRACK-GROWTH EQUATION
WITH MEASURED CRACK-GROWTH RATES

Equation 8 as derived from the mean regression curve of fatigue test data (Fig. 2)
is shown in Figure 7 and compared with the various stages of crack growth in the test
beam shown in Figure 3. The straight-line estimate for crack growth as a penny-
shaped crack from crack initiation until penetration of the extreme fiber is indicated.
Also shown are the data points for the measured crack-growth rates on the inside and
outside surface of the flange for growth as a three-ended crack.

It is apparent from Figures 7 and 3 that most of the life is spent growing the crack
from its initial equivalent flaw radius, a_e = 0.04 in., to its penetration of the extreme
fiber of the flange, a_f = 0.375 in. The corresponding range of ΔK for the test beam
was between 8 $ksi\sqrt{in.}$ and 25 $ksi\sqrt{in.}$ under a constant amplitude stress range of 36
ksi while 435,000 cycles elapsed. The transition from a penny-shaped crack to a
three-ended crack only required about 16,000 cycles. An additional 10,000 cycles
were required to grow the crack large enough to cause net-section yielding. Final
failure terminated testing at 467,000 cycles.

It is also apparent from Figure 7 that most of the life was spent while growth
occurred in a region of small ΔK. This is particularly true for lower applied stress

Figure 4. Two small fatigue cracks that initiated from pores in the longitudinal fillet weld and grew perpendicular to the axis of the weld (~x5.5).
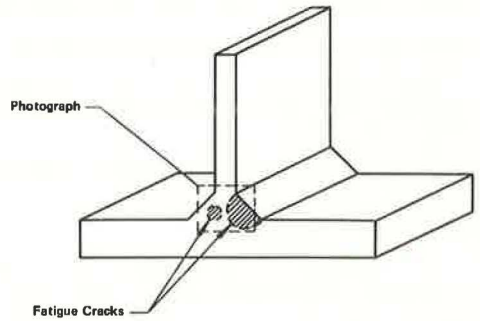

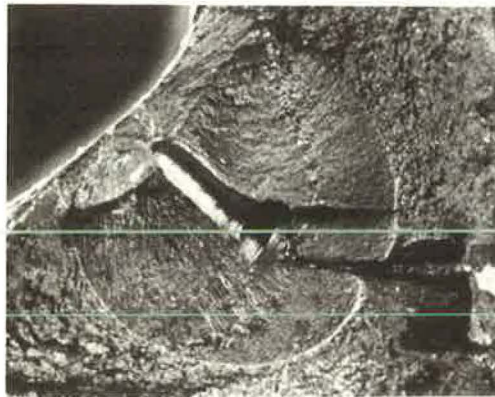Figure 5. Small crack with penetration to the fillet weld surface (~x6.3).

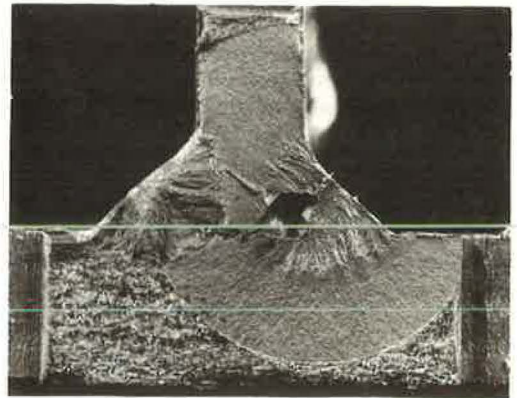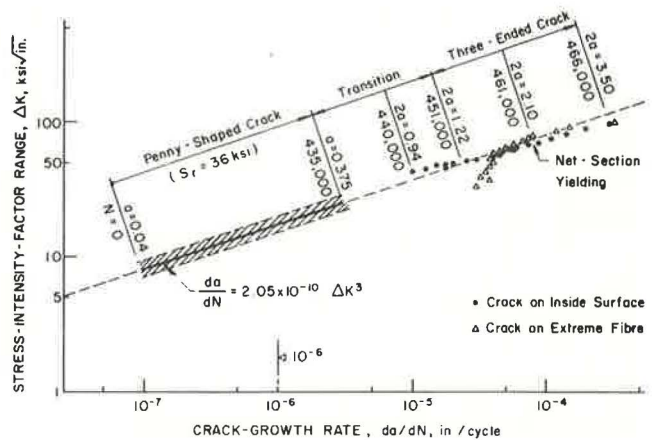Figure 6. Crack in flange-to-web junction approaching the extreme fiber of the tension flange (~x2.1).

Figure 7. Stages of crack growth and corresponding growth rates for a crack in a plain-welded beam.

ranges as shown in Figure 8. The ΔK-regions applicable to growth as a penny-shaped crack are indicated for the test beams subjected to the stress ranges used in this study. Crack initiation took place at ΔK-values below 10 ksi $\sqrt{in.}$ in all test beams. Most of the life was spent at growth rates smaller than 10^{-6} in. per cycle.

The derived crack-growth relationship given by Eq. 8 is also compared with data from crack-growth specimens (Fig. 8). It was necessary to extrapolate the curve into the higher growth-rate region to compare it with available growth-rate data. The extrapolated curve falls within the scatterband reported by Crooker and Lange (3). This scatterband contains data from tests on carbon and low-alloy steels with yield strengths comparable to the yield strengths of the steel beams. A conservative upper bound for growth rates on ferrite-pearlite steels was proposed by Barsom (1) as

$$da/dN = 3.6 \times 10^{-10} \Delta K^3 \tag{9}$$

This relationship is parallel to Eq. 8.

Because much of the growth in the plain-welded beams took place in the weld metal and heat-affected zone, a comparison of the theoretical curve with Maddox's data (13) is relevant. An approximate envelope for Maddox's data on four different weld metals is shown. Three had about equal yield strength (67 ksi), and the fourth had a higher yield point equal to 90 ksi. Also included in the scatterband are test data for a simulated heat-affected zone in mild steel material with the same yield strength. The correlation with these crack-growth data is good.

It is apparent from Figure 8 that the Crooker-Lange scatterband does not cover the critical region of interest for plain-welded beams. Most studies of crack-growth rates have been limited to larger ΔK-values and higher crack-growth rates because of the difficulties encountered in the slow-growth region. However, the theoretical curve (Eq. 8) extrapolated into the higher ΔK-regions shows the same general trend reported by others on basic crack-growth specimens (Fig. 8). The theoretical curve is just above the crack-growth data and underestimates their growth rate. This is surprising because the penny-shaped crack assumes the best condition for the crack in the welded beams and neglects the influence of free surfaces. This underestimate in growth rate may be due to crack initiation or an overestimate of the stress intensity.

The exponent, n, of the predicted crack-growth equation was about equal to 3.00 (Eq. 8). It represents the slope of the fatigue test data on plain-welded beams fabricated from three grades of steel. Crooker and Lange (3) observed from a review of the literature that the value of the slope, n, fell between 2 and 4 for a large range of steels. Gurney (6) reported the slope of the curve to be a linear function of yield stress of the material. A general trend observed in crack-growth studies is for the value of the exponent, n, to decrease with increasing yield strength of the material. This trend was not as pronounced in the welded-beam study. The value of the exponent, n, did not appear to vary greatly from 3.

Careful evaluation of the coefficients n and C is needed for a wider range of rates of growth. Most of the data generally used to fit the straight-line approximation only extend over a small range of ΔK. In other cases, data points at the extremes cause rotation of the line. Substantial overestimates or underestimates of the fatigue life of a structural component might result if crack-growth relationships are used to extrapolate beyond the range of the test data.

Very Slow Growth

Johnson and Paris (12) have suggested that a threshold exists for crack growth. A recent investigation by Paris (16) on ASTM 9310 steel has provided more information on this phenomenon of very slow growth. An approximate mean line fit to Paris' data is compared in Figure 9 and Eq. 8. A drastically reduced growth rate for $\Delta K \simeq 5.2$ ksi $\sqrt{in.}$ is observed. Deviations from the straight-line approximation are also found for large ΔK-values, which indicates an increased growth rate and applies mainly to low-cylce fatigue problems.

Harrison (7) has reviewed the literature for runout data on a variety of specimens. He concluded that "for all materials with the exception of pure aluminum, cracks will

not propagate if $\Delta K/E < 1 \times 10^{-4} \sqrt{\text{in}}$." Harrison's runout levels for four types of steel are also shown in Figure 9 and range between 3.3 ksi $\sqrt{\text{in}}$. for mild steel and 5.3 ksi$\sqrt{\text{in}}$. for austenitic steel.

Predictions of Fatigue Life Using Different Crack Models

Additional crack models were used to assess their influence on the prediction of the fatigue life. Figure 10 shows the results for the various models used. Six A 441 steel beams were selected for the comparison. The actually observed fatigue lives of these six beams are shown by solid circles together with the mean and the 95 percent confidence interval for all test beams failing from porosity.

The defects that caused crack growth and failure of the six beams were examined. They were assumed to be characterized by a circumscribed ellipse with half-axes a and b. The following models were used to estimate the fatigue life of each individual beam by using the known dimensions of the circumscribed ellipse and the crack-growth Eq. 8.

The open circles shown in Figure 10 (model a) correspond to the life estimates for the penny-shaped crack with equivalent crack radius. The equivalent crack radius was computed from the equivalence of the K-value with the circumscribed elliptical crack.

Penny-shaped cracks were assumed to inscribe and circumscribe the ellipse. The shortest life estimates resulted from the circumscribed crack and the longest from the inscribed crack. These two estimates constitute "upper and lower bounds" and are indicated by the horizontal T-symbols shown in Figure 10 (model b).

Additional life estimates were made based on the elliptical crack model. Growth was assumed in the direction of the minor axis 2a with constant major axis 2b until the size of the circumscribed crack was reached. The computation of the increment of life from an elliptical to a circular crack was done by using an available computer program (5). Numerical integration was employed because of the variable correction factor, $f(a)$. This increment of life was added to the estimate for the circumscribed penny-shaped crack. The total life estimate is indicated by the triangles shown in Figure 10.

The comparison between the estimates for each individual beam provided by the different models and the observed fatigue life permit the following observations.

1. The observed fatigue data were contained within the bounds from the estimates of the circumscribed and inscribed circles in all but one case.

2. Most of the estimates from models a and c fell within the two limits of dispersion representing the 95 percent confidence interval of all the beam test data. Hence, the selection of a penny-shaped crack model did not introduce more scatter than was experimentally observed from fatigue test data.

Prediction of Fatigue Life Using Measured Crack-Growth Rates

Maddox (14) and Harrison (8) have demonstrated that good predictions of the fatigue life can be obtained from crack-growth data. Barsom's (1) conservative estimate of crack-growth rate, Eq. 9, for ferrite-pearlite steels was used to predict the fatigue life of the beams failing from porosity. The result is shown in Figure 11 together with the applicable welded beam test data, the corresponding mean line, and 95 percent confidence interval.

Also shown in Figure 11 is the prediction based on Paris' data (16), which indicates a threshold level for runout at about 23 ksi. This prediction was obtained by using the straight-line segments shown in Figure 9, which approximate the data from the study on very slow growth. The threshold values by Harrison (7), also shown in Figure 9, were used to estimate runout. Runout tests are predicted to occur at levels as high as 20 ksi for low-alloy steel, as shown by the horizontal lines in Figure 11.

The predictions based on the crack-growth data underestimate the mean fatigue life of the test beams at the higher stress range levels. This was expected from the comparison of the crack-growth data. Because any assumption other than the penny-shaped crack model for the welded beams would further reduce the life prediction based on crack-growth data, a crack-initiation period may be responsible for the slight

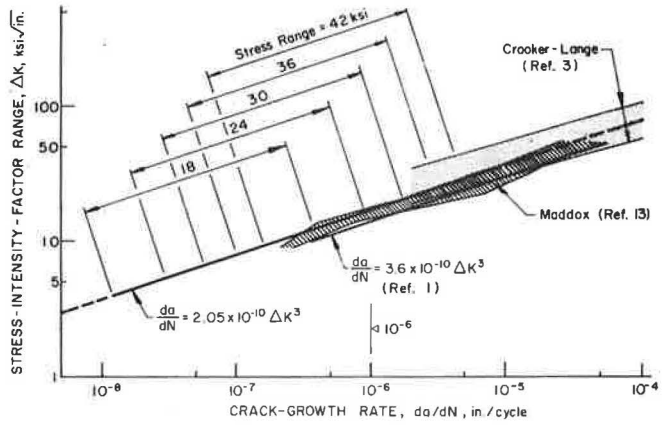**Figure 8.** Ranges for crack growth as a penny-shaped crack.

Figure 9. Approximate mean line of Paris' data for very slow growth and Harrision's limiting ΔK-values for nonpropagating cracks.
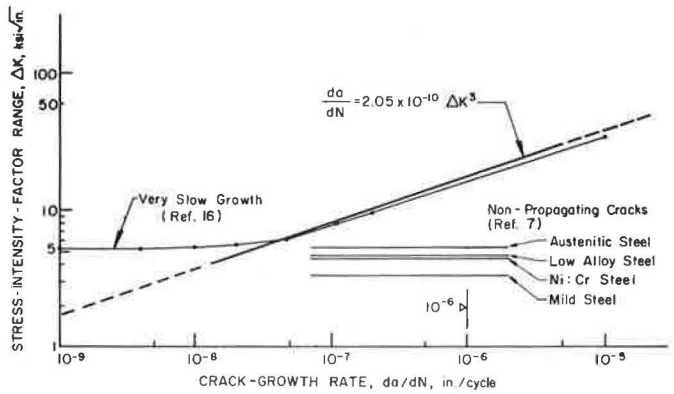

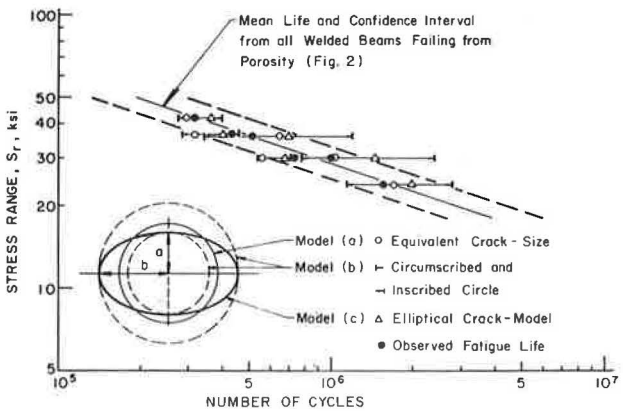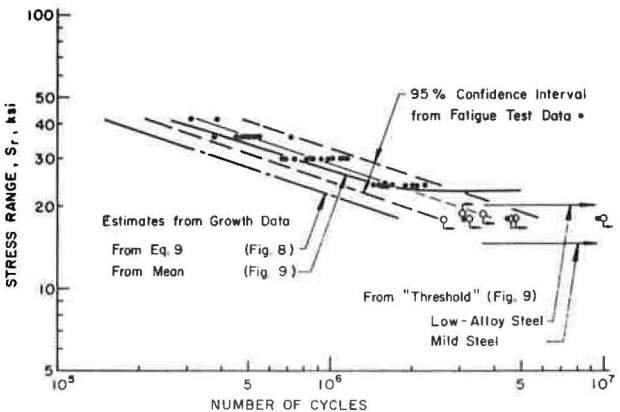**Figure 10.** Prediction of fatigue life using crack models.

Figure 11. Comparison of a predicted low bound and a mean line with mean life and scatterband from test data.

underestimate. Other factors that could be responsible for the underestimate in life are an overestimate of the initial crack size, an overestimate of the stress intensity, and a slower growth rate under plane-strain conditions (2).

The scatter in the test data shown in Figure 11 was previously related to the variation in shape, size, and severity of the porosity. Other factors contribute to the variation in test data. Beams with seemingly equal defects still experience variation in the fatigue strength because of variation in the crack-tip radius, crack-growth rates, and other uncontrolled variables.

SUMMARY AND CONCLUSIONS

The following findings of this study are based on a detailed examination of the test data, fracture surfaces, initial flaw conditions provided by the experimental work, and the theoretical studies of stable crack growth.

1. Fractographic examination of the initial flaw conditions revealed porosity to be the most common defect in plain-welded beams. The distribution of the size and location of the pores in the longitudinal fillet weld was random. The welded-beam fatigue data fell within a narrow scatterband when plotted as the logarithmic transformation of stress range and cycles to failure.

2. Fracture-mechanics concepts provided a rational way to analyze and characterize the behavior of welded beams. These concepts were applied to describe numerically the effective initial flaw conditions in welded beams and to derive a crack-growth rate versus range of stress-intensity relationship from welded-beam fatigue data.

3. A penny-shaped crack was found to model crack growth from porosity in welded beams. An equivalent crack with a 0.04-in. radius described the average pores observed in the welded beams.

4. The derived crack-growth equation exhibited the same trend as measured data from crack-growth specimens. It provided a lower estimate of the growth rate. Among other factors, this difference was attributed to crack initiation, a possible overestimate of the stress intensity, and slower growth in the plane-strain condition for the welded beams.

5. Available crack-growth data were shown to only cover a small region of growth rates. Extrapolation into regions outside the data could be misleading, particularly when used for fatigue-life estimates.

6. Very little information is available for growth rates below 10^{-6} in. per cycle. This was found to be the region most critical for the fatigue behavior of welded and rolled beams. More than 75 percent of the life was spent in this region growing a crack from its initial size to a visible crack.

7. It was shown that the initial flaw size was the controlling factor for the fatigue life of welded beams. An increase in flange thickness and larger weld sizes should not result in an increase in allowable defect size.

8. The variation of the fatigue data within the scatterband was found to be related in part to the variation in the initial flaw condition and in part to the variation in fatigue crack-growth rates or other uncontrolled variables.

ACKNOWLEDGMENTS

REFERENCES

1. Barsom, J. M. Fatigue-Crack Propagation in Steels of Various Yield Strengths. U.S. Steel Corp., Applied Research Laboratory, Monroeville, Pennsylvania, 1971.

2. Clark, W. G., Jr., and Trout, H. E., Jr. Influence of Temperature and Section Size on Fatigue Crack Growth Behavior in Ni-Mo-V Alloy Steel. Engineering Fracture Mechanics, Vol. 2, No. 2, Nov. 1970, pp. 107-123.

3. Crooker, T. W., and Lange, E. A. How Yield Strength and Fracture Toughness Considerations Can Influence Fatigue Design Procedures for Structural Steels. Welding Research Supplement, Vol. 49, No. 10, Oct. 1970, pp. 488-496.

4. Fisher, J. W., Frank, K. H., Hirt, M. A., and McNamee, B. M. Effect of Weldments on the Fatigue Strength of Steel Beams. NCHRP Rept. 102, 1970, 112 pp.

5. Frank, K. H., and Fisher, J. W. Analysis of Error in Determining Fatigue Crack Growth Rates. Lehigh University, Fritz Engineering Laboratory, Rept. 358.10, March 1971.

6. Gurney, T. R. An Investigation of the Rate of Propagation of Fatigue Cracks in a Range of Steels. The Welding Institute, Members' Rept. E18/12/68, Dec. 1968.

7. Harrison, J. D. An Analysis of Data on Non-Propagating Fatigue Cracks on a Fracture Mechanics Basis. Metal Construction and British Welding Jour., Vol. 2, No. 3, March 1970, pp. 93-98.

8. Harrison, J. D. The Analysis of Fatigue Test Results for Butt Welds With Lack of Penetration Defects Using a Fracture Mechanics Approach. Welding in the World, Vol. 8, No. 3, 1970, pp. 168-181.

9. Hirt, M. A., Yen, B. T., and Fisher, J. W. Fatigue Strength of Rolled and Welded Steel Beams. ASCE, Jour. Struct. Div., Vol. 97, No. ST7, July 1971, pp. 1897-1911.

10. Hirt, M. A. Fatigue Behavior of Rolled and Welded Beams. Lehigh University, Department of Civil Engineering, PhD dissertation, Oct. 1971.

11. Irwin, G. R. Analysis of Stresses and Strains Near the End of a Crack Traversing a Plate. Transactions, ASME, Series E, Vol. 24, No. 3, Sept. 1957, pp. 361-364.

12. Johnson, H. H., and Paris, P. C. Sub-Critical Flaw Growth. Engineering Fracture Mechanics, Vol. 1, No. 1, June 1968, pp. 3-45.

13. Maddox, S. J. Fatigue Crack Propagation in Weld Metal and Heat Affected Zone Material. The Welding Institute, Members' Rept. E/29/69, Dec. 1969.

14. Maddox, S. J. The Propagation of Part-Through-Thickness Fatigue Cracks Analysed by Means of Fracture Mechanics. The Welding Institute, Members' Rept. E/30/69, Dec. 1969.

15. Paris, P. C. The Fracture Mechanics Approach to Fatigue. Proc., Tenth Sagamore Army Materials Research Conference, Syracuse University Press, Syracuse, 1964, p. 107.

16. Paris, P. C. Testing for Very Slow Growth of Fatigue Cracks. Closed Loop, MTS Systems Corp., Vol. 2, No. 5, 1970, pp. 11-14.

FULL-SCALE TORSION TESTS OF
PRESTRESSED CONCRETE I-BEAMS

Eugene Buth and Howard L. Furr, Texas Transportation Institute,
  Texas A&M University

•IN modern concrete highway bridges, torsional loadings are created in a variety of loading situations both during construction and during the service life of the structure. Overhanging deck forms cantilevered from edge beams are a primary source of torsional loading during construction of a prestressed beam, cast-in-place deck structure. Torsional loads occur, under traffic, in beams in skewed and curved structures and in other more liberal designs. These requirements have emphasized the need for a better understanding of practical methods for analyzing torsional stresses in prestressed concrete beams. A simple method of analysis and a reliable failure or strength criterion, verified by experimental data, is urgently needed.

Research on torsion of prestressed beams has been reported by Hsu (1), Zia (2), and Wyss and Mattock (3). Several methods of analysis and failure theories have been proposed in this work. Hsu indicated that, although the maximum tensile stress theory of failure did not accurately predict the torsional strength of concrete beams, the effect of prestressing derived from this theory appeared to be valid. Zia concluded that elastic torsion theory is applicable to prestressed concrete members but that neither Rankine's, nor Coulomb's, nor Cowan's failure theory satisfactorily agreed with test results. He showed that a modification to Cowan's theory, an approximation to Mohr's failure theory, closely predicted the torsional strength of concrete members, within the range of variables encountered in practice. Wyss and Mattock, in their study of prestressed concrete I-beams subjected to combined torsional and flexural loadings, concluded that these quantities may be reasonably and accurately determined by using elastic theory.

This paper reports torsion tests that were conducted on two full-scale Texas Highway Department (THD) Type B prestressed highway bridge beams to provide experimental data on this subject. The tests were conducted at the THD facilities in Austin, Texas.

The following notation is used in this paper.

T = externally applied torque, ft-lb
K = torsional stiffness constant in classical elastic theory, in.^{4}
ϕ = stress function
δ = grid spacing, in.
$\Delta, \Delta^2 \ldots$ = first, second, ... forward differences
G = shear modulus of elasticity, psi
θ = angle of twist, rad/in.
σ_t = principal tensile stress, psi
τ = shearing stress, psi
f_c' = compressive strength of concrete, psi
e = eccentricity of prestressing strands, in.
L = length of beam
ϵ = strain, μin./in.
C = constant = $K\tau/T$

THEORETICAL INVESTIGATION

Elastic theory (4) for a homogeneous member of uniform cross section subjected to pure torsion was used to calculate the theoretical stresses developed in the beams by

the applied torque. This technique is the same as that applied by Tamberg (5) in his study of AASHO girders. The governing differential equation for the elastic torsional theory is

$$(\partial^2\phi/\partial x^2) + (\partial^2\phi/\partial y^2) = -2G\theta \tag{1}$$

where

ϕ = stress function;
G = shear modulus of elasticity, psi; and
θ = angle of twist, rad/in.

In the application of this theory, the cross section of the beam is divided into a 2-in. square grid. The grid is symmetric with respect to the vertical axis of symmetry of the section. The differential equation written in finite difference form for an interior point is

$$1/\delta^2 \left[\phi_{i+1} + \phi_{i+2} + \phi_{i+3} + \phi_{i+4} - 4\phi_i)\right] = -2G\theta \tag{2}$$

For points near the boundary where the grid pattern is not complete, the finite difference equation is modified. The finite difference equation, when written for each point in the grid, will result in a system of equations that can be solved simultaneously to yield values of ϕ for each point in the grid.

The shear stress attributable to the "applied torque only" can then be determined by the following relationship:

$$\tau_x = \partial\phi/\partial y \quad \text{or} \quad \tau_y = \partial\phi/\partial x \tag{3}$$

The first partial derivative is evaluated by using the forward differences method. The equation is

$$\tau = 1/\delta^2 \left[(\Delta\phi - 1/2\Delta^2\phi) + (1/3\Delta^3\phi) - (1/4\Delta^4\phi) + \dots)\right] \tag{4}$$

Δ, Δ^2, ... = the first, second, etc., forward difference. Values of ϕ for the cross section of a THD Type B beam are given in Table 1. Values of shear stress, in terms of $G\theta$, at various points on the boundary of the cross section are shown in Figure 1.

The relationship between applied torque and angle of twist per unit length is given by

$$T = KG\theta \tag{5}$$

where

T = applied torque, ft-lb;
K = torsional stiffness constant, in.[4];
G = shear modulus of elasticity, psi; and
θ = angle of twist, rad/in.

EXPERIMENTAL INVESTIGATION

Specimens, Instrumentation, and Loading Frame

Two standard THD Type B pretensioned, prestressed, draped strand beams, nominally 50 ft long were tested. Those beams, fabricated 27 months earlier for other purposes, were designed to THD specifications for normal bridge use and were not specifically designed for torsional tests. Dimensions and details of the beams are shown in Figures 2 and 3. One beam was made of lightweight concrete, lightweight coarse aggregate, and natural sand; the other was made of normal-weight concrete. Additional information about these specimens can be found elsewhere (6).

Table 1. Values of ϕ at various grid points in a THD Type B prestressed concrete beam.

Grid Point	Value of ϕ	Grid Point	Value of ϕ	Grid Point	Value of ϕ	Grid Point	Value of ϕ
1[a]	4.55Gθ[b]	13	20.62Gθ	25	7.77Gθ	37	8.53Gθ
2	9.99	14	25.47	26	12.55	38	13.09
3	13.19	15	27.16	27	7.03	39	6.13
4	14.96	16	5.87	28	11.39	40	13.00
5	15.54	17	16.00	29	6.78	41	15.63
6	5.96	18	22.99	30	10.95	42	8.61
7	14.24	19	25.46	31	6.73	43	13.70
8	19.79	20	6.50	32	10.87	44	15.44
9	23.11	21	17.03	33	6.84	45	6.59
10	24.23	22	20.70	34	11.06	46	9.76
11	4.20	23	9.92	35	7.26	47	10.74
12	13.23	24	15.27	36	11.66		

[a]See Figure 1 for grid point locations. Values of ϕ are symmetric about the vertical centerline of the cross section.
[b]Multiply each value of ϕ by Gθ.

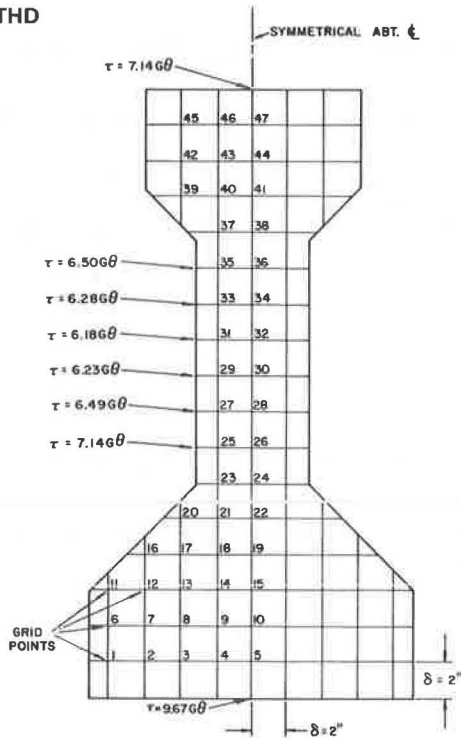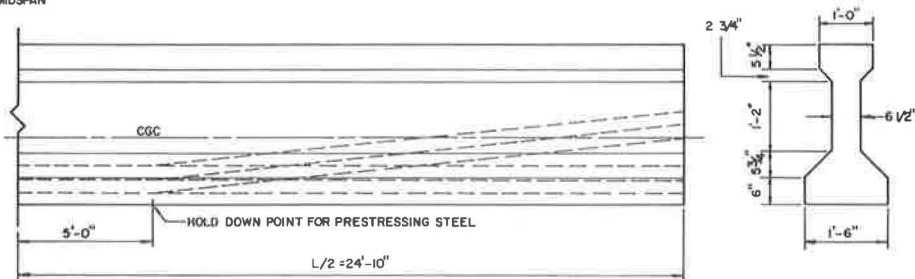**Figure 1. Cross section of THD Type B prestressed beam.**

Figure 2. THD Type B prestressed concrete bridge beam.

TYPE B BEAM

An existing testing frame, which was designed and constructed by THD for structural testing of prestressed bridge beams, was used to apply the load to the beams. This facility, with a failed beam installed, is shown in Figure 4. No extensive provisions were made to allow for changes in the length of the beam. However, longitudinal motion was restrained only by friction of the hinge pin. Load was applied to both ends of the beam with hydraulic jacks, and bourdon gauges were used to determine the amount of load.

Rotational displacements of each end of the beam were determined by using a precise level and two scales hanging from crossbars attached to each end of the beam. This setup is shown in Figure 5.

Electrical resistance rectangular strain-gauge rosettes were installed on the surface of each beam at the locations shown in Figure 6. The gauges had 120 ohms of resistance and were 2.362 in. long. The gauges were installed while the beam was simply supported in the testing frame; no external load was applied. The strains due to dead load and prestress already existed when the gauges were installed and balanced; therefore, the strains measured by the gauges were those due to the applied torque only. The orientation of the gauges was such that the three arms made angles of 0, 45, and 90 deg with the longitudinal axis of the beam. Manual switching and balancing units and servo-controlled digital readout equipment were used to read the gauges.

Torque increments of 5.88 ft-kips (1,000 psi on the bourdon gauges) were applied to the beam. After each load increment, the rotational displacement of each end of the beam and the strain at each gauge location were determined.

Normal-Weight Beam Test

The first sign of distress in this beam was noted at the support on the south end when, at a torque of 35.2 ft-kips, a small piece of concrete was sheared out of the beam. A diagonal crack then appeared in the web extending to the top flange adjacent to this support. Examination of this specimen showed that this was a local condition caused by high pressure of the twisting frame against the beam and not a condition caused by or influencing the torsional strength of the beam. Once the cracking and the redistribution of stress at the point of loading occurred, there was no further distress.

At a torque of 41.2 ft-kips, a 2-in. long diagonal crack was observed at about mid-depth of the web 15 ft from the north end of the beam on the east side. The crack did not grow with added torque, and it is believed that the crack was caused by a small local imperfection. It did not appear to influence the strength of the beam. The first extensive diagonal crack caused by the torsional load was observed when the applied torque was 88.8 ft-kips. This crack extended from the bottom flange diagonally through the web and upper flange on the west side of the beam near the south end.

The crack that resulted in failure occurred at an applied torque of 91.2 ft-kips and passed through the hold-down point of the prestressing steel on the north end of the beam. The crack was initially observed to extend from a point where the bottom flange joins the web diagonally to the top of the beam. The crack projected across the top flange and diagonally down the other side of the beam forming a helical shape. The two ends of the helix were connected by a longitudinal crack in the bottom flange. The crack pattern developed in this beam is shown in Figure 7, and the failure crack is shown in Figure 8.

Lightweight Beam Test

The same type of local cracking occurred early in the test at the loading frame on the south end as it did with the normal-weight beam. At a torque of 41.2 ft-kips, a diagonal crack occurred adjacent to the support at the south end, but neither of these cracks grew any further as loading continued. At 82.3 ft-kips, diagonal cracking began to occur in the top flange and web. These cracks developed at several locations along the length of the beam while the torque was being held at 82.3 ft-kips. The crack pattern developed in this beam is shown in Figure 9, and the failure crack is shown in Figure 10.

20

Figure 3. Stresses due to dead load plus prestress.

Midspan

+238 psi   +169   +122   +88   +137   +113

-1869   -1817   -1752   -1776   -1787   -1772

0'   5'   10'   15'   20'   25'

Normal Weight Beam

Midspan

+230 psi   +203   +133   +174   +233   +217

-1824   -1800   -1782   -1782   -1827   -1814

0'   5'   10'   15'   20'   25'

Lightweight Beam
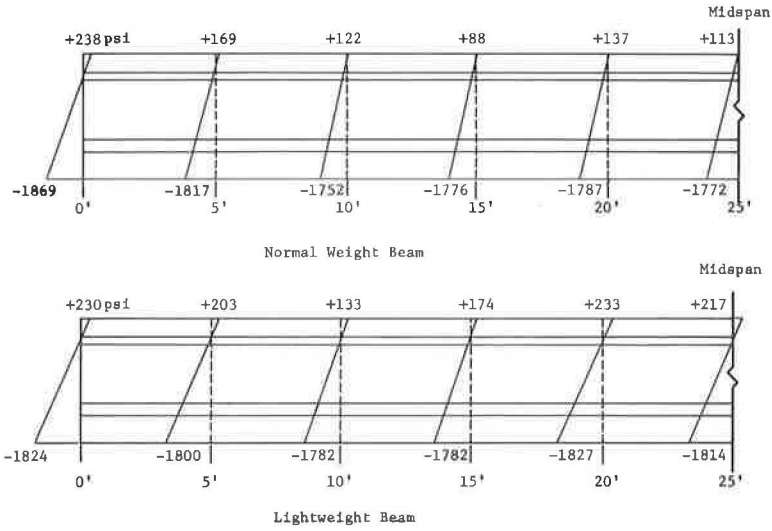
Figure 4. Testing frame with failed specimen.

Figure 5. Testing frame showing scales used to determine rotational displacements of end of specimen.

Figure 6. Cross section of THD beam showing dimensions and locations of strain-gauge rosettes.

+ GAGES AT MID SPAN
O GAGES AT 15' EITHER SIDE OF MID SPAN
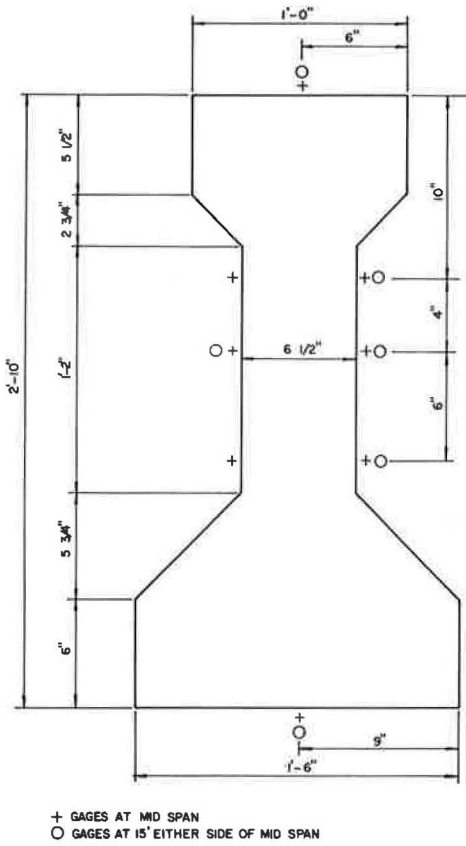
Figure 7. Cracking pattern in normal-weight beam.
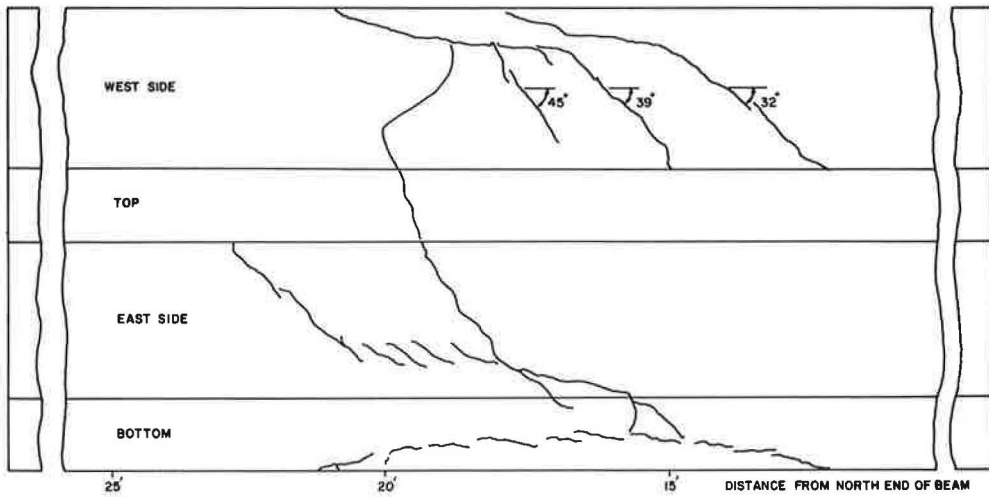
Figure 8. Failure crack in normal-weight beam.
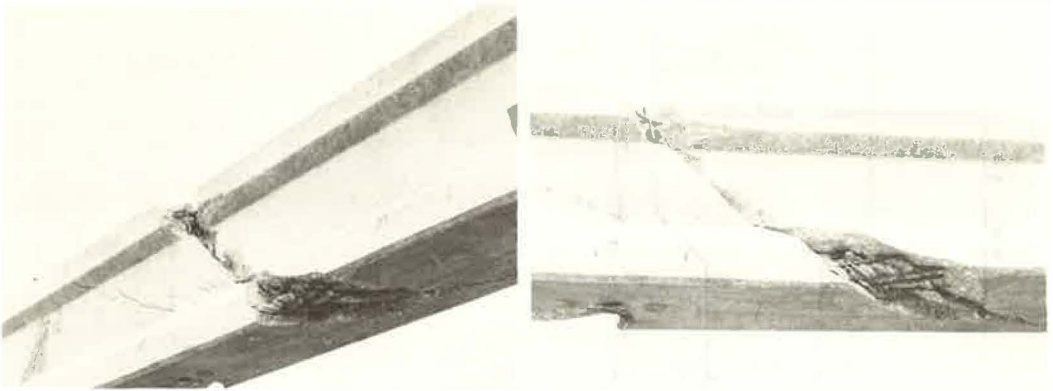
Figure 9. Cracking pattern in lightweight beam.
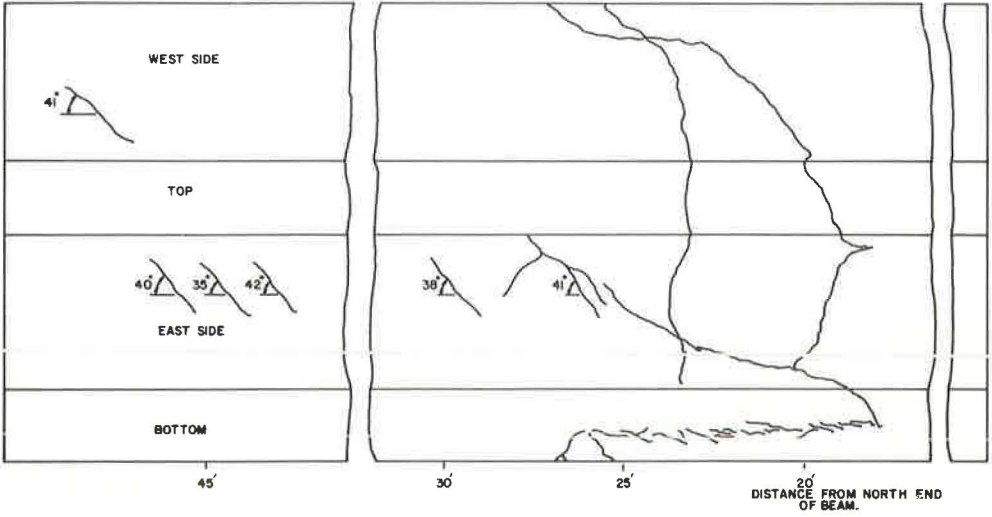
Figure 10. Failure crack in lightweight beam.
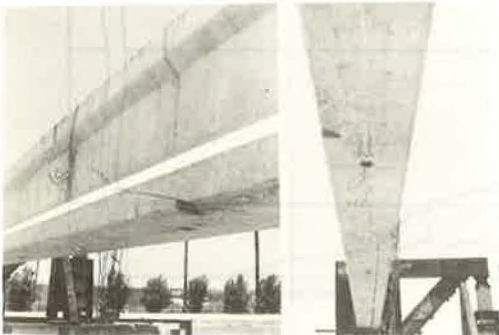
Experimental Strains

The strains measured by the arms of the strain gauge rosettes at 45-deg angles to the longitudinal axis of the beam were the principal strains due to the applied torque. This fact was verified experimentally by the nil strains measured in the longitudinal and transverse directions. The magnitudes of these strains (in μin./in.) at levels of torque of 76.8, 82.4, 88.8, and 91.2 ft-kips for the normal-weight beam are shown in Figure 11 and at levels of torque of 64.8, 70.4, 76.8, and 82.4 ft-kips for the lightweight beam shown in Figure 12.

COMPARISON OF THEORETICAL WITH EXPERIMENTAL RESULTS

The relations between the torque and the angle of twist for the two beams are shown in Figures 13 and 14. In each figure a line has been drawn through the portion of the curve most nearly approximating a straight line. This line is assumed to be the slope of the torque-rotation relationship. By using these data with $K = 7,600$ in.^{4} in the expression $T = KG\theta$ or $(1/K)(T/\theta) = G$, one finds G to be 2.30×10^6 and 1.65×10^6 psi for the normal-weight and lightweight beams respectively. This compares with corresponding values of 2.44×10^6 and 1.56×10^6 psi as determined by ASTM C 215 for the two beams.

If the stresses due to the applied torque are combined with those due to prestress and dead load, the resulting principal stresses (neglecting stress concentrations at the reentrant corners) are greatest in the middle of the face of the top flange at points 5 ft on either side of midspan of the beam. The expressions relating maximum tensile stress to applied torque are

$$\sigma_t = 68.5 + \sqrt{4,700 + 127.3 \ T^2} \qquad (6)$$

and

$$\sigma_t = 116.6 + \sqrt{13,600 + 127.3 \ T^2} \qquad (7)$$

for the normal-weight and lightweight beams respectively. If the tensile strength of the concrete is taken as $0.1f'_c$, the resulting torques necessary to cause cracking of the concrete are 53.5 ft-kips for the normal-weight beam and 54.2 ft-kips for the lightweight beam.

Two standard 6 by 12 cylinders were available for each of the beams. Splitting tensile tests were conducted on these cylinders in the Texas Transportation Institute laboratory. The splitting tensile strengths were 540 psi for the lightweight concrete and 560 psi for the normal-weight concrete. If these values are used in the preceding expressions, the torques necessary to cause cracking are 36.1 ft-kips for the lightweight beam and 44.1 ft-kips for the normal-weight beam. For the normal-weight beam, the first observed extensive diagonal crack occurred at a torque of 88.5 ft-kips. However, the shape of the torque rotation curve indicates that some unobserved cracking may have occurred at a torque as low as 76.5 ft-kips. The torque-rotation curve for the lightweight beam indicates that unobserved cracking may have occurred at 65.0 ft-kips and some as low as 47.0 ft-kips.

Computations were made for selected points on the two beams at selected values of applied torque for comparisons between theoretical and experimental shear stresses. The experimental values were calculated by using the expression $\tau_{exp} = 2G\epsilon$, and the theoretical values were determined by using the relationships shown in Figure 1, with $G\theta$ replaced by T/K. These values are compared in Tables 2 and 3.

Stress Concentrations

The torsional shear stress is increased in magnitude at reentrant corners of a cross section. The amount of stress concentration is dependent on the angle of the corner and the radius that exists between the two adjoining faces. Calculations were made to determine the shear stress at the reentrant corners between the top flange and the web

Figure 11. Strains for normal-weight beam.
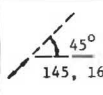
45°	169, 203, 248, 239	
145, 168 184, 129	149, 168, 193, 161 WEST SIDE	93, 110, 140, 98
	141, 155, 196, 144	
144, 142, 158, 110	144, 174, 219, 227 TOP	122, 122, 90, 73
145, 156, 183, 132	149, 155, 194, 143	111, 121, 130, 99
141, 162, 206, 154	151, 172, 201, 190 EAST SIDE	114, 131, 168, 140
159, 174, 187, 142	169, 180, 210, 173	132, 149, 177, 134
199, 224, 260, 194	161, 182, 194, 151 BOTTOM	174, 190, 199, 157
40'	25'	10' Distance from north end of beam

Figure 12. Strains for lightweight concrete beam.
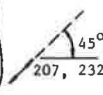
45°	187, 201, 208, 220	
207, 232, 254, 269	177, 199, 217, 236 WEST SIDE	191, 207, 226, 278
	182, 202, 213, 233	
218, 242, 257, 271	160, 167, 175, 182 TOP	172, 190, 210, 207
237, 259, 272, 293	200, 212, 224, 238	215, 237, 260, 237
190, 204, 232, 251	157, 181, 197, 219 EAST SIDE	146, 168, 181, 165
239, 270, 287, 298	202, 224, 240, 264	218, 240, 224, 299
271, 303, 341, 391	312, 369, 425, 520 BOTTOM	269, 292, 334, 391
40'	25'	10' Distance from north end of beam.

Figure 13. Torque-rotation relation for normal-weight beam.

Figure 14. Torque-rotation relation for lightweight concrete beam.

Table 2. Theoretical and experimental torsional stresses for lightweight beam.

Applied Torque (ft-kips)	Point[a]	$\tau_{exp} = 2G\epsilon$[b]	$\tau_{theory} = \dfrac{CT}{K}$	$\dfrac{\tau_{theory}}{\tau_{exp}}$
64.8	A40	680	730	1.17
	E40	846	988	1.17
70.4	A40	755	793	1.05
	E40	945	1,070	1.13
76.8	A40	802	865	1.08
	E40	1,064	1,170	1.10
82.4	A40	846	928	1.10
	E40	1,220	1,253	1.03
64.8	A25	499	730	1.46
	E25	973	988	1.02
70.4	A25	521	793	1.52
	E25	1,151	1,070	0.93
76.8	A25	546	865	1.58
	E25	1,326	1,170	0.88
82.4	A25	568	928	1.63
	E25	1,622	1,253	0.77
64.8	A10	537	730	1.36
	E10	839	988	1.18
70.4	A10	593	793	1.34
	E10	911	1,070	1.17
76.8	A10	655	865	1.32
	E10	1,042	1,170	1.12
82.4	A10	635	928	1.46
	E10	1,220	1,253	1.03

[a] Points A are on centerline of face of top flange; points E are on the centerline of bottom flange. Numerical suffix indicates distance from end of beams.
[b] $G = 1.56 \times 10^6$ psi.

Table 3. Theoretical and experimental torsional stresses for normal-weight beam.

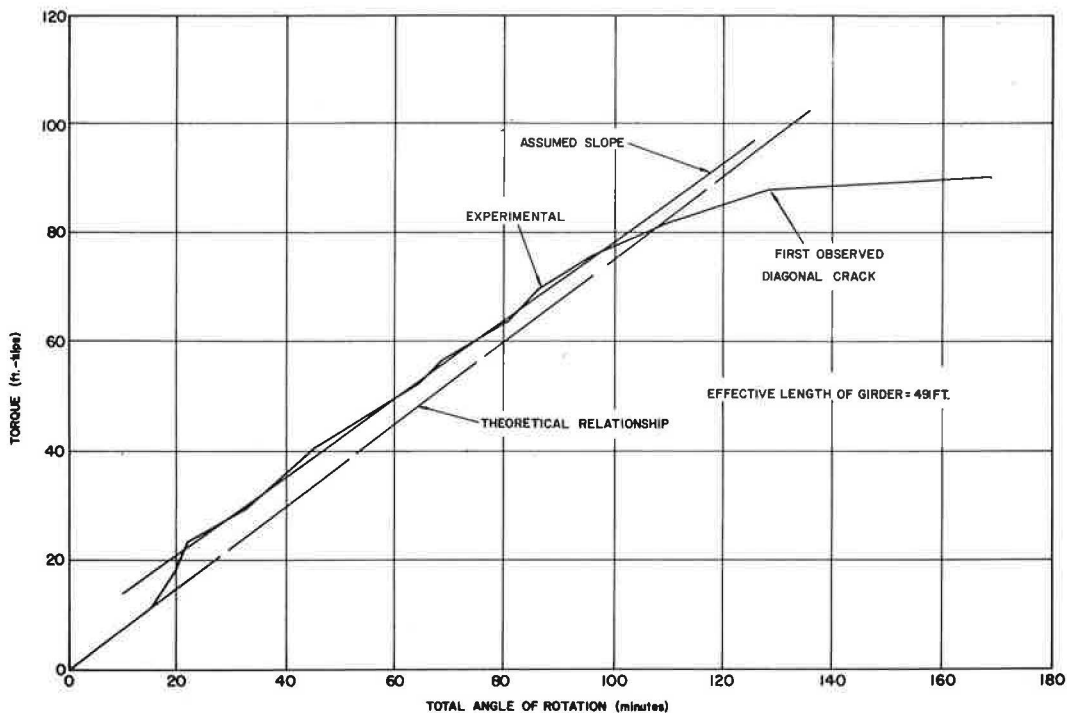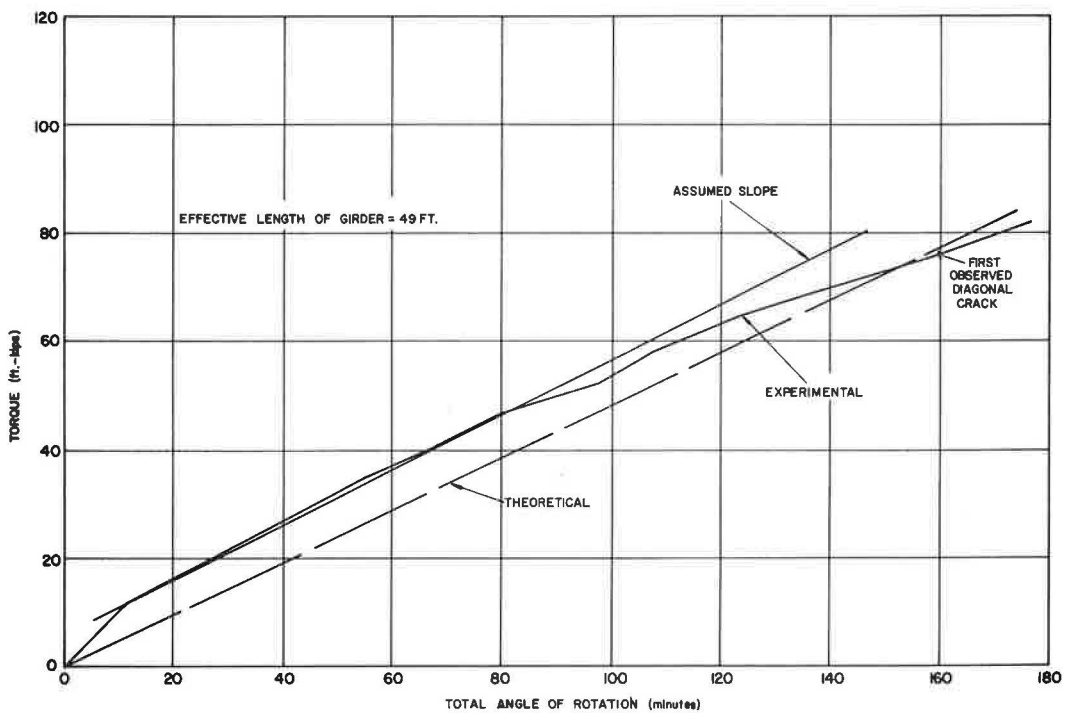| Applied Torque (ft-kips)	Point	$\tau_{exp} = 2G\epsilon$[a]	$\tau_{theory} = \dfrac{CT}{K}$	$\dfrac{\tau_{theory}}{\tau_{exp}}$
76.8	A40	703	866	1.23
	E40	971	1,172	1.21
82.4	A40	693	928	1.34
	E40	1,093	1,258	1.15
88.8	A40	771	1,001	1.30
	E40	1,269	1,355	1.07
91.2	A40	537	1,028	1.91
	E40	948	1,392	1.47
76.8	A25	703	866	1.23
	E25	786	1,172	1.49
82.4	A25	849	928	1.09
	E25	888	1,258	1.42
88.8	A25	1,069	1,001	0.94
	E25	947	1,355	1.43
91.2	A25	1,108	1,028	0.93
	E25	737	1,392	1.89
76.8	A10	595	866	1.46
	E10	849	1,172	1.38
82.4	A10	595	928	1.60
	E10	927	1,258	1.36
88.8	A10	439	1,001	2.28
	E10	971	1,355	1.40
91.2	A10	356	1,028	2.89
	E10	766	1,392	1.82

[a] $G = 2.44 \times 10^6$ psi.

Figure 15. Comparison of stress at reentrant corner with stresses in top flange.
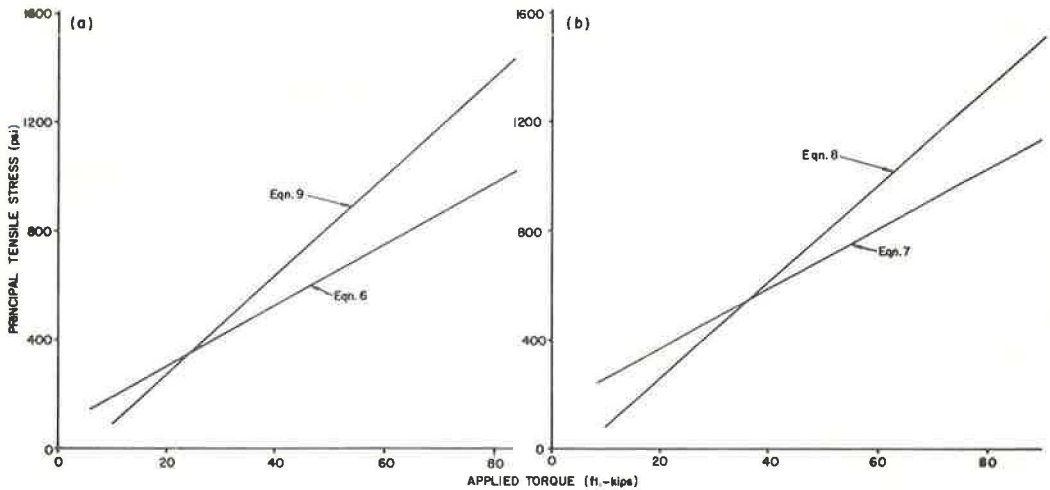
and between the bottom flange and the web of the beams. The values of these shear stresses are 11.80 Gθ and 10.90 Gθ for the reentrant corners at the top and bottom flanges respectively. For the top-flange reentrant corners at points 5 ft from either side of midspan of the beam, the expressions for principal tensile stress are

$$\sigma_t = -134 + \sqrt{17,950 + (11.80 \; G\theta)^2} \tag{8}$$

and

$$\sigma_t = -165 + \sqrt{27,200 + (11.80 \; G\theta)^2} \tag{9}$$

for the lightweight and normal-weight beams respecitvely. Equations 6 and 9 are compared in Figure 15a, and Eqs. 7 and 8 are compared in Figure 15b. From these figures, it is seen that the location of the point on the beam where the maximum tensile stress occurs is dependent on the relative magnitude of the applied torque and the bending stresses. The stresses at the reentrant corner do not exceed those in the top flange for low-value torques. For values of torque near the failure torque, the concentrated stresses at the reentrant corner significantly exceed those in the top flange. It should be remembered that the stress concentrations are confined to a very small area and that significantly lower stresses exist on either side of the corner. Localized plastic yielding could account for the fact that pronounced early failure did not occur at the reentrant corner in the tests.

CONCLUSION

On the basis of the two tests and the analysis conducted in this study, the following observations and conclusions are indicated.

1. When subjected to a torsional load, the prestressed concrete beams failed in tension along a diagonal line that made an angle of approximately 40 deg on the sides and 50 deg on the top flange. The ends of this crack were connected by a line on the bottom flange running longitudinally with the axis of the beam.

2. The effective values of shearing modulus, G, of 2.30 and 1.65 x 10^6 psi found in the full-scale torsion tests compare well with values of 2.44 and 1.56 x 10^6 psi determined by ASTM C 215 for the normal-weight and lightweight beams respectively. Thus, the procedure followed in the theoretical calculations along with the concrete properties used in these calculations results in torsional stiffness values that compare well with experimental values.

3. Theoretically derived torsional capacity using 0.1f$'_c$ as the ultimate tensile strength was about 60 percent of the experimental torsional capacity, which is on the conservative side. If strengths obtained from split cyclinder tests are used as the ultimate strength, the theoretical torsional capacity is about 50 percent of the experimental torsional capacity.

REFERENCES

1. Hsu, T. T. C. Torsion of Structural Concrete—Uniformly Prestressed Rectangular Members Without Web Reinforcement. Jour. Prestressed Concrete Institute, April 1968.
2. Zia, P. Torsional Strength of Prestressed Concrete Members. Jour. of the American Concrete Institute, Vol. 57, April 1961.
3. Wyss, A. N., and Mattock, A. H. A Study of I-Section Prestressed Concrete Girders Subject to Torsion, Shear and Bending. Dept. of Civil Engineering, University of Washington, Seattle, Final Rept. on Research Project Y-1180, June 1971.
4. Timoshenko, S., and Goodier, J. N. Theory of Elasticity, 2nd Ed. McGraw-Hill, New York, 1951.
5. Tamberg, K. G. Elastic Torsional Stiffness of Prestressed Concrete AASHO Girders. Jour. of the American Concrete Institute, Vol. 62, No. 4, April 1965.

28

6. Furr, H. L., Sinno, R., and Ingram, L. L. Prestress Loss and Creep Camber in Highway Bridge With Reinforced Concrete Slab on Pretensioned Prestressed Concrete Beams. Texas Transportation Institute, Texas A&M University, Res. Rept. 69-3 (Final), October 1968.

INVESTIGATION OF PRESTRESSED REINFORCED CONCRETE FOR HIGHWAY BRIDGES

M. A. Sozen and C. P. Siess, University of Illinois

This report provides a guide to the work accomplished in the course of an extensive research project on the use of prestressed concrete for highway bridges. The project was active over the period 1951-1969. It covered various topics related to flexural strength, shear strength, time-dependent deformations, anchorage-zone stresses, and bond characteristics of prestressed concrete beams. The scope of the analytical and experimental investigations in each area is outlined. The report also contains a list of references where complete information on different phases of the investigation can be found.

●IN October 1950, George F. Burch, then Bridge Engineer for the Illinois Division of Highways, requested the University of Illinois Civil Engineering Department to submit a proposal for research that might help to answer certain questions about the use of prestressed concrete in highway bridges, questions that had been discussed in the Committee on Bridges and Structures of the American Association of State Highway Officials. This proposal led to a comprehensive investigation of the strength and behavior of prestressed concrete bridge beams, which was conducted through the years 1951-1969 as a cooperative research project of University of Illinois, the Illinois Division of Highways, and the U. S. Department of Transportation, Federal Highway Administration, Bureau of Public Roads.

The objectives of the project, which were reviewed annually by an advisory committee with emphasis on their ultimate relation to bridge design, covered flexural strength, shear strength, time-dependent effects, anchorage-zone stresses, and bond. The resulting research produced a fund of basic information on the structural performance of prestressed concrete, which influenced directly the development of design specifications and methods in the United States and other countries. This paper provides a summary of the activities on the project.

The aims of the project as well as the research methods were formed under three influences.

1. The project was initiated only 2 years after the completion of the Walnut Lane Bridge in Philadelphia, the first prestressed concrete highway bridge in the United States. Prestressed concrete was new, full of promise, and somewhat mysterious. The claims made for its qualities in the popular professional literature were often unsubstantiated and sometimes irrelevant.

2. The basis of structural design in reinforced concrete was in the process of changing from working stresses to strength.

3. Prior to the initiation of the project on prestressed concrete, an extensive and successful investigation of concrete bridge floors had just been concluded at the University of Illinois. In that project, fundamental information was gathered and used to develop design methods by using a three-pronged approach that consisted of (a) theoretical formulation of the problem, which lead to selection of the critical variables to be investigated experimentally; (b) experimental studies, which provide tests of the

theoretical predictions and sometimes lead to modifications of the theory and further tests of critical variables; and (c) development of simplified design methods with explicitly defined domains of applicability.

The entrepreneurial claims made for prestressed concrete on the basis of superficial evidence made it essential to establish whether prestressed concrete would have its own set of design criteria or whether the criteria for reinforced concrete would be applicable to prestressed concrete. The change in the design basis from stress to strength created a need for fundamental information. The manifest success of the methods used in the investigation of concrete bridge floors provided the confidence and the convincing evidence for planning a long-range study starting with investigations of fundamental problems.

Thus, as various different problems were considered throughout the history of the investigation, the method used was the classic experimental method of hypothesize-test-rehypothesize. The final step was that of producing design methods for use in practice. The research program was always aimed at developing information about broad and basic problems rather than specific design conditions. For example, the entire problem of the flexural strength of prestressed concrete sections was studied analytically and experimentally to develop design criteria for unbonded prestressed concrete beams. Although this approach required time to reach practical results, it eliminated backtracking and reduced the number of limitations and doubts that often surround the results of single-purpose programs designed for immediate solutions.

Various phases of the project are described in the following sections.

FLEXURAL STRENGTH

At the time of inception of the project, a general theoretical understanding of the flexural strength of reinforced concrete sections was still to be developed. Sufficient data under different conditions had not yet been obtained to provide a firm and general perspective of factors such as the limiting strain and effective strength of the concrete in a beam in relation to a test cylinder. Prestressed concrete introduced additional variables (the prestress level and reinforcement with a stress-strain curve that could not easily be idealized as elastoplastic) and brought doubts to bear on what had been one of the stable foundations of the theory of flexural strength for ordinary reinforced concrete sections (the distribution of strain over the depth of the section) because of the need for deriving comparable solutions for unbonded beams as well as beams with fully and partially bonded reinforcement.

The concepts involved in determining the flexural strength of prestressed reinforced concrete sections are shown in Figure 1, which shows the conditions of strain and stress at failure for a rectangular beam reinforced in tension. Notation related to the geometry of the cross section is defined in the figure. The symbols for strain and stress have the following significance:

ϵ_u = limiting strain of concrete in compression,
ϵ_{sa} = increase in the steel strain beyond the strain $(\epsilon_{se} + \epsilon_{ce})$,
ϵ_{ce} = concrete strain at level of reinforcement caused by effective prestress,
ϵ_{se} = strain in reinforcement corresponding to effective prestress,
ϵ_{su} = total strain in reinforcement at failure,
f_{cu} = average stress in beam concrete at ultimate, and
f_{su} = reinforcement stress at beam failure.

The steel strain increase, ϵ_{sa}, is related to the limiting concrete strain, ϵ_u, by the expression

$$\epsilon_{sa} = F \epsilon_u \left[(1/k_u) - (1) \right] \tag{1}$$

where F is a strain compatibility factor that is influenced primarily by the bond between concrete and steel and the loading conditions. From equilibrium, it can be shown that

$$k_u = p f_{su}/f_{cu} \tag{2}$$

which can be substituted in Eq. 1 to yield

$$\epsilon_{sa} = F \epsilon_u \left[(f_{su}/pf_{su}) - (1) \right] \qquad (3)$$

The total steel strain at beam failure is

$$\epsilon_{su} = \epsilon_{se} + \epsilon_{ce} + F \epsilon_u \left[(f_{su}/pf_{su}) - (1) \right] \qquad (4)$$

Equation 4 provides a direct relation between f_{su} and ϵ_{su} as represented qualitatively by curve 1 shown in Figure 2. Another relation between steel stress and strain is isolated by the inherent stress-strain curve for the steel. For a particular case, for which curve 1 may be plotted with the help of Eq. 4, the solution for f_{su} is at the intersection of the two curves shown in Figure 2. The flexural capacity of the section is almost directly proportional to f_{su}. Therefore, the relative effects of the critical variables on flexural strength can be evaluated by using Figure 2.

The stress-strain curve for prestressing reinforcement can be divided ideally into a linear and a nonlinear portion. In relation to the strength of the beam, indicated by the stress f_{su}, it follows from Figure 2 that, if curve 1 intersects the linear portion of curve 2, any factor that shifts the position of curve 1 becomes critical. If curve 1 intersects the nonlinear portion of curve 2, flexural strength of the beam is insensitive to variations in factors affecting the position of curve 1.

A series of 82 beam tests was made in the course of the investigation to establish the effects of various parameters that control the location of curve 1 as indicated by Eq. 1. The concrete strength, reflected in the term f_{cu} of Eq. 1, was varied from 1,270 to 8,320 psi. The reinforcement ratio, p, varied from 0.1 to 1.0 percent. Bond conditions, which affect the compatibility factor F, were varied by testing bonded, totally unbonded, and partially unbonded beams. The effective prestress ranged from 20,000 to 180,000 psi.

A typical example of the type of studies carried out is shown in Figure 3, which shows the variation of the failure stress in the reinforcement, f_{su}, with the ratio p/f_{cu} at different values of the effective prestress ranging from 0 ($\epsilon_{se} = 0$) to 150,000 psi ($\epsilon_{se} = 0.005$). It is evident from Figure 3 that, below $p/f_{cu} = 1.5 \times 10^{-6}$ (1/psi), the flexural strength of the beam is insensitive to the effective prestress. The curves also indicate that a reduction in prestress from 150,000 to 120,000 psi is not important for strength throughout the range of p/f_{cu} values covered and that, at prestress levels over 120,000 psi ($\epsilon_{se} = 0.004$), there is little variation in f_{su} as the abscissa changes from 1×10^{-6} to 3×10^{-6}. Large variations in concrete strength are not of significance in this range.

Analyses shown in Figure 3 not only helped to plan experimental studies (concentrating experimental work in ranges where the analytical results show little sensitivity to changes in the parameters studied may produce trivial test results) but also indicated the ranges where design simplifications are possible.

For example, it is evident from Figure 3 that for bonded beams the variation of the steel stress with the parameter p/f_{cu} can be represented closely by a straight line. Figure 4 shows the exact solution for the steel stress with the predictions of an approximate method described by the expression

$$f_{su} = f'_s \left[(1) - (0.5) (pf'_s/f'_c) \right] \qquad (5)$$

where f'_s is the strength of the reinforcement.

The work on flexural strength of prestressed concrete included studies toward the development of design specifications as well as analytical and experimental research. This phase of the project is summarized elsewhere (4).

One portion of the studies made in relation to design involved analytical studies of the interrelations among design criteria for flexure. Prestressed concrete bridge beams were designed to satisfy one set of requirements based on service load stresses, such as maximum stresses immediately after prestress and maximum stresses at design load, and another set of requirements based on minimum factors of safety. These

dual sets of criteria hindered the selection of optimum sections. Consequently, a comprehensive study was made of the interrelations among design criteria for composite and noncomposite sections, leading to various aids for design as well as an explicit understanding of the effects of the design requirements. These studies are summarized elsewhere (3).

SHEAR STRENGTH

One of the early misconceptions about prestressed concrete was the belief that prestressing eliminated the need for web reinforcement. For service loads, it could be shown by calculation that the inclined principal tensile stresses were negligible or nonexistent. This is generally correct, but it does not mean that the prestressed concrete beam is not susceptible to shear failure. The first few beam tests demonstrated quite clearly that prestressed concrete beams could fail in shear with the beam developing considerably less strength and less ductility than it would have if it had failed in flexure.

Figure 5 shows the measured load-deflection curves of two prestressed concrete I-beams with similar properties except for web reinforcement. Beam 1 had no web reinforcement, and it failed in shear. Beam 2 had sufficient web reinforcement to develop a flexural failure. The undesirability of a bridge beam susceptible to a shear failure and the need for web reinforcement are clear from the comparison.

The investigation was concerned primarily with developing design methods for the determination of the optimum amount and type of web reinforcement in prestressed concrete bridge beams. Because of the lack of rational concepts related to shear failure, this task required considerably more experimental work than the investigation of flexural strength, with a substantial effort spent on understanding the behavior and modes of failure of beams without web reinforcement.

Initial tests and analyses of rectangular prestressed concrete beams resulted in the definition of shear-compression failures, which explained in an intelligible manner many features of shear failures in prestressed as well as ordinary reinforced concrete beams (5). This was followed by a study of prestressed I-beams, which related the shear-compression theory explicitly to the development of strains in the beam. It also showed that this mode of failure was only one of several possible modes and that the critical stage in the load history of a prestressed beam was the development of the inclined crack that could be initiated either in an uncracked portion of the beam or in a region influenced by flexural cracking (6). Subsequent studies showed the negative effect of draped reinforcement (i.e., that draping the strands could actually reduce the shear strength of the beam rather than increase it) and the quantitative relation between flexural cracking and inclined cracking (7, 8, 9). After a stable perspective had developed about the strength and behavior of beams without web reinforcement, work was started on beams with web reinforcement. This phase of the work (11) demonstrated that, although theoretically incorrect, the truss analogy would serve satisfactorily as a basis for the determination of web reinforcement in prestressed concrete beams and that the amount of web reinforcement was proportional to the difference between the shears corresponding to flexural failure and to initiation of inclined cracking.

During the course of this investigation of shear, a total of 250 beam tests was made. Loading conditions included simply supported beams, continuous beams, and beams subjected to simulated moving loads. Beams with rectangular cross sections as well as composite and noncomposite I-beams were tested. Concrete strength, prestress level, and amount and type of web reinforcement were major variables. The entire work is reported elsewhere (6, 10, 11).

The investigation had a strong impact on design methods for prestressed concrete. The concepts of inclined cracking, which developed during the progress of the investigation, are currently used in the ACI Building Code. As a result of the findings in this study, it has also become general practice to relate the shear capacity of the concrete to the inclined cracking load.

Figure 1. Conditions of strain and stress at failure for beams reinforced in tension only.
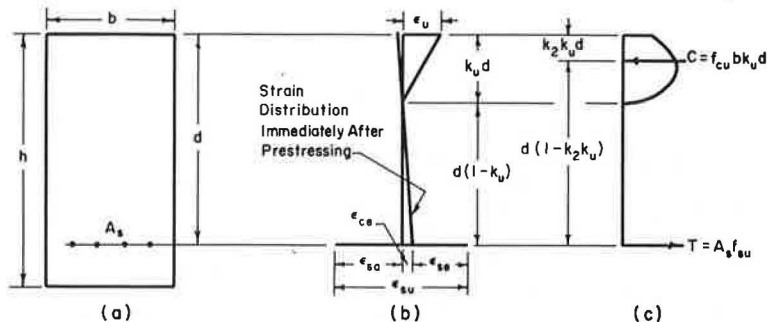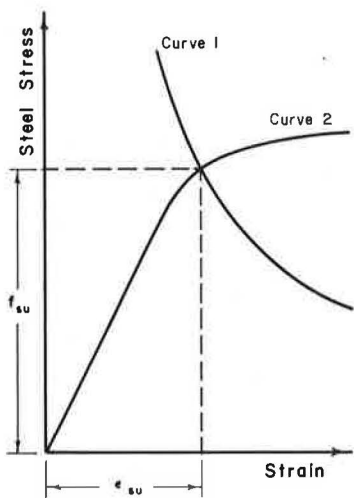

Figure 2. Graphic solution.

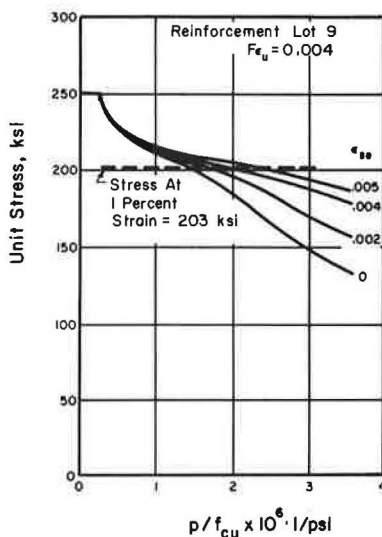Figure 3. Effect of ϵ_{se} on reinforcement at failure.

Figure 4. Comparisons of "exact" values of f_{su} with those derived from the joint committee approximate method and the proposed approximate method.
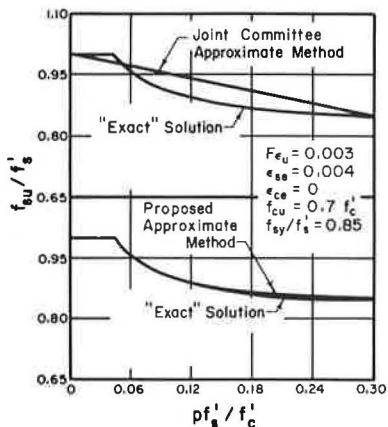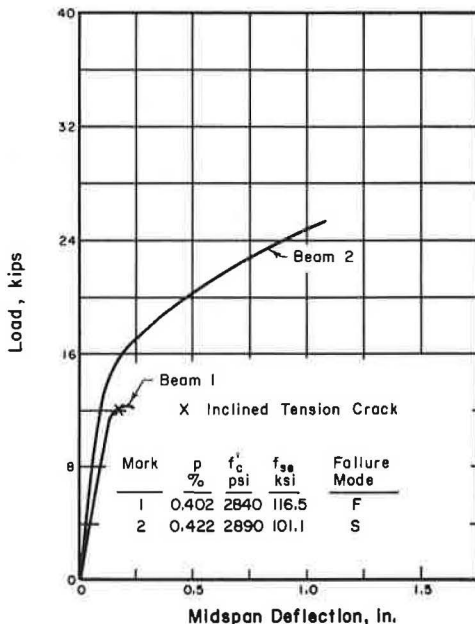

Figure 5. Load-deflection curves for beams failing in flexure and shear.

TIME-DEPENDENT EFFECTS

Stress relaxation of prestressing reinforcement and time-dependent deflections of prestressed concrete beams were studied in this phase of the investigation.

In the early 1950s, there were limited data on long-time stress-relaxation characteristics of prestressing reinforcement in general and virtually no data on prestressing steel manufactured in the United States. Consequently, a series of tests was initiated using the vibration technique (12) and continued for a 10-year period. The final paper (14) on this project reports data from 57 tests made at the University of Illinois and 444 tests made in other laboratories. On the basis of these data, design expressions were developed for estimating stress-relaxation losses as a function of time and the initial prestress level.

Prestressed concrete beams develop time-dependent deflections because of stress relaxation of the steel and creep and shrinkage of the concrete. Because the prestressing force varies with time, concrete creep occurs under varying stress. Furthermore, the prestressed bridge beam is typically subjected to sudden changes in its loading conditions in the early part of its life history, such as applications of prestress and casting of a deck, which complicate the process for calculating time-dependent deflections. An analytical investigation was initiated, complemented by laboratory tests, to study the feasibility of various methods of calculating time-dependent deflections. The main difference between the methods used was the manner of treating creep under varying stress. It was found that a simple procedure, the rate-of-creep method, was adequate for most practical cases (13). The study was extended to discuss the time-dependent deflection problem in typical composite highway bridges.

DESIGN OF ANCHORAGE-ZONE REINFORCEMENT

Longitudinal cracks have been observed in the anchorage zones of both post-tensioned and pretensioned prestressed concrete bridge girders. On some occasions, these cracks have led to collapse of the girder. A program of tests and analyses was initiated to investigate this phenomenon and to develop design methods for the proportioning of transverse reinforcement to restrain anchorage-zone cracking.

The experimental program included 66 tests of simulated anchorage zones. The results of these tests were studied in conjunction with data from 111 tests reported by other investigators. The experimental data covered a wide range of variables critical to the behavior of the anchorage zone: (a) size and shape of cross section; (b) eccentricity of the prestressing force; (c) ratio of the loaded area to the cross-sectional area; (d) distribution of the prestressing force; (e) type of prestressing (post-tension or pretension); (f) concrete quality; (g) amount, type, and location of transverse reinforcement; and (h) time-dependent effects.

Theoretical studies of the stress distributions in the anchorage zone resulted in a simplified analytical solution to the problem, which permitted the analysis of the critical cracking stresses in beams of all cross sections. More importantly, this analysis provided an intelligible basis for the design of transverse reinforcement to restrain anchorage-zone cracking. The entire study is summarized in a paper by Welsh and Sozen (17), which discusses the fundamental aspects of the anchorage-zone problem, describes the method of design, and presents an illustrative example.

BOND CHARACTERISTICS OF PRESTRESSING STRAND

In the early applications of prestressed concrete, a firm knowledge of bond was not considered to be critical because most of the bridge members were long and slender and some elements were post-tensioned and anchored mechanically. However, research on anchorage-zone stresses and shear strength indicated that the development length of the strand was critical in determining the susceptibility of the prestressed element to the development of longitudinal and inclined cracks near the anchorage zone. Consequently, an extensive investigation of the bond characteristics of prestressing wire and strand was initiated as one phase of the investigation.

The experimental program included 486 pullout tests and 5 beam tests to investigate the following parameters.

1. Strand diameter: seven-wire strands varying from $\frac{1}{4}$ to $\frac{1}{2}$ in. were tested.
2. Concrete strength: compressive strength of the concrete ranged from 2,400 to 7,600 psi.
3. Settlement of concrete: depth of concrete beneath strand was varied from 2 to 30 in.
4. Consistency of concrete: tests were made with concretes having slumps from 0.2 to 7.5 in.
5. Curing conditions: tests were made with moist-cured and dry-cured concrete, primarily to vary shrinkage.
6. Lateral pressure: a special test setup made it possible to make pullout tests with the concrete subjected to lateral pressure ranging up to 2,500 psi.
7. Age of concrete: specimens were tested from 1 to 64 weeks after casting.
8. Sustained load: pullout tests were made with the strand subjected to a constant load for periods up to 15 months.

The results of the entire investigation are reported elsewhere (18), which, in addition to presenting a hypothesis for the nature of bond between strand and concrete, contains recommendations for use in practice of the information developed.

REFERENCES

1. Billet, D. F., and Appleton, J. H. Flexural Strength of Prestressed Concrete Beams. Jour. American Concrete Institute, Vol. 25, No. 10, June 1954, pp. 837-854.
2. Siess, C. P. The Strength of Prestressed Concrete Members. Proc., Symposium on the Strength of Concrete Structures, Cement and Concrete Association, London, May 1956, pp. 123-157.
3. Khachaturian, N., Ali, I., and Thorpe, L. T. Investigation of Prestressed Reinforced Concrete for Highway Bridges, Part II: Analytical Studies of Relations Among Various Design Criteria for Prestressed Concrete. Univ. of Illinois Eng. Exp. Station Bull. 463, Aug. 1962.
4. Warwaruk, J., Sozen, M. A., and Siess, C. P. Investigation of Prestressed Reinforced Concrete for Highway Bridges, Part III: Strength and Behavior in Flexure of Prestressed Concrete Beams. Univ. of Illinois Eng. Exp. Station Bull. 464, Sept. 1962.
5. Zwoyer, E. M., and Siess, C. P. The Ultimate Strength in Shear of Simply-Supported Prestressed Concrete Beams Without Web Reinforcement. Jour. American Concrete Institute, Vol. 26, No. 2, Oct. 1954, pp. 181-200.

6. Sozen, M. A., Zwoyer, E. M., and Siess, C. P. Investigation of Prestressed Concrete for Highway Bridges, Part I: Strength in Shear of Beams Without Web Reinforcement. Univ. of Illinois Eng. Exp. Station Bull. 452, April 1959.

7. MacGregor, J. G., Sozen, M. A., and Siess, C. P. Effect of Draped Reinforcement on Behavior of Prestressed Concrete Beams. Jour. American Concrete Institute, Vol. 32, No. 6, Dec. 1960, pp. 649-699.

8. MacGregor, J. G., Sozen, M. A., and Siess, C. P. Strength of Prestressed Concrete Beams With Web Reinforcement. Jour. American Concrete Institute, Vol. 62, No. 12, Dec. 1965, pp. 1503-1519.

9. MacGregor, J. G., Siess, C. P., and Sozen, M. A. Behavior of Prestressed Concrete Beams Under Simulated Moving Loads. Jour. American Concrete Institute, Vol. 63, No. 8, Aug. 1966, pp. 835-842.

10. Hawkins, N. M., Sozen, M. A., and Siess, C. P. Behavior of Continuous Prestressed Concrete Beams. Proc. Internat. Symposium on Flexural Mechanics of Reinforced Concrete, ASCE, 1965, pp. 259-294.

11. Olesen, S. Ø., Sozen, M. A., and Siess, C. P. Investigation of Prestressed Reinforced Concrete for Highway Bridges, Part IV: Strength in Shear of Beams With Web Reinforcement. Univ. of Illinois Eng. Exp. Station Bull. 493, July 1967.

12. Siess, C. P., and McLean, G. Relaxation of High-Tensile Strength Steel Wire for Use in Prestressed Concrete. ASTM Bull. 211, Jan. 1956, pp. 46-52.

13. Corley, W. G., Sozen, M. A., and Siess, C. P. Time-Dependent Deflections of Prestressed Concrete Beams. HRB Bull. 307, 1962, pp. 1-25.

14. Magura, D. D., Sozen, M. A., and Siess, C. P. A Study of Stress Relaxation in Prestressing Reinforcement. Jour. Prestressed Concrete Institute, Vol. 9, No. 2, April 1964, pp. 13-57.

15. Gergeley, P., and Sozen, M. A. Design of Anchorage-Zone Reinforcement in Prestressed Concrete Beams. Jour. Prestressed Concrete Institute, Vol. 12, No. 2, April 1967, pp. 1-13.

16. Lenschow, R. J., and Sozen, M. A. A Practical Analysis of the Anchorage-Zone Problem in Prestressed Beams. Jour. American Concrete Institute, Vol. 62, No. 11, Nov. 1965, pp. 1421-1439.

17. Welsh, W. A., Jr., and Sozen, M. A. Investigation of Prestressed Reinforced Concrete for Highway Bridges, Part V: Analysis and Control of Anchorage-Zone Cracking in Prestressed Concrete. Univ. of Illinois Eng. Exp. Station Bull. 497, Sept. 1968.

18. Stocker, M. F., and Sozen, M. A. Investigation of Prestressed Reinforced Concrete for Highway Bridges, Part VI: Bond Characteristics of Prestressing Strand. Univ. of Illinois Eng. Exp. Station Bull. 503, Aug. 1970.

TIME-DEPENDENT BEHAVIOR OF CONCRETE MADE WITH HAWAIIAN AGGREGATES

Harold S. Hamada, Samuel Zundelevich, and Arthur N. L. Chiu,
University of Hawaii

The results from experimental studies on creep and shrinkage behavior of axially loaded cylinders and the camber and deflection behavior of simply supported rectangular prestressed concrete beams are reported. The nominal compressive strength of the Hawaiian aggregate concrete is 5,000 psi. The specimens were stored at 73 F and 50 percent relative humidity. Two lightweight and one normal-weight concrete mixes were used to manufacture the specimens. The cylinders were loaded to 0.25 f'_c, 0.40 f'_c, and 0.60 f'_c. The beams were loaded at third points with 750-lb loads. The span length of the beam was 15 ft. All Hawaiian aggregate concretes show larger ultimate shrinkage strain when compared with data in published literature. Hawaiian lightweight concretes have smaller ultimate shrinkage strain than does the Hawaiian normal-weight concrete.

•LIGHTWEIGHT and normal-weight concrete is widely used in construction in the state of Hawaii. Because of its wide usage, there is a need for a better understanding of the initial and time-dependent behavior of concrete members.

This paper discusses the results obtained from experimental studies on the creep and shrinkage behavior of axially loaded cylinders and the camber and deflection behavior of simply supported rectangular prestressed concrete beams. All specimens were made from concrete using Hawaiian aggregates.

Much research work has been done on the long-term behavior of manufactured lightweight and normal-weight concrete, and many theories have been advanced to describe the empirical information. However, no universally accepted theory exists. The published experimental information indicates that many variables affect the long-term behavior of concrete that is stressed.

Testing is the only satisfactory means of assessing the long-term creep and shrinkage behavior of concrete that is made from local aggregates. For this study, standard concrete cylinders were used; they either were free of stress for investigating shrinkage behavior or were subjected to constant axial stress for investigating creep behavior.

Accurate prediction of camber in prestressed concrete beams and girders becomes especially important in bridge construction to ensure required cast-in-place slab thickness and conformance with grade profiles. Initial and time-dependent deflections are important in building construction because excessively large deflections result in unsightly cracks.

For this study, simply supported rectangular concrete beams, manufactured with local aggregates, were used for investigating camber and deflection behavior. Calculated values using available procedures are compared with assessed loss of prestress, axial shortening, camber, and deflection.

The following notation is used in this paper.

CF_{LA} = correction factor for delayed time of loading;
C_L = creep coefficient defined as the ratio of creep strain to initial strain at the time of applying additional dead load;
C_t = creep coefficient at time t;

$\overline{C}_t$ = average value of creep coefficient at time t;

C_{t_1} = creep coefficient for the noncomposite beam due to subsequently applied loads;

C_u = ultimate creep coefficient;

D = parameter in creep equation;

Fo = prestressing force at transfer (after elastic loss);

ΔF_t = total loss of prestress at time minus the initial elastic loss;

n = number of gauges;

t = time;

t_{LA} = age of concrete when loaded, days;

$\Delta(t)$ = deflection at any time t;

$(\Delta_i)_{Fo}$ = initial camber due to the initial prestress force, Fo;

$(\Delta_i)_{DL}$ = initial deflection caused by the beam's own weight;

$(\Delta_i)_L$ = initial deflection caused by additional loading;

ϵ_o = creep strain of i th gauge;

ϵ_o^i = initial strain of i th gauge;

$\overline{\epsilon}_o^i$ = average value of initial strain, and

ϵ_u = ultimate creep strain.

UNIAXIALLY LOADED CONCRETE CYLINDERS

Laboratory Procedures

Standard 6-in. diameter concrete cylinders were loaded in uniaxial compression in accordance with ASTM C 512-69 recommendations. The constant axial load was maintained by placing steel coil springs in series with the concrete specimens.

The concrete specimens were moist-cured for the first 7 days after manufacture and housed in a controlled-environment room thereafter. The room temperature was maintained at 73.4 ± 2 F, and the relative humidity was maintained at 50 ± 4 percent. All specimens were loaded 28 days after manufacture.

Concrete Mixes

The nominal compressive strength selected was 5,000 psi. Three coarse aggregates were selected: (a) basalt rock from Kapaa Quarry, Oahu; (b) lightweight volcanite cinder, commercially called cinderlite, from Molokai; and (c) lightweight trachyte pumice, commercially called volcanite, from Hawaii. Concrete made from the basalt rock weighed approximately 152 lb/ft^3, whereas concretes made from the other two aggregates were lighter (124 lb/ft^3 for cinderlite and 121 lb/ft^3 for volcanite) and hereafter will be referred to as lightweight concrete.

The design mixes for the 5,000-psi concrete are given in Table 1. These mixes were obtained from a commercial vendor, and the mixes are used in construction projects. The actual 28-day compressive strengths for the mixes are as follows: basalt, 5,883 psi; cinderlite, 5,513 psi; and volcanite, 4,445 psi. Average values were obtained from testing a minimum of three cylinders for each mix. Many cylinders were tested prior to the 28th day to determine the effect of age on compressive strength.

Mathematical Expressions for Creep

For this paper, the mathematical expression selected to represent creep strain as a function of time is taken from Meyers et al. ([1]):

$$C_t = (t^{0.6})/(t^{0.6} + D) C_u \tag{1}$$

The values for C_u and D are to be determined from tests.

Other mathematical functions have been proposed: for example, the hyperbolic formula by Ross ([2]) and Lorman ([3]); the power function by Shank ([4]); and the logarithmic function by Thomas ([5]), Hansen ([6]), and McHenry ([7]). Other forms have also been proposed, but they will not be discussed here. Kajfasz and Szulc ([8]) have published a study on the various expressions.

Test Results

The constant-stress tests were designed to sustain three stress levels: $0.25\ f'_c$, $0.40\ f'_c$, and $0.60\ f'_c$. It was speculated that the first two stress levels were within the linear portion of the stress-strain curve, and the third stress level would fall in the nonlinear range.

Figures 1, 2, and 3 show the creep plus shrinkage strain histories for the three concrete mixes. Initial strains due to elastic shortening at the time of loading are also shown. The horizontal axis shows time after the application of loads on the specimens. Each point in the figures represents an average of nine readings taken from three cylinders. Three gauge lines, spaced 120 deg along the circular perimeter, were selected on each cylinder. Change in cylinder length was measured with an 8-in. Whittemore gauge.

Figure 1 shows the data for the normal-weight concrete. The actual stress levels were different from the desired values, but all three stress levels fell in the linear range of the stress-strain curve. The curves passing through the data points are drawn arbitrarily to delineate each stress level.

Figure 2 shows the data for the concrete made from volcanite aggregates with the stress levels at $0.29\ f'_c$, $0.45\ f'_c$, and $0.67\ f'_c$. Although the first two stress levels were in the linear range, the third stress level was definitely in the nonlinear range of the stress-strain curve. For the first two stress levels, the creep plus shrinkage strains were not significantly different from those shown in Figure 1. However, the initial strains were much larger than those for the basalt mix, indicating a lower elastic modulus for the volcanite mix.

Figure 3 shows the data for the concrete made from cinderlite aggregates with stress levels at $0.23\ f'_c$, $0.36\ F'_c$, and $0.55\ f'_c$. By using the ratio of applied stress to initial strains, we can observe the following:

$$(0.23\ f'_c/450) \simeq (0.36\ f'_c/839) \simeq (0.55\ f'_c/1,171) \simeq \text{elastic modulus}$$

Because these three ratios for the initial strains are nearly equal, the three curves shown in Figure 3 are for the linear range of the stress-strain curve.

Comparison of Figures 1 and 3 may show that the creep plus shrinkage strain of the lightweight cinderlite is less than that of the normal-weight concrete. However, the initial strains of the lightweight concrete are greater, and therefore the total strain (creep plus shrinkage plus initial strains) is greater for the lightweight concrete.

Figures 4, 5, and 6 show the time variation of the creep strain. These curves are similar to those shown in Figures 1, 2, and 3, except that shrinkage strains have been subtracted. The variation of shrinkage strain with time may be obtained from these figures by taking the difference between the appropriate curves. Special shrinkage strain versus time curves will not be presented. Shrinkage strains are discussed in more detail in subsequent portions of this paper.

The curves shown in Figures 4, 5, and 6 are based on the equation

$$\overline{\epsilon}_c = \epsilon_u(t^{0.6})/(t^{0.6} + D) \tag{2}$$

The constants C_u and D, which are shown in Figures 4, 5, and 6, have been determined by least square fitting of the experimental data. It is noted that the creep coefficient for the normal-weight concrete is greater than that of the lightweight concrete. The creep coefficient for lightweight concrete from Hawaiian aggregates compares favorably with those given by Shideler (9).

In the process of determining C_u and $\overline{\epsilon}_u$ from the experimental data, the following problem was observed. The coefficients C_u and D were obtained by least square fitting of the average values of the creep coefficient.

Table 1. Design mixes for 5,000-psi concrete.

Mix	Material	Size	Source	ASTM Designation	Quantity
Mix 47[a]					
Coarse aggregate	Basalt	$^3/_4$ in.	Kapaa	C-33	1,575 lb
Fine aggregate	Basalt	Number 4	Kapaa	C-33	1,008 lb
	Sand	—	Molokai	C-33	546 lb
Cement	Type I	—	Hawn/Perm	C-150	7.2 sacks
Admixture	Plastiment	—	Sika	C-494	3 oz/sack
Mix 67[b]					
Coarse aggregate	Cinder	$^3/_4$ in.	Molokai	C-330	1,000 lb
Fine aggregate	Coral	Number 4	Barbers Point	C-33	619 lb
	Sand	—	Molokai	C-33	705 lb
Cement	Type I	—	Hawn/Perm	C-150	7.3 sacks
Admixture	Plastiment	—	Sika	C-494	3 oz/sack
Mix 77V[c]					
Coarse aggregate	Volcanite	$^3/_4$ in.	Hawaii	C-330	1,200 lb
Fine aggregate	Volcanite	Number 4	Hawaii	C-330	1,010 lb
Cement	Type I	—	Hawn/Perm	C-150	8.0 sacks
Admixture	Plastiment	—	Sika	C-494	3 oz/sack

[a]Mix 47 = 5,000-psi 3F with plastiment (5.0-3FP1-7.2).
[b]Mix 67 = 5,000-psi cinderlite with plastiment (5.0-CCP1-7.5).
[c]Mix 77V = 5,000-psi volcanite with plastiment (5.0-VOP1-8.0).

Figure 1. Creep plus shrinkage strains versus time after loading for basalt concrete.
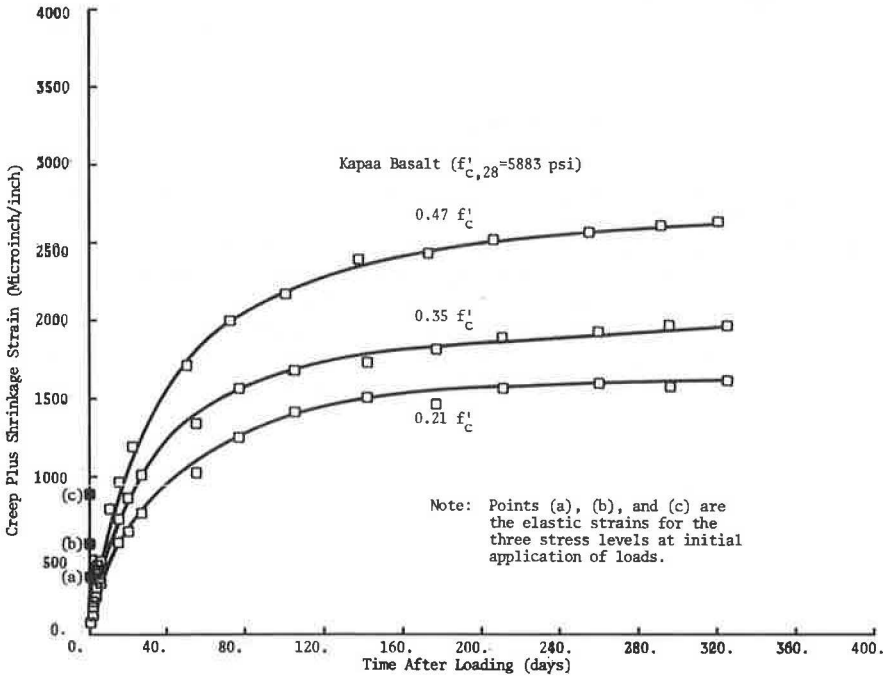
Figure 2. Creep plus shrinkage strains versus time after loading for volcanite concrete.
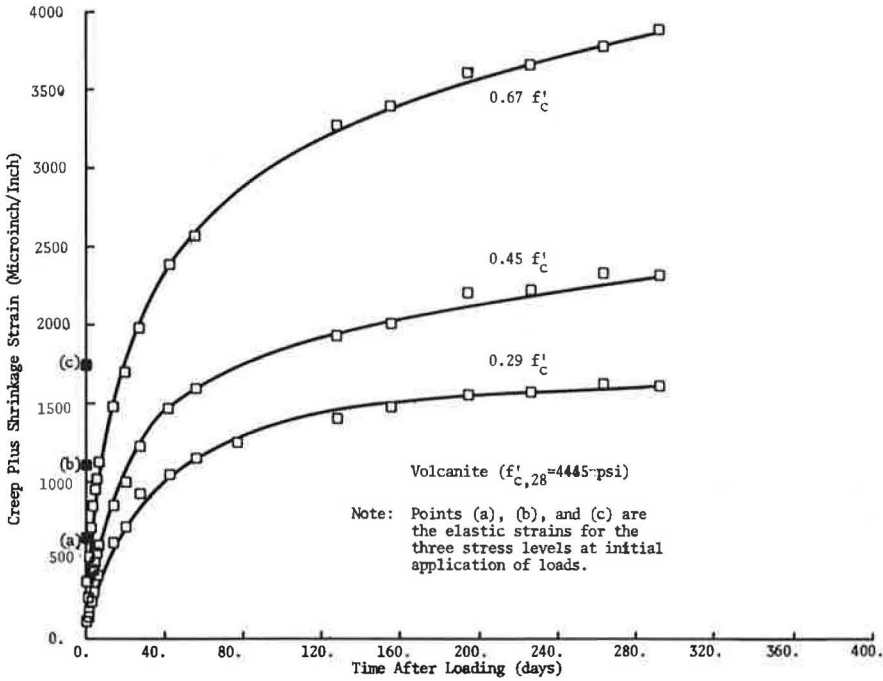
Figure 3. Creep plus shrinkage strains versus time after loading for cinderlite concrete.
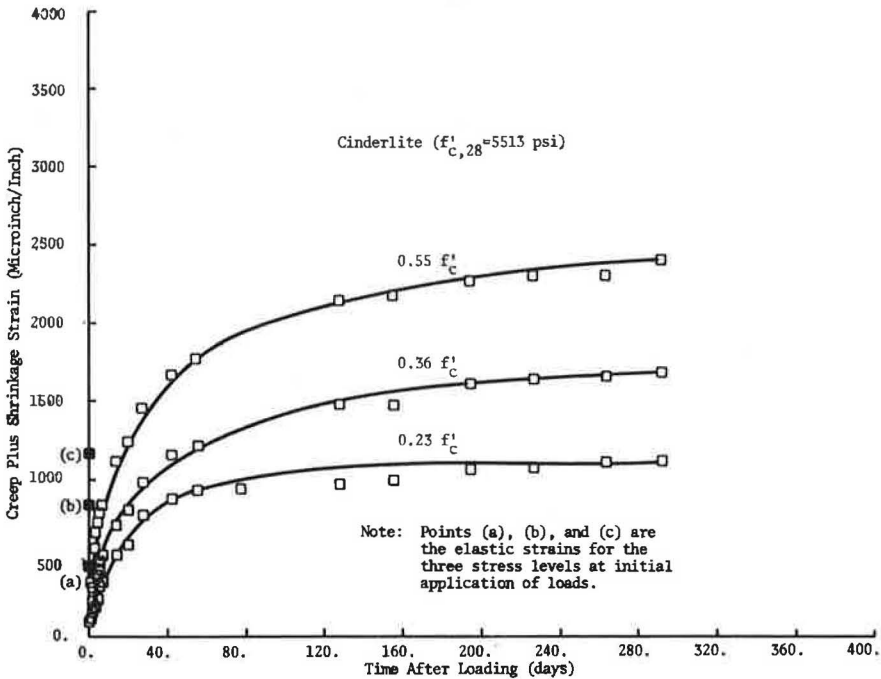
Figure 4. Creep strain versus time after loading for basalt concrete.

Stress Level	C_u	D	$\bar{\epsilon}_o$
O 0.21 f_c'	3.19	11.65	368
□ 0.35 f_c'	3.01	12.42	576
△ 0.47 f_c'	3.52	16.65	895
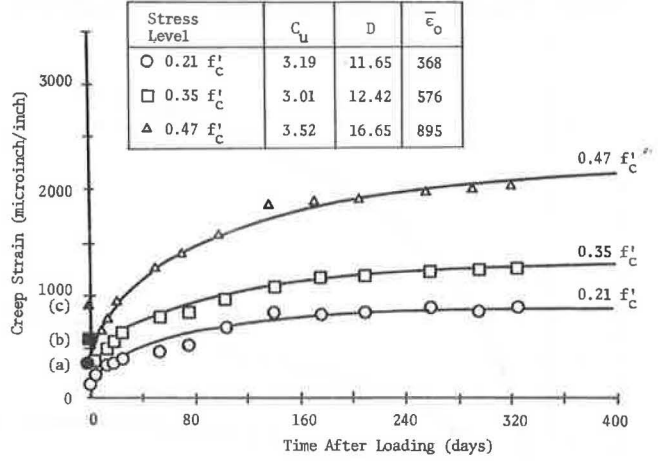
Figure 5. Creep strain versus time after loading for volcanite concrete.

Stress Level	C_u	D	$\bar{\epsilon}_o$
O 0.29 f_c'	2.54	24.89	647
□ 0.45 f_c'	2.24	17.60	1111
△ 0.67 f_c'	2.52	12.79	1744
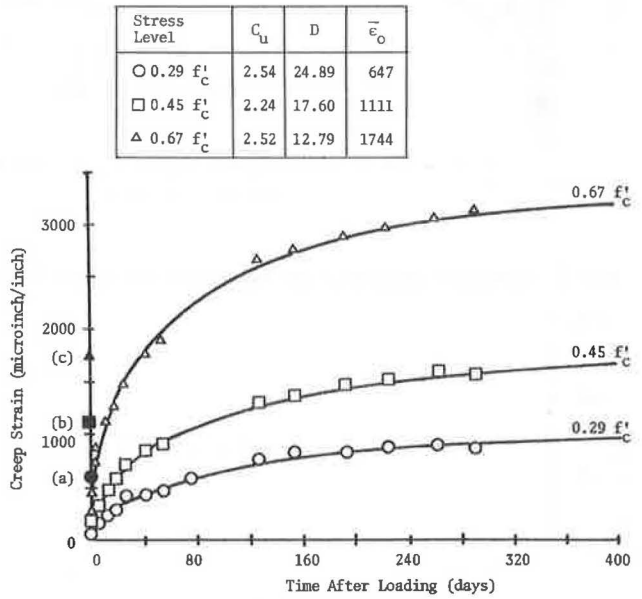
Figure 6. Creep strain versus time after loading for cinderlite concrete.

Stress Level	C_u	D	$\bar{\epsilon}_o$
O 0.23 f_c'	1.90	9.14	450
□ 0.36 f_c'	1.97	10.84	839
△ 0.54 f_c'	2.54	7.31	1170
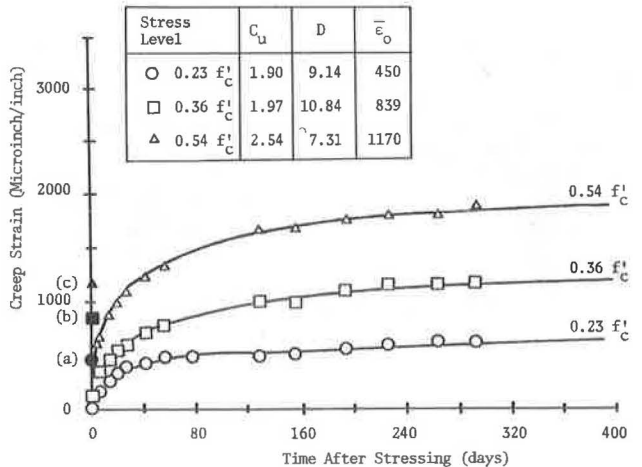
$$\overline{C}_t = \left[\sum_{i=1}^{n} (\epsilon_{c_i}/\epsilon_{o_i}) \right] \bigg/ n \qquad (3)$$

The average initial strain was determined by the equation

$$\overline{\epsilon}_o = \left[\sum_{i=1}^{n} (\epsilon_{o_i}) \right] \bigg/ n \qquad (4)$$

Now if one uses the product of $\overline{\epsilon}_o$ and C_u as the value of the ultimate creep strain ϵ_u in Eq. 2, the resultant curves will not adequately represent the data points. The ultimate creep strain ϵ_u must be determined separately. This observation may suggest that the creep coefficient is not a good parameter to use because it does not adequately demonstrate the variation in the experimental data in both numerator ϵ_{c_i} and denominator ϵ_{o_i}.

SIMPLY SUPPORTED PRESTRESSED CONCRETE BEAMS

Simply supported rectangular prestressed concrete beams were used to investigate the camber and deflection characteristics. These beams were manufactured with the same types of aggregates as were used for the cylinders. Type I standard cement and plastiment as a retardant admixture were used.

By using the different mixes, with a nominal strength $F_o = 5,000$ psi, three sets of specimens were cast separately. Each set consisted of three beams to study deflections and three beams to study camber (one unstressed beam 7 ft 9 in. long was poured for each set to determine shrinkage strains). The beams were 4 in. by 6 in. in cross section, 15 ft 6 in. long, and simply supported over a 15-ft span. Two $\frac{3}{8}$ in., 7-wire, 270^k strands located at 1.75 in. from the bottom were used for the prestressing. In addition to their own weights, the deflection specimens support two concentrated 750-lb loads at one-third points of the span as shown in Figure 7.

Strain readings were taken with a Whittemore gauge at different times in accordance with ASTM C 512-69. The gauge point locations are also shown in Figure 7. Camber and deflection values from dial gauge readings compared very well with values calculated by using strain-gauge point readings.

EXPRESSIONS USED TO CALCULATE CAMBER AND DEFLECTION

Several mathematical expressions are available to model the deflection behavior of prestressed concrete members. Reference 10 contains a simplified version from the more accurate expression developed by Branson (11). The terms in Branson's expression can be rearranged, and the total deflection, excluding the effects of non-prestressed reinforcement, can be expressed as the sum of different components shown in Eq. 5 and Figures 8 and 9.

$$\Delta(t) = \Delta_1 + \Delta_2(t) + \Delta_3 + \Delta_4(t) \qquad (5)$$

where

$$\Delta_1 = (\Delta_1)_{F_o} - (\Delta_1)_{DL} \qquad (6)$$

is the result of the initial camber (positive) due to initial prestressing force and the initial deflection due to the beams's own weight;

$$\Delta_2(t) = \{-(\Delta F_t/F_o) + [1 - (\Delta F_t/2F_o)] C_t\} (\Delta_1)_{F_o} - C_t(\Delta_1)_{DL} \qquad (7)$$

44

Figure 7. Prestressed concrete beams.

PRESTRESSING
STRANDS   CROSS SECTION

TYPICAL ARRANGEMENT
OF 8" WHITTEMORE
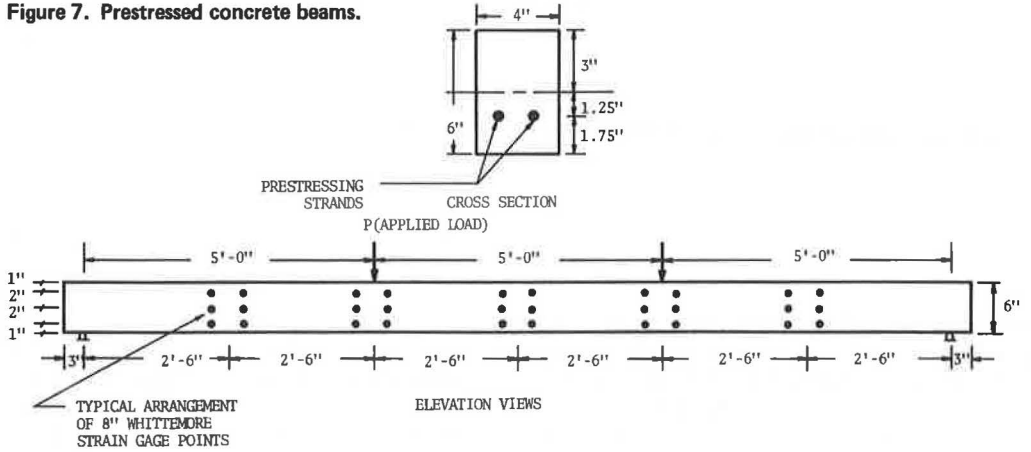STRAIN GAGE POINTS

ELEVATION VIEWS

Figure 8. Camber and deflection behavior of simply supported prestressed concrete beams.
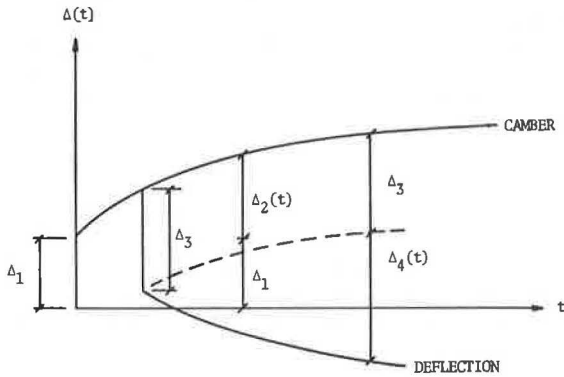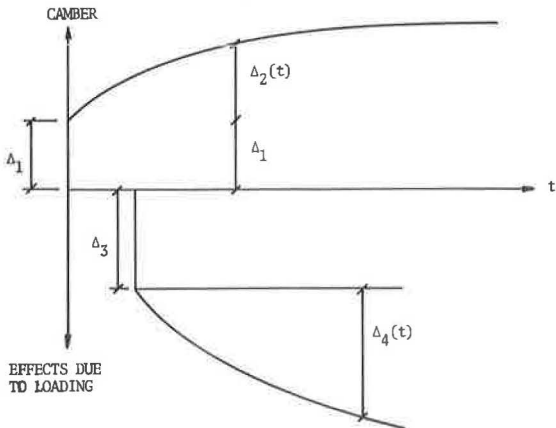

Figure 9. Components of deflection of a simply supported prestressed concrete beam.

is the result of time-dependent effects due to initial camber;

$$\Delta_3 = -(\Delta_1)_{load} \tag{8}$$

is the change in deflection due to additional loading; and

$$\Delta_4(t) = -C_{t_1}(\Delta_1)_{load} - [-(\Delta F_1/2Fo) C_L - (\Delta F_t/2Fo) C_t] (\Delta_1)_{Fo} \tag{9}$$

is the time-dependent effect due to loading and includes the gain in prestress due to the lengthening of fiber at the level of the prestressing steel.

The equations adequately model the deflection behavior of a prestressed concrete member if proper values for concrete strength, modulus of elasticity, ultimate shrinkage strain, and ultimate creep coefficient are used. Conditions other than standard have to be considered by using correction factors to account for differences. Of particular importance are the values of the creep coefficient at any time and the correction factor due to age of loading represented by Eqs. 10 and 11. These equations were presented in detail elsewhere (1).

$$C_t = [t^{0.6}/(D + t^{0.6})] C_u \tag{10}$$

$$CF_{LA} = 1.25 t_{LA}^{-0.118} \tag{11}$$

The parameters, C_u and D, are given in Figures 4, 5, and 6.

RESULTS

This section discusses the experimental results obtained from the study: compressive strength, modulus of elasticity, shrinkage, creep, loss of prestress, camber, and deflection.

Compressive Strength

Results from compression tests indicate that the cinderlite and volcanite mixes have higher early strengths than do the basalt mix.

The calculated modulus of elasticity, using the ACI formula, was always higher than the measured value. This could be one of the reasons why measured initial deflection values were higher than calculated values.

Shrinkage

Table 2 compares ultimate shrinkage strains and free shrinkage values derived from measurements on the free-standing beams. The measured shrinkage values are higher than those suggested by Meyers et al. (1); the latter could be used if no other information is available. However, variations in ultimate shrinkage values cause only minor changes in the answers when predicting camber and deflections. The time-dependent components of deflection, as calculated from Branson's method (using measured constants and measured shrinkage strains), were compared with calculated values by using suggested shrinkage strains. It was found that the behavior can be predicted with acceptable accuracy in both cases.

Creep

In contrast to the cylinder specimens, where the stresses are uniform and maintained constant, the beam specimens show stresses varying along the depth of the member and decreasing with time. To assess the experimental coefficients under such conditions, we obtained ultimate creep coefficients from the measured data. The procedure was to

fit the curves of the average measured camber $[\Delta_1 + \Delta_2(t)]$ and the average measured effects on deflection due to a subsequently applied load $[\Delta_3 + \Delta_4(t)]$. However, to minimize the effects of the discrepancy in the initial camber and in the change in deflection, we normalized the camber and the effects on deflection due to applied loads by dividing the initial camber Δ_1 and instantaneous change in deflection due to loading Δ_3 respectively. If different coefficient values were used with the available expressions for the loss of prestress, camber, and deflection, the value yielding the best visual fit between experimental and calculated curves is selected as the most suitable. Branson's method and measured values of concrete strength and ultimate shrinkage strains were used in the calculations.

The normalized average measured camber and the normalized effects on deflection due to applied loads are shown in Figures 10, 11, and 12 for basalt, cinderlite, and valcanite. Also shown in the figures are curves using experimental constants and ultimate creep coefficients ($C_{u_{basalt}} = 3.7$, $C_{u_{cinderlite}} = 3.3$, and $C_{u_{volcanite}} = 3.0$) obtained by applying the method described in the previous paragraph. Notice that the theoretical curves for the basalt and volcanite mixes fit the experimental curves at every point; this proves the adequacy of Eq. 11. The small discrepancies observed for the cinderlite mix indicate that the values of the parameters in Eq. 11 for the cinderlite mix may be different from those shown (13). Eq. 10 yields excellent results for the three mixes.

Experimental values obtained from the beams as well as from the cylinders are compared with suggested ultimate creep coefficients in Table 2. Differences in values may be attributed to the sensitivity of the creep coefficient to variation of stresses along the depth of the section, to decreasing magnitude of the stresses due to the loss of prestress, and to the delayed time of loading. (The volume-surface ratio for the beams was approximately equal to the volume-surface ratio for the cylinders.)

Loss of Prestress

The initial time-dependent strains for each beam at all five sets of gauge points were measured at different times after stressing. A typical strain diagram at a mid-span section is shown in Figure 13.

The loss of prestress was evaluated by using the strain at the level of the steel and by adding to it 75 percent of the calculated relaxation as suggested by Branson (11). The value of 75 percent takes into account the fact that stress relaxation occurs under decreased strain caused by creep and shrinkage. Experimental loss of prestress at midspan for each concrete mix is shown in Figure 14.

Measured values were compared with calculated values by using the methods suggested in Ref. 10 and by using Branson's method (11) along with suggested and measured constants. It was concluded that Branson's method with suitable constants will predict the loss of prestress more accurately. The method suggested in Ref. 10 is simplified to avoid extensive calculations in design.

Camber and Deflection

Camber and deflection histories for each beam measured with dial gauges are shown in Figures 15, 16, and 17. The average measured camber and average measured effects on deflection are separated and shown in Figures 18, 19, and 20.

Figures 18, 19, and 20 also show the camber and effects on deflection due to applied loads by using the respective recommended constants and formulas suggested elsewhere (10, 11). Also shown in the figures are curves obtained by Branson's method but which use creep coefficients experimentally determined from the beams and the cylinders. By using the experimental values from the beams, camber and deflection behavior can be predicted with better accuracy. The method suggested in Ref. 10 predicts the camber with acceptable accuracy but is less accurate in predicting the effects on deflection due to applied loads. This is because of simplifications made on ultimate creep coefficients for delayed time of loading. The essential difference between the method in Ref. 10 and Branson's method is that the former has been simplified to aid the designer.

Table 2. Comparison of experimental and suggested values for ultimate shrinkage strains and ultimate creep coefficients.

Type of Aggregate	Ultimate Shrinkage Strain, × 10⁻⁶ in./in.		Ultimate Creep Coefficient		
	Experimental	Suggested[a]	Experimental (from beams)	Experimental (from cylinders)	Suggested[a]
Basalt	1,050	714	3.7	3.24	2.69
Cinderlite	938	714	3.3	2.17	2.34
Volcanite	878	726	3.0	2.44	2.33

[a]Derived from Ref. 1.

Figure 10. Comparison of normalized camber and normalized effects of subsequently applied loads with suggested values (basalt).
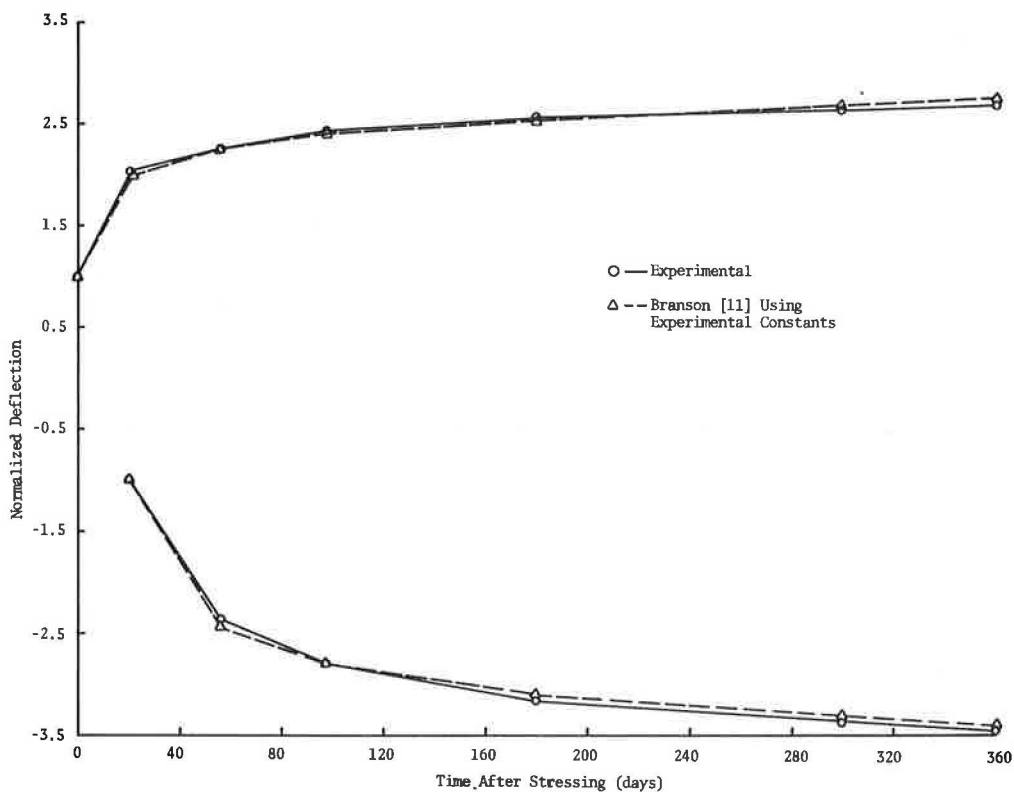
Figure 11. Comparison of normalized camber and normalized effects of subsequently applied loads with suggested values (cinderlite).
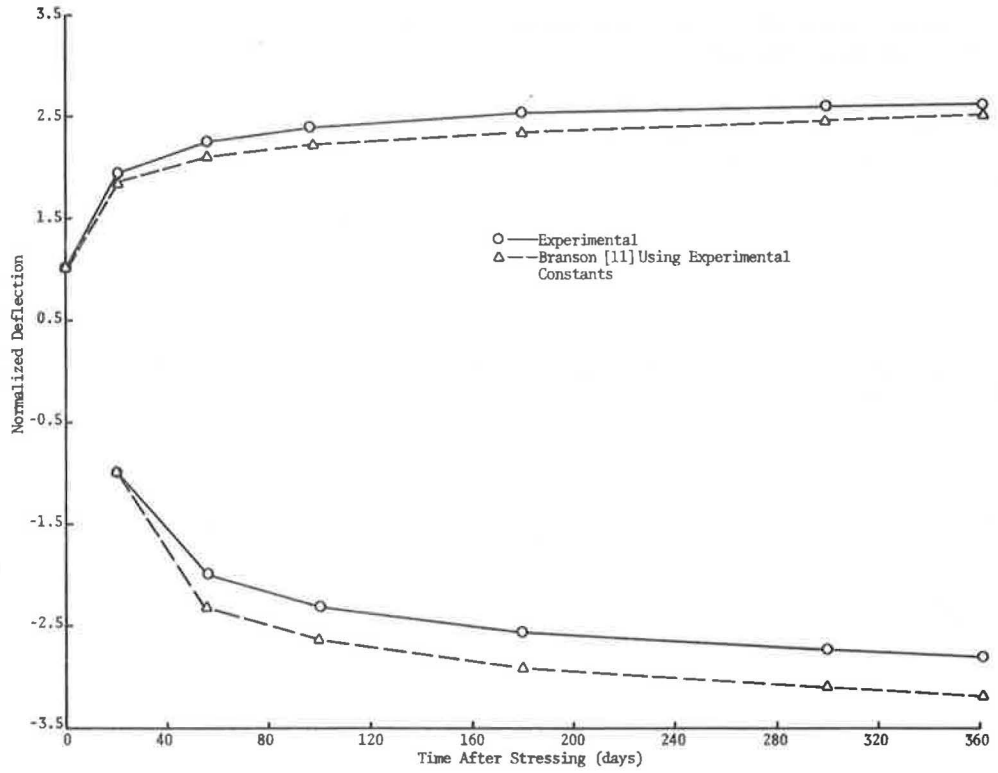
Figure 12. Comparison of normalized camber and normalized effects of subsequently applied loads with suggested values (volcanite).
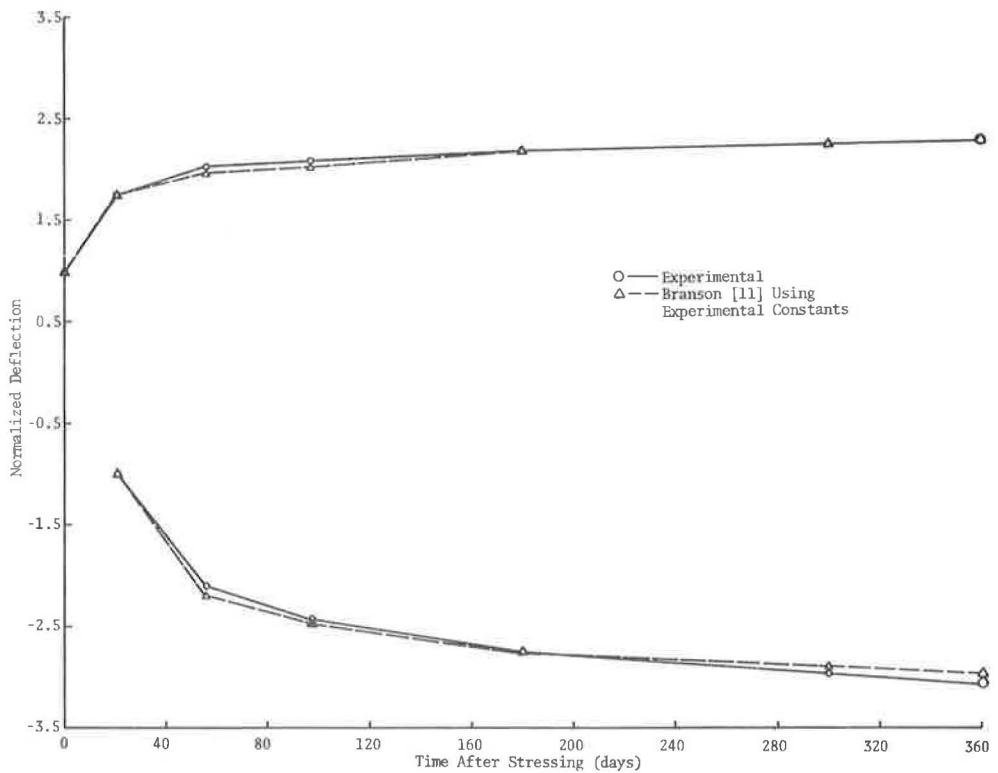
Figure 13. Typical measured strain diagrams at midspan for different times after stressing.
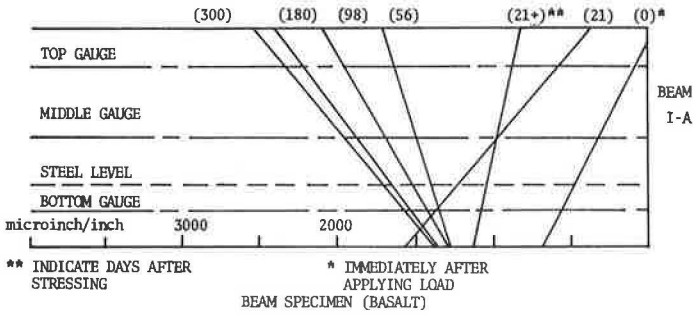
Figure 14. Experimental loss of prestress at midspan for each concrete mix.

50
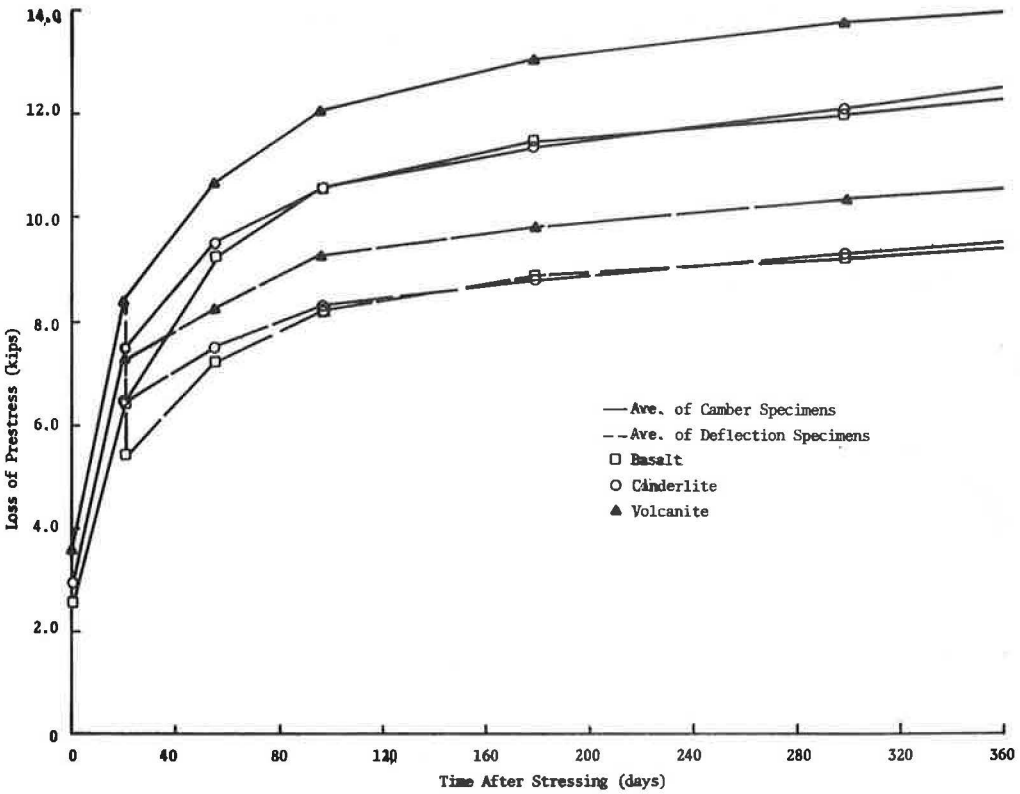
Figure 15. Measured deflection at midspan (basalt).
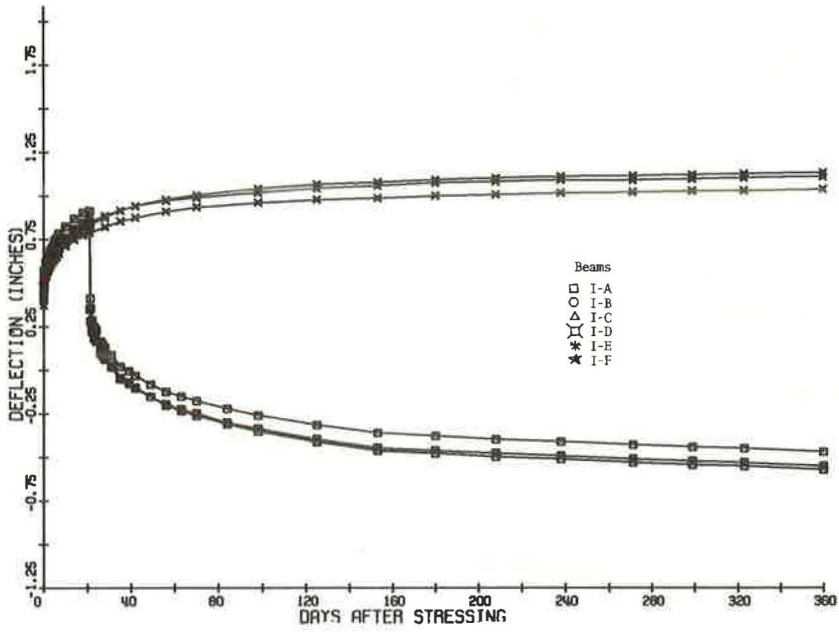
Figure 16. Measured deflection at midspan (cinderlite).
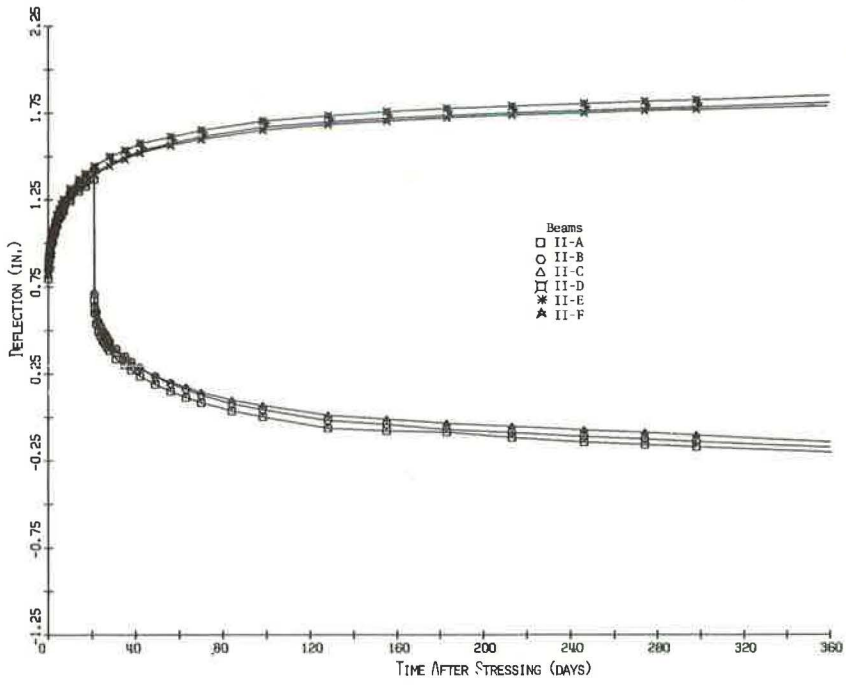
Figure 17. Measured deflection at midspan (volcanite).
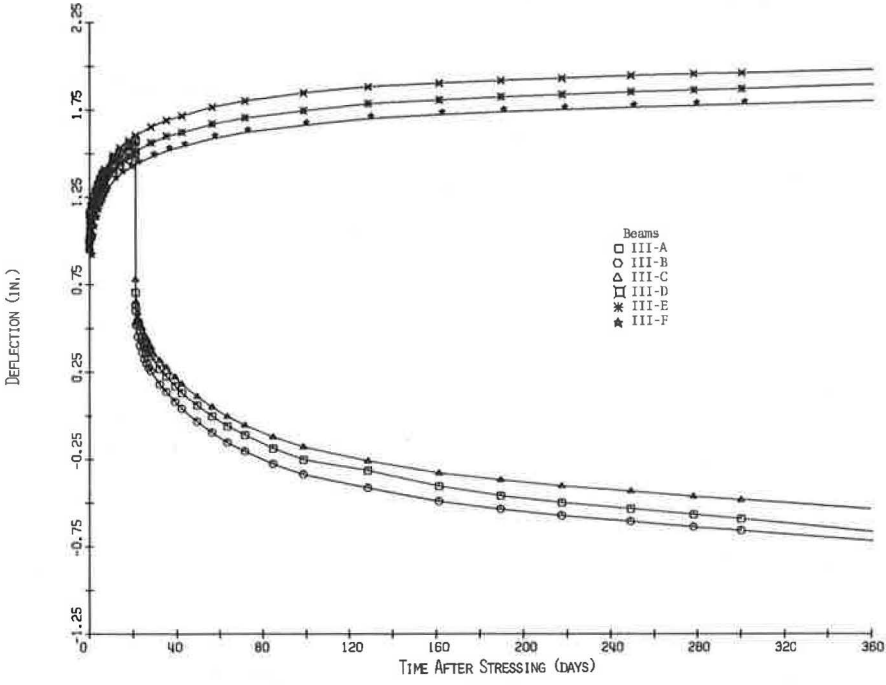
Figure 18. Comparison of camber and effects on deflection due to subsequently applied loads with suggested values using experimental strength (basalt).

52
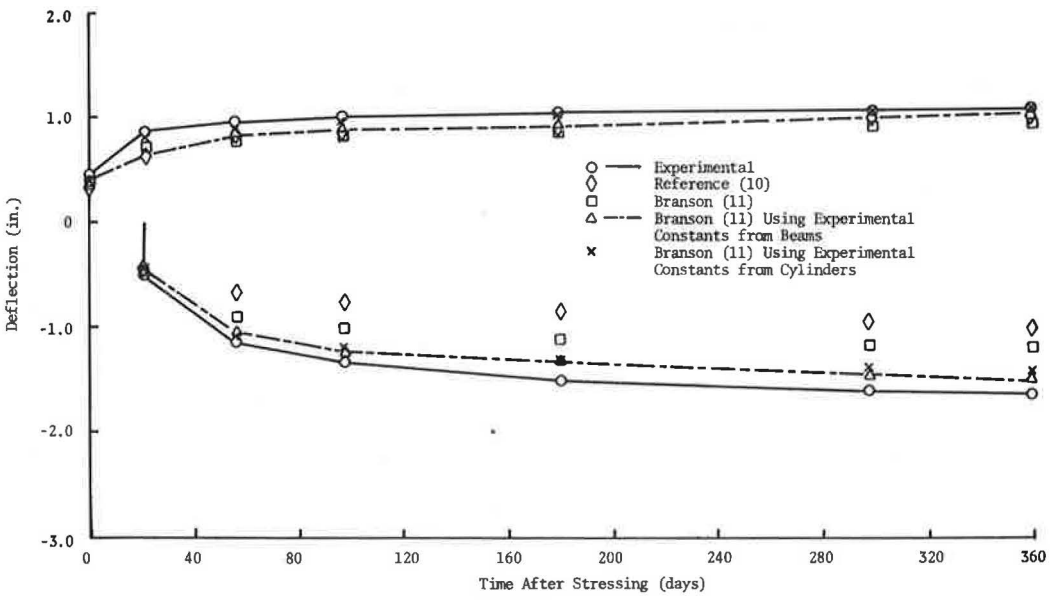
Figure 19. Comparison of camber and effects on deflection due to subsequently applied loads with suggested values using experimental strength (cinderlite).
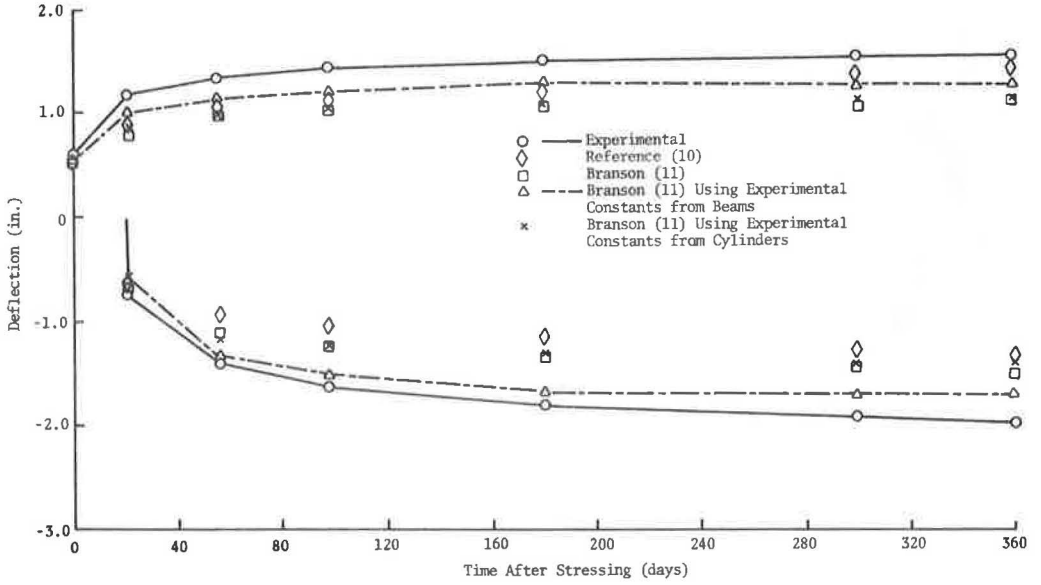
Figure 20. Comparison of camber and effects on deflection due to subsequently applied loads with suggested values using experimental strength (volcanite).
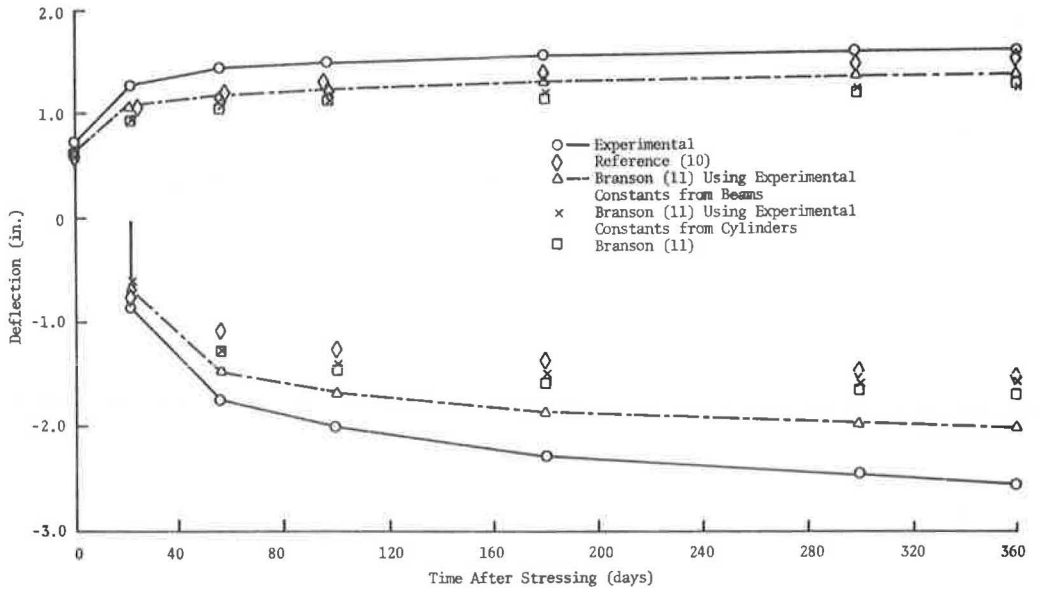
CONCLUSIONS

The following statements can be made on the basis of the study results.

1. Volcanite concrete has higher early strength relative to cinderlite and basalt concretes.

2. The moduli of elasticity for Hawaiian aggregate concretes are lower than the elastic modulus calculated from the ACI formula.

3. All Hawaiian aggregate concretes show larger ultimate shrinkage strains when compared with the data in published literature.

4. Hawaiian lightweight concretes have smaller ultimate shrinkage strain than the Hawaiian normal-weight concrete.

5. Differences in the ultimate creep coefficients, which were determined from uni-axially stressed concrete cylinders and prestressed concrete beams, may be attributed to large sensitivity to the loss of prestress, which is most difficult to assess.

6. The creep coefficient for basalt concrete is larger than the creep coefficients for cinderlite and volcanite concretes. However, this does not necessarily mean that the basalt concrete creeps more because the creep strain is determined from the product of the creep coefficient and initial strains.

7. Branson's method for predicting initial and time-dependent loss of prestress, axial shortening, camber, and time-dependent deflection are recommended. The data show that this method accurately estimates these effects if appropriate coefficients are used for concrete made from Hawaiian aggregates.

ACKNOWLEDGMENT

REFERENCES

1. Meyers, B. L., Branson, D. E., Schumann, C. G., and Christianson, M. L. The Prediction of Creep and Shrinkage Properties of Concrete. Iowa State Highway Commission Res. Rept. 70-5, Aug. 1970.

2. Ross, A. D. Concrete Creep Data. The Structural Engineer, London, Aug. 1937, p. 314.

3. Lorman, W. R. The Theory of Concrete Creep. Proc. ASTM, Vol. 40, 1940, p. 1,082.

4. Shank, J. R. The Plastic Flow of Concrete. Ohio State Univ. Bull. 91, 1935.

5. Thomas, F. G. A Conception of the Creep of Unreinforced Concrete, and an Estimation of the Limiting Values. The Structural Engineer, London, Vol. 11, No. 2, Feb. 1933.

6. Hansen, T. C. Creep and Stress Relaxation of Concrete, A Theoretical and Experimental Investigation. Proc. Swedish Cement and Concrete Research Institute, Stockholm, 1960, p. 98.

7. McHenry, D. A New Aspect of Creep in Concrete and Its Application to Design. Proc. ASTM, Vol. 43, 1943, p. 1,069.

8. Kajfasz, S., and Szulc, J. Approximation of Experimental Data by a Creep Function. Materiaux et Constructions, Vol. 3, No. 18, 1970, p. 381.

9. Shideler, J. J. Lightweight Aggregate Concrete for Structural Use. Portland Cement Association Bull. D 17, Skokie, Illinois, 1957.

10. Branson, D. E. Design Procedures for Computing Deflections. ACI Jour., Proc., Vol. 65, No. 9, Sept. 1968, p. 730.

11. Branson, D. E., Meyers, B. L., and Kripanarayanan, K. M. Loss of Prestress, Camber and Deflection of Noncomposite and Composite Structures Using Different Weight Concretes. Iowa State Highway Commission Res. Rept. 70-6, Aug. 1970.

54

12. Hamada, H. S., Watari, J., and Chiu, A. N. L. Creep and Shrinkage of Concrete Made From Hawaiian Aggregates. Dept. of Civil Eng., Univ. of Hawaii, Tech. Rept. R 71-2 (to be published).
13. Zundelevich, S., Lee, D. N. L., and Chiu, A. N. L. Camber and Deflection Behavior of Simply Supported Prestressed Concrete Beams Manufactured With Hawaiian Aggregates. Dept. of Civil Eng., Univ. of Hawaii, Tech. Rept. R 71-1 (to be published).

FACTORS AFFECTING GIRDER DEFLECTIONS DURING BRIDGE DECK CONSTRUCTION

M. H. Hilton, Virginia Highway Research Council

Problems involved in obtaining the desired thickness of bridge decks were investigated. The study, which was limited to decks longitudinally screeded during construction, included (a) field measurements of the girder deflections during construction and (b) theoretical frame analysis of the girder deflections under the field-loading conditions. Two simply supported steel-plate girder spans were investigated. When full-span length longitudinal screeding is used, the finished grade elevations are set on the screeding edge of the machine and remain independent of the bridge girder deflections, and thus the forming elevations, will in turn have a bearing on the final thickness of a bridge deck. In addition, all factors that in effect cause the deck forming to be too high at the time the concrete is screeded to grade have the potential of causing an inadequate deck thickness. The most significant factors were found to be (a) plan dead-load deflection values that are in error, (b) differential temperatures existing between the top and bottom flanges of the girders during concrete placement as opposed to those that may have existed when the forming elevations were established, and (c) the transverse position of the concrete dead loading at the time a final screeding pass is made over a given point on a span.

•AS bridge design trends have tended toward longer, more flexible spans and as construction techniques have become more sophisticated, the design thickness of bridge decks is often more difficult to obtain during construction. When deficient deck thicknesses occur, there are virtually no reliable corrective measures for restoring lost structural strength; where insufficient cover over the reinforcing steel results, permanent maintenance problems may develop.

During bridge deck construction there are two basic methods for screeding the concrete deck to grade: the transverse and the longitudinal (by nature of the screeding machine's orientation to the alignment of the bridge). This study was concerned only with the longitudinal placement and screeding technique, which is used by many contractors.

Longitudinal screeding machines, such as the one shown in Figure 1, are most often used on simple spans 100 ft or less in length. The transverse screed rails supporting the machine are normally set to the finished grade at each end of the span. The finished grade of intermediate points on the deck are set on the longitudinal strike-off edge of the screeding machine. If the structure of the machine is stable, then the elevations remain fixed and are independent of the girder deflections occurring during concrete placement. Consequently, the final thickness of the bridge deck will be dependent on the deflections of the girders at the time the concrete deck is struck off the grade. Accordingly, all factors influencing the girder deflections during construction have a direct bearing on the final thickness of a bridge deck.

When longitudinal screeding is used, one factor of concern involves the effect on deflections of interconnecting diaphragms between the bridge girders. Conventional

---

procedures for computing plan dead-load deflection values normally assume that diaphragm connections are hinged, i.e., that each girder is free to deflect independently under the dead load of that portion of the concrete deck it would carry. When concrete is placed down one side of a bridge span, as is the case when a deck is to be longitudinally screeded, the deflections of girders directly under the load will be partially restrained by the interconnecting diaphragm action with the unloaded girders. Thus, if the concrete deck is struck off to grade over one girder before concrete is placed over the remaining girders, then the deflection of this girder will not be as much as calculated, and the deck will not be adequate. An earlier theoretical analysis (1) and field investigation (2) indicated that deficient deck thicknesses could result where longitudinal screeding follows too closely behind concrete placement. These studies, however, assumed full rigidity at all diaphragm connections. For bolted connections, the assumption of a rigid joint may not be applicable under the variable loading conditions that exist during deck placement. This paper presents the results of field measurements and a theoretical analysis of semirigidly connected simple-span bridge girders that were used to investigate the actual versus the theoretical deflections occurring during bridge deck construction.

Other factors that could have a bearing on girder deflections during construction were investigated. These included thermal effects such as the heat of hydration of the concrete during deck placement and solar heating of the top flanges of the steel girders prior to concrete placement. To determine the order of magnitude of the influence of the thermal factors, we measured temperatures on the steel girders during the field investigations.

PURPOSE AND SCOPE

The following were the main objectives of the study:

1. To investigate the girder deflections at progressive stages of concrete deck placement and to evaluate the adequacy of the conventional method of computing plan dead-load deflections for a bridge deck that is to be placed and screeded longitudinally over the full-span length;

2. To estimate—by use of a comparison of the theoretical and field data—the degree of diaphragm connection rigidity on the particular spans studied;

3. To investigate the theoretical effects of diaphragm connection rigidity on the deflections of a girder system and to compare the results with field deflection data obtained during progressive stages of deck placement; and

4. To obtain field data on the differential thermal conditions between the upper and lower flanges of steel girders due to solar heating prior to deck placement and the subsequent hydration heat of concrete.

The general scope of the study was limited to simple-span steel-girder bridges with bolted diaphragm connection type designs. The study was limited to bridge decks constructed by use of longitudinal placement and screeding of the concrete.

STRUCTURES STUDIED

One span on each of 2 bridges was instrumented for field study. These were span 3 of the Route 607 and span 4 of the Route 15 bridges over Interstate 64.

The Route 607 span was composed of 6 parallel girders; the Route 15 span was composed of 7. Figure 2 shows the dimensions and the locations of the test instrumentation for the Route 607 span.

INSTRUMENTATION, TESTS, AND PROCEDURES

The data collection techniques and measurement devices were selected to be of minimum obstruction and delay to the contractors during construction of the bridge and roadway grading. For obvious reasons, concrete placement operations could not be delayed for long periods of time. Thus, the number of measurements taken during each delay in deck placement was limited to that which could be handled in approximately 10 to 15 minutes.

Instrumentation

A high-precision modified Wild "N-III" level, capable of direct readings to 0.001 in., was used for measuring the girder deflections. The level was mounted on a trivet that in turn was set in stationary lugs on the top of a pier cap at one end of the test span. In addition, the level was centered on the cap directly above one of the circular pier columns.

Special design rod and scale units (Fig. 3) were attached to the lower flanges of each girder at the quarter-span and midspan length points. Engineer's scales with $\frac{1}{2}$-in. major graduations were attached to the rods, and a reference scale was mounted to the pier cap at the end of the span opposite the position of the level instrument.

A 24-channel Honeywell thermocouple recorder powered by a portable generator was used to collect temperature data on the steel girders. Thermocouples were placed on the top and bottom flanges of the girders at the quarter-span and midspan length points. The top flanges were emphasized, however, because it was expected that temperature variations would be greatest on the top side due to the concrete placement operation and other factors affecting the sun's radiation. A complete cycle of 24 thermocouples was made every 12 minutes during operation of the recorder.

Both of the structures instrumented were designed with neoprene bearing pads located at the expansion ends of the spans. The dead-load deflections of these pads were measured by using dial gauges that were set as close to the centerline of bearing of each girder as was possible. In addition, deflection measurements were taken at a fixed-end steel bearing point to determine the order of magnitude of the vertical movement at these types of assemblies.

Strain measurements, which will not be discussed in this paper, were taken on some of the diaphragm members as indicated in Figure 2.

Test on the Plastic Concrete

Tests made on the plastic concrete were restricted to the measurement of those properties that would have the most direct influence on the bridge girder deflections during deck placement. The following tests and measurements were made on both spans.

1. The time of initial and final set (ASTM C403-68) was run on 3 representative batches of the deck concrete.

2. Unit weight determinations (ASTM C138-63) were made at intervals selected to be generally representative of the concrete placed in each area between the girders.

3. The temperature of the concrete was measured at discharge from the mixer trucks, and the ambient air temperature was recorded continuously during the placement operations.

Field Study Procedures

Initial readings were taken on all systems just prior to the beginning of deck placement operations. Subsequent measurements were taken by delaying placement operations when the concrete deck load was, as nearly as practical, midway between adjacent girders (with the exception that the first delay for measurements was made between the second and third girders from the beginning side of the span). Final measurements were taken when all the concrete was in place with the exception of the thermal data, which were collected for several hours after completion of the decks.

Temperature data were recorded automatically throughout the placement operations. In addition, temperature and deflection measurements were taken on the Route 607 span several days prior to concrete placement to investigate the independent effects on girder elevations of differential temperatures resulting from solar radiation.

During deck concreting, a record of the time and sequence of events was maintained. With the exception of the placement delays for measurements, the contractor's normal procedures were used during construction.

The deck concrete on each of the 2 spans was placed during warm and sunny weather. The air temperature during decking operations ranged from 66 to 89 F and from 64 to 92 F respectively for the Route 15 and Route 607 spans.

58

Figure 1. Longitudinal bridge deck screeding machine.

Figure 2. Locations and dimensions of test instrumentation for Route 607 span.
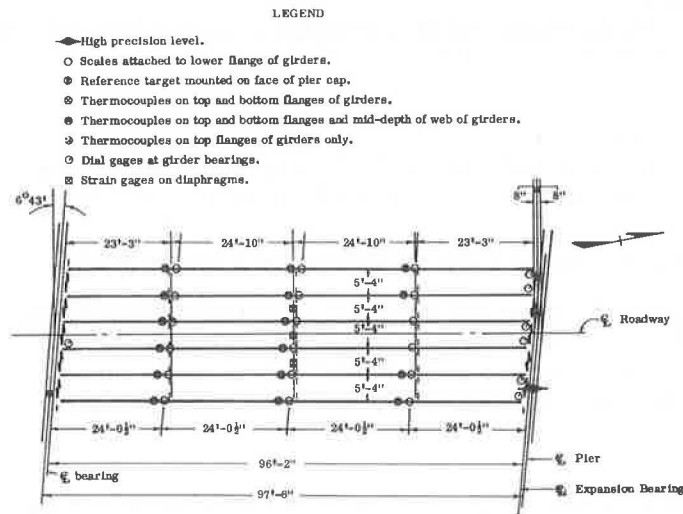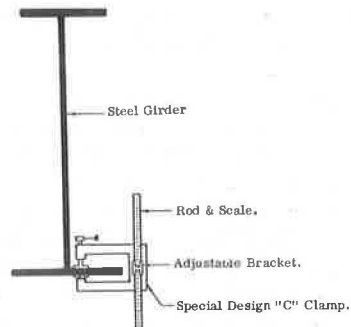

Figure 3. Typical rod and scale unit attached to the lower flange of a bridge girder.

ROUTE 607 SPAN RESULTS

Solar Radiation and Thermal Differentials

The Route 607 span runs in a general north-south direction. Accordingly, the morning sun falls on the east side of the superstructure and gradually passes over to the west side in the afternoon. During several sunny days in June and July, differential thermal and deflection readings were taken on the girders while only the deck forming was in place. With the deck forming in place, of course, the lower flanges of the interior girders were shielded from the sun. The exterior girder on the east side was exposed to the sun in the morning, and the exterior girder on the west side was exposed to the afternoon sun. In addition, the vertical forming on each side of the span tended to shield the top of the east girder in the morning and the top of the west girder late in the afternoon. A transverse section of the steel framing of this span is shown at the top of Figures 4a and 4b, which show respectively the average differential temperatures recorded between the top and bottom flanges of the girders and the resulting upward midspan deflections of the girders.

At 7:00 a.m. on July 1, the temperature differential between the top and bottom flanges was virtually neutral (Fig. 4a), and the corresponding girder elevations at midspan were recorded at that time and used as a reference (Fig. 4b). Comparisons of the temperature differentials at 10:00 a.m., 1:15 p.m., and 3:45 p.m. with the corresponding midspan deflections generally show that the upward deflection of the steel girders increases with increasing temperature differentials. In addition, a transfer of the thermal loading between girders via the diaphragm connections is indicated by the smooth transverse deflection pattern. Upward midspan deflections of 0.43 in. were recorded on girders 5 and 6 at 3:45 p.m. All the girders reached an upward deflection level of approximately $3/8$ in. above the reference level during the early afternoon. As will be discussed in more detail later, thermal deflections of this order of magnitude could have a significant bearing on bridge deck thicknesses.

It can also be noted that the differential temperatures varied transversely across the span width because of its orientation to the angle of the sun. Thus, not only did the midspan girder elevations vary significantly in magnitude, but also the slope of the transverse pattern of upward deflections reversed during the course of the day. This transverse "warping" effect, due to the sun moving toward the west, is shown in Figure 5, where the midspan girder elevations for 2 days are referenced to the elevations existing at 12:00 noon. A difference in the relative elevation of girders 6 and 1 on the order of $1/4$ in. occurred between 12:00 noon and 3:45 p.m. on June 30. It can also be noted from Figure 5 that, during days of similar climatic conditions and at nearly the same time of day, the differential temperatures and thus the upward deflections of the girders are quite similar. For the 2 comparative days illustrated, the maximum difference in elevation was $1/32$ in. at girder 6. It might be concluded from these data that, for 2 days having similar weather, temperature, and solar conditions, the elevations of the girders will be close to identical at approximately the same time of day. It is apparent, however, that exact girder elevations cannot be established when any degree of solar radiation is present.

During the thermal studies, temperatures on the order of 120 F were measured on the top flanges of the girders, but at middepth of the web the temperatures recorded were about the same as those on the lower flanges. It is likely that some of the heat from the top flanges is conducted down into the web but becomes insignificant before reaching the middepth level.

Although the maximum temperature differentials recorded between the upper and lower flanges in this study were on the order of 25 F, it is possible to experience differentials of a higher order of magnitude. In a study of the thermal behavior of a box section type bridge in the London area, for example, Capps ([3]) has reported extreme temperature differentials on the order of 50 F.

It is important to note that solar radiation can cause changes in the elevations of bridge girders during daytime deck placement operations. When girder elevation changes are considered relative to the initial elevations measured for calculation of forming elevations, significant deck thickness can be lost if the span is longitudinally

Figure 4. Upward midspan girder deflections due to differential temperatures between the top and bottom flanges of each girder.
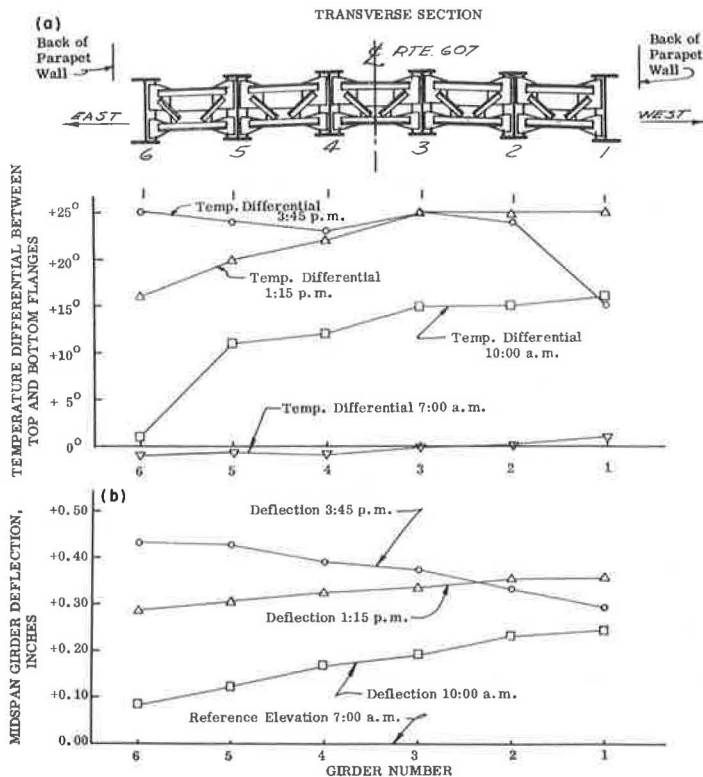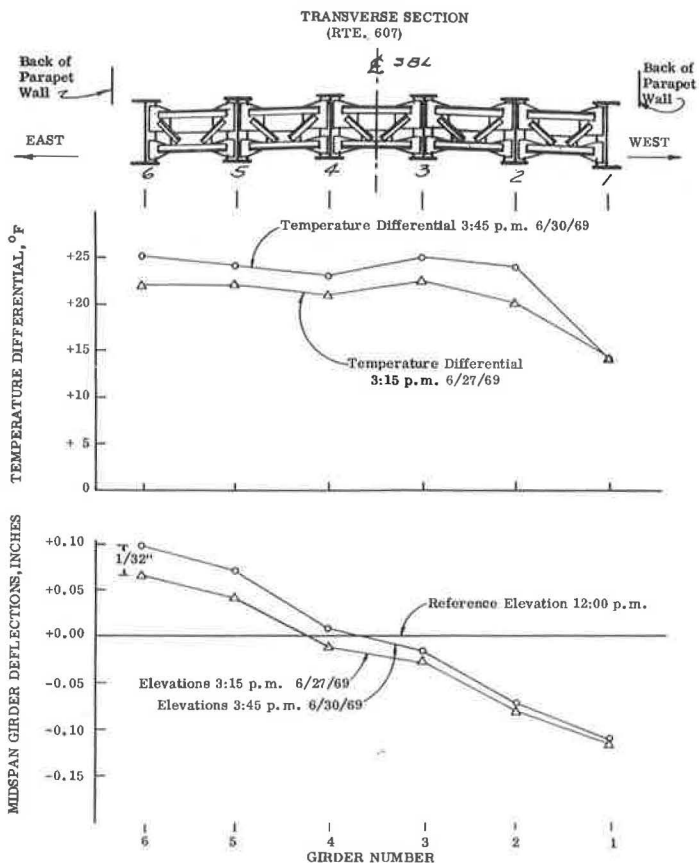

Figure 5. Midspan girder deflections and temperature differentials.

screeded (Fig. 6). If no temperature differential exists between the top and bottom flanges of a simply supported bridge girder, it is in a thermally neutral position (Fig. 6a). Under conditions of solar radiation, differential temperatures will generate an expansive force, F, in the upper flange, which is resisted by an opposing force in the lower flange to create a bending moment, M. The resulting effect is an upward deflection of the girder (Fig. 6b). If the deck forms are established to grades complying with the neutral position of the girder (but the concrete deck is screeded to grade under differential thermal conditions), the thickness of the deck will be decreased by an amount Δ (Fig. 6c).

The effects of solar radiation can be minimized by doing the following: Deck forming elevations should be established when the thermal conditions on the girders will approximate those anticipated at the time of concrete placement; and/or the deck forms should be adjusted vertically at a time when the thermal condition of the girders will approximate the condition expected to prevail at the time the concrete is screeded to grade. The latter precaution is important because the in-place forming will shield the lower portion of the girders from solar radiation and thus cause high differential temperatures on hot, sunny days. Solar thermal effects can be virtually negated, of course, by very early or very late deck placement operations.

In addition to solar radiation, other general factors such as the temperatures of the plastic concrete and the ambient air can cause thermal differentials during deck placement. Typical data showing the net effect of all these factors are discussed later.

Plan Girder Deflections

Deflections given on the bridge plans for simply supported spans are usually calculated by assuming each girder to be free to deflect as an individual unit. Thus, plan dead-load deflections are calculated by assuming that each interior girder, for example, will carry an equal portion of the concrete deck. By using this method, we found that the midspan deflections for the Route 607 interior girders were equal to 1.0 in. The plans, however, gave the value as $1\frac{5}{8}$ in., or 0.63 in. too high. Had the plan value been used, the forms would have been set too high; and with the longitudinal screeding the deck thickness would have been deficient by 0.63 in. (assuming that the correct conventionally calculated deflection represents the true situation and that all thermal factors are neglected). However, an inadequate deck thickness had resulted earlier on another bridge deck, and the contractor had made adjustments in the forming elevations to avert a similar occurrence on the test spans.

Plan deflection errors on the high side, as other studies (2) have shown, are a major cause of inadequate deck thickness when longitudinal screeding is used and would have caused a deficient deck on the study spans if adjustments had not been made during construction.

Field Versus Theoretical Girder Deflections

The field deflection measurements taken during the deck placement operation naturally incorporate the existing thermal conditions on the girders. Accordingly, the actual midspan deflections of the girders for each deck loading increment are shown in Figure 7. Additional measurements taken approximately 3 hours after completion of the deck finishing (2:55 p.m. data, Fig. 7) clearly show that continued heating of the top girder flanges results in an upward deflection of the span. Viewed as a proportion of the total dead-load deflection at 11:40 a.m., this average 18 percent "thermal uplift" demonstrates the remarkable forces generated by thermal differentials.

The general transverse pattern of the midspan girder deflections for all loading intervals shows that the structural steel framing is acting as a unit due to the diaphragm connections between the girders. Thus, the basic questions are as follows:

1. How do the actual deflections for each loading increment compare to those conventionally calculated?

2. How do the actual deflections compare with those computed by assuming rigid or semirigid connections between all the girders?

To study the latter question, we used a theoretical analysis of deflections of semirigidly connected girders. This analysis, which was developed by Lisle (4), utilizes

a modified stiffness matrix and has been programmed in Extended ALGOL 60 for solution on a Burroughs B5500 computer. The program can be used for computing deflections of bridge girder systems with any degree of end fixity at the diaphragm connections. Thus, an end fixity factor of 1 would represent a rigid connection, and 0 would represent a pinned connection. Any value between 0 and 1 would represent a semirigid connection.

In using the program, the structural framing of a span is considered as a series of segments—each segment usually terminating at a connection. The moments of inertia of each segment are calculated by using conventional procedures. The differential thermal conditions existing on the girders at each loading increment can be accounted for in the program by applying calculated moments at the girder ends (as shown in Fig. 6) and at changes in the sectional dimensions of the girders.

For the loading on the frame, the actual unit weights of the concrete were used. The total weight of the concrete was determined from the unit weights and the volumes placed in each loading increment. The total weight was proportioned to each girder according to the plan dimensions. Because much of the concrete on the span had not been screeded to grade at each loading increment, this procedure was considered to be reasonable. Thus, the programmed loading corresponded as nearly as was practical to that existing during the field deflection measurements.

Diaphragm Connection Rigidity

A thorough theoretical analysis of a wide range of end fixity factors (EFF) was made for each loading increment shown in Figure 7. In general, very little difference was found between the deflections obtained by assuming EFF's ranging from 0.10 to 1.0. An EFF of 0.20, however, appeared to match the actual deflection patterns the closest. Consequently, the theoretical comparisons presented in this paper are based on semirigid diaphragm connections having an EFF of 0.20. For most practical purposes, this could be assumed to be virtually a rigid connection.

Actual and Theoretical Deflection Comparisons

Figures 8 through 11 compare the actual and the computed midspan deflections for each loading increment. The computed deflection values are shown both excluding and including the superimposed differential thermal conditions on the girders. The conventional deflections are based on a unit weight of 150 lb/ft^3 for concrete, which is commonly used for calculating plan deflections. The following observations are made from the data presented in the figures for several of the loading conditions.

1. In general, the deflections by the frame analysis including thermal conditions are in very good agreement with the field deflections.

2. The frame analysis excluding thermal conditions shows that the girder deflections would be considerably greater if differential thermal conditions did not exist.

3. Both the field and the frame analysis results were markedly different from the conventionally calculated deflections.

4. With reference to girder 2 during the third loading increment (Fig. 8), it can be observed that the concrete placement was 2 to 2½ bays ahead of the final pass of the screeding machine over girder 2. (A bay is defined as the distance between adjacent girders.) Excluding thermal effects, the frame analysis deflection value is very nearly equal to the conventional deflection. With reference to the same point on Figure 9, which would constitute a 3- to 3½-bay lead, the deflection value for girder 2 is almost identical to that observed under the loading condition shown in Figure 8. Thus, the greater is the lag of the final screeding pass, the greater is the chance of the actual deflections being the same as the conventional plan deflections and the less the chance of the deck thickness being inadequate. For the span in question, a final screeding pass lag of 3 bays behind concrete placement appears to be ideal when conventionally calculated deflections are used for establishing forming elevations.

5. General observations from the data presented indicate that the final screeding pass over the concrete averages a 2- to 3-bay lag behind concrete placement. Quite often, however, only a 2-bay lag was noted over some areas.

Figure 6. Possible effects of solar radiation on bridge deck thickness when longitudinal screeding is used.
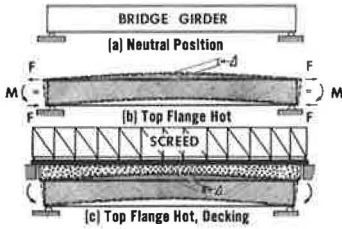
Figure 7. Midspan girder deflections due to concrete deck placement (Route 607, span 3).

Figure 8. A comparison of actual field midspan deflections with computed deflections (loading interval 3, 9:15 a.m., Route 607, span 3).

64

Figure 9. A comparison of actual field midspan deflections with computed deflections (loading interval 4, 9:45 a.m., Route 607, span 3).
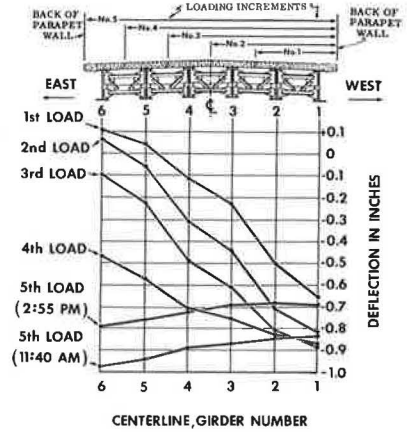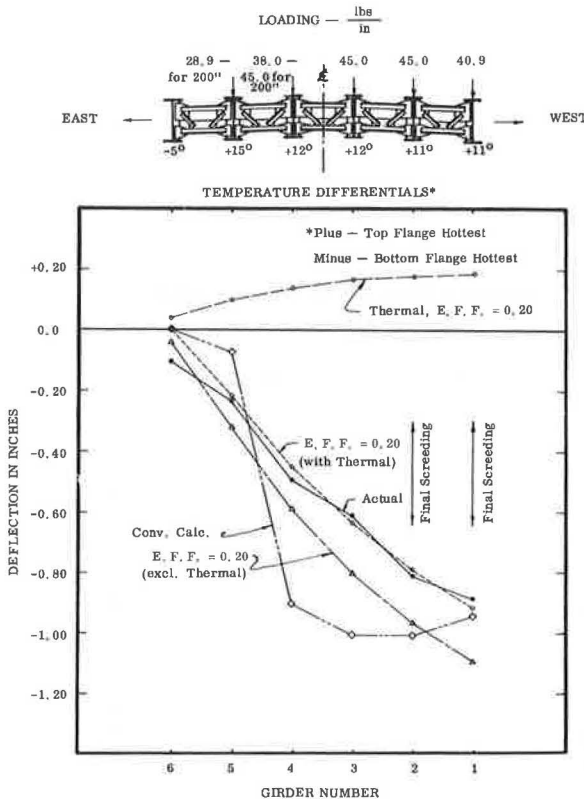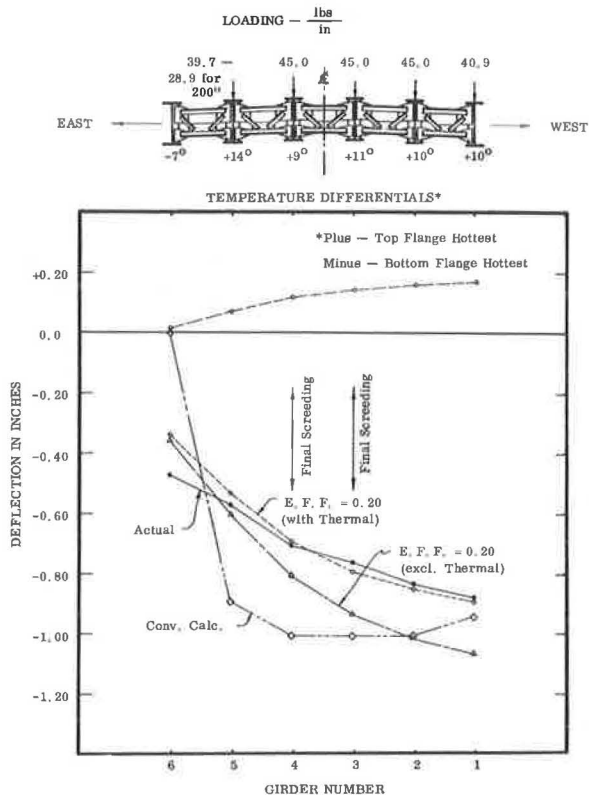

Figure 10. A comparison of actual field midspan deflections with computed deflections (loading interval 5, 2:50 p.m., Route 607, span 3).
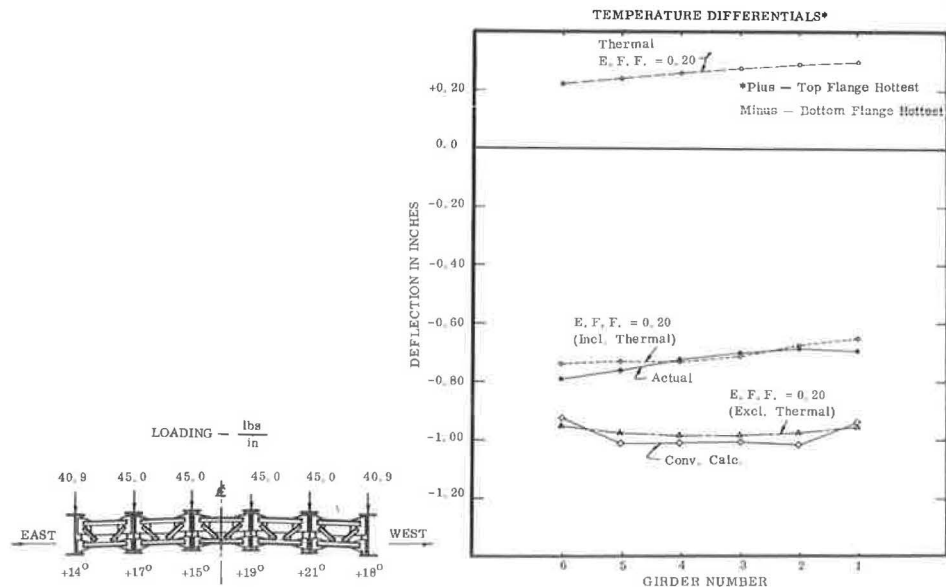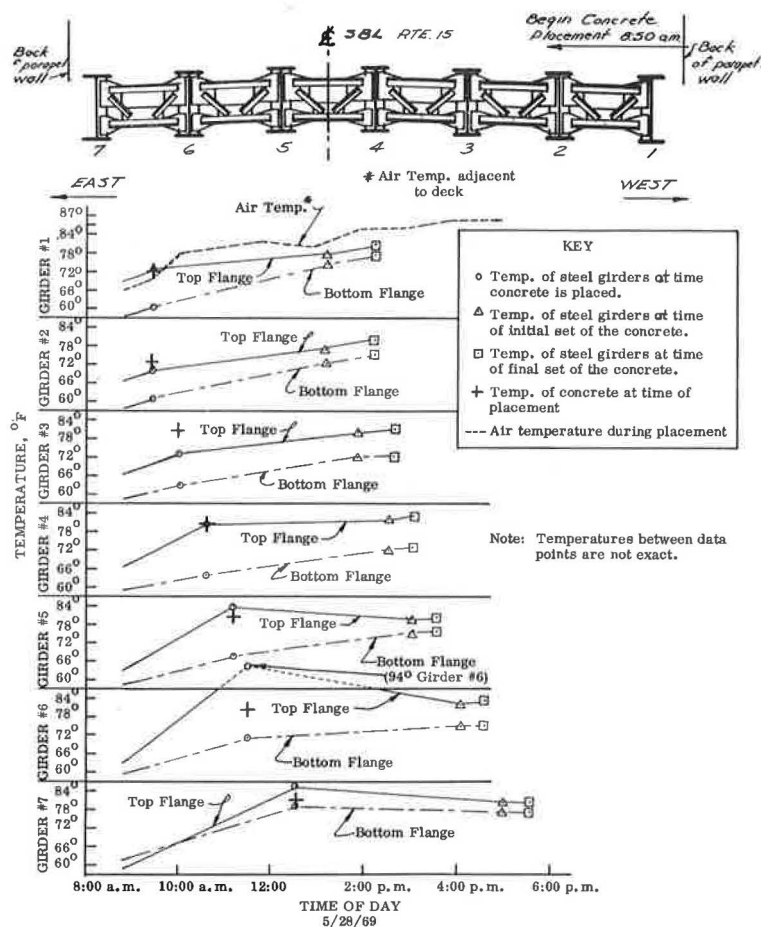
Figure 11. Temperature conditions during bridge deck placement (Route 15, span 4).

6. In one instance, the final pass of the screed was made with only a 1-bay lag. The difference between the field and conventional deflections at the final pass over girder 4 is 0.30 in. (Fig. 9). The deck thickness could possibly have been deficient by 0.30 in. in that vicinity if the forms had been set utilizing conventional deflections and if the initial girder elevations (taken for bolster calculations) had been measured when the girders were in a thermally neutral condition.

7. If we consider a hypothetical situation that would include the same conditions listed in the preceding situation, an average 0.40-in. deficient deck thickness could occur between girders 3 and 4 during the third loading increment (Fig. 8) if only a 1-bay lag were used in screeding the deck to grade.

8. The thermal uplift of the span, which occurred in a 3-hour period subsequent to completion of the deck finishing, was verified by the frame analysis results, which check very closely with the field deflections at that time (Fig. 10). The final midspan deflection of the span as calculated from the frame analysis is in excellent agreement with the conventionally calculated deflection (Fig. 10).

Bearing Pad Deflections

The results of measurements made at the neoprene expansion bearing pads during placement of the concrete on the Route 607 span indicated only slight vertical movements. The greatest pad deflection, 0.035 in., occurred under the first girder loaded with the plastic concrete. In general, the first pads that were loaded compressed the most, and the last several pads that were loaded compressed to a lesser degree. The average pad compression, which was on the order of 0.02 in., would have an additive but insignificant effect on deck thickness and does not warrant consideration in design or field calculations.

Measurements taken at a steel bearing assembly on the fixed end of the span indicated very slight vertical movements. The maximum compression measured was 0.01 in.—considerably less than the average at the neoprene bearings.

ROUTE 15 SPAN RESULTS

The results of the field measurements and data analysis on the Route 15 span were much the same as those presented for the Route 607 span. Because the latter results have been discussed in considerable detail, treatment of the Route 15 data will be confined to observations of the thermal conditions during deck placement.

Thermal data taken during placement of the Route 15 span are shown in Figure 11, and the following observations are presented.

1. The data clearly indicate that temperature differentials exist on the steel girders during summer daytime deck placement operations.

2. The temperature on the top flanges of the girders increased rapidly because of solar radiation until the concrete was placed over them.

3. After the concrete had been placed, the average rate of rise of the temperature on the top flanges was usually less than that of the ambient air temperature. On girders 5, 6, and 7, where the concrete was placed after 10:30 a.m., a net cooling of the top flanges prior to final set (4,000-psi penetration resistance) resulted.

4. The general rate of temperature rise on the bottom flanges was slightly less than the average rate of increase in the ambient air temperature (with the exception of girder 6 on the east side, which was exposed to morning solar radiation). The temperature on the bottom flanges of the girders was always less than the ambient air temperature adjacent to the deck.

Although the heat of hydration of the concrete prior to final set may have had some effect on the increased temperature of the top flanges of girders 1, 2, and 3, the evidence suggests that solar radiation, increasing ambient air temperature, and initial temperature of the plastic concrete were responsible for the increase.

DISCUSSION OF RESULTS

Although there was usually a reasonable lag between concrete placement and the final longitudinal screeding pass over a given area, occasionally there was only a 1-

or 2-bay lag. There would appear to be a need to compensate for such instances when conventional plan deflections are used to establish forming elevations. If one considers the hypothetical situation discussed in the Route 607 results, a 40 percent reduction in the plan girder deflections would have been needed to avert a 0.40-in. deficient deck thickness. On the other hand, if deck forming elevations were established to minimize the potential thermal differentials, only a 26 percent reduction in conventional plan deflections would be needed. Clearly, a routine reduction in conventional plan deflection values of at least 25 percent appears warranted where a sufficient lag between concrete placement and screeding cannot be ensured.

The results indicated that the bolted diaphragm connections act in a semirigid fashion on the 2 spans tested, but for most practical calculations they could be assumed to be rigid. Use of conventionally calculated dead-load deflections appears to be adequate as long as final longitudinal screeding follows concrete placement by approximately 3-bay lengths. This result, however, must be qualified to structures similar to those tested. Bridges on heavy skews, for example, would represent a different situation, and the use of conventional plan dead-load deflection values and longitudinal screeding could be quite risky.

CONCLUSIONS

The following conclusions are based on the results of the field and analytical study and pertain only to bridge decks constructed by use of the full-span longitudinal concrete placement and screeding technique.

1. Differential temperatures between the top and bottom flanges of steel girders can be quite high—due to solar radiation—when the deck forms are in place. The resulting effect is an upward deflection of the girders. If bridge deck forms are established to grades complying essentially with a thermally neutral condition on the girders, but the concrete deck is screeded to grade during differential thermal conditions, a deficient deck thickness could result. Upward midspan deflections on the order of 0.40 in. due to solar radiation were measured on a 96-ft 2-in. long steel girder span.

2. It is apparent that exact steel girder elevations cannot be established when any degree of solar radiation is present. On different days having similar weather, temperature, and solar conditions, however, the elevations of the girders will be almost identical at approximately the same time of day.

3. The heat of hydration of plastic concrete prior to initial set would have an insignificant effect on girder deflections for warm-weather deck placement conditions. The evidence suggests that solar radiation, changes in air temperature, and initial temperature of the plastic concrete influence girder temperatures more than does the heat of hydration. In this respect, it should be noted that differential girder temperatures could develop during cold-weather concrete placement as well as during warm-weather placement.

4. The average compression of the neoprene bearing pads (due to the dead load of the concrete deck) was on the order of 0.02 in., which does not warrant consideration in the calculation of dead-load deflections.

5. This study and others (2) indicate that there is a tendency for plan dead-load deflections to be in error on the high side. Thus, the deck forms would be set too high, and with full-span longitudinal screeding a deficiency in deck thickness would result. Plan deflection errors are believed to be due to the inclusion of the dead weights of all superstructure components in the calculations rather than the use of concrete deck weights only.

6. The field deflection measurements show that the structural steel framing of each of the 2 spans tested acted as a unit because of the diaphragm connections between the girders.

7. A comparison of the field deflection data with a theoretical analysis of deflections of semirigidly connected girders suggests that the bolted diaphragm connections on the 2 study spans act in a semirigid fashion. It was estimated from the comparison that the connections have an end fixity factor of approximately 0.20, which in effect is not greatly different from a rigid connection with an end fixity factor of 1.0.

8. For the 2 spans tested, the conventionally calculated dead-load deflection values were found to check very close to the actual field deflections when concrete placement was $2\frac{1}{2}$ to 3 bays beyond the girder in question. Thus, if the final screeding pass had lagged behind concrete placement by at least 3 bays, the conventionally calculated dead-load deflections would have been acceptable for both study spans. This result, however, must be qualified to structures similar to the 2 study spans. Bridges with high skew angles, for example, would likely present a different situation.

9. At a point where roughly three-quarters of the deck concrete had been placed, however, there was a tendency on both study spans for the final pass of the longitudinal screeding machine to follow too closely behind concrete placement. It is concluded that the plan dead-load deflection values, after being checked to ensure correctness, should be reduced by 25 percent to compensate for such occurrences on simple-span structures.

ACKNOWLEDGMENTS

REFERENCES

1. Zuk, W. Preliminary Report on the Theoretical Investigation of Bridge Beam Distortion During Construction. Virginia Highway Research Council, Sept. 1967.
2. Hilton, M. H., Zuk, W., and McKeel, W. T., Jr. Investigation of Shy Deck Thickness on the Route 264 Bridge Over Brambleton Avenue. Virginia Highway Research. Council, Feb. 1968.
3. Capps, M. W. R. The Thermal Behavior of the Beachley Viaduct/Wye Bridge. Road Research Laboratory, Harmondsworth, England, RRL Rept. 234, 1968.
4. Lisle, F. N. Theoretical Deflections of Semirigidly Connected Bridge Girder Systems During Construction. Master's thesis, Univ. of Virginia.

PREFORMED ELASTOMERIC BRIDGE JOINT SEALERS: INTERIM GUIDE FOR DESIGN AND CONSTRUCTION OF JOINTS

George S. Kozlov, New Jersey Department of Transportation

As a result of several years of research that culminated in the construction of two experimental bridges, it now becomes possible to present engineers with procedures for the design and construction of adequately sealed bridge joints. These procedures are offered as an interim solution until research provides further evidence or improvements or both. The paper suggests armored joint construction sealed with preformed elastomeric sealers as the most advantageous solution to the problem of sealing joints in bridges.

•SINCE 1965 the New Jersey Department of Transportation has been conducting a research study dealing with preformed sealers for bridge decks. The results of this study were presented in three previous papers (1, 2, 3). In the first of these papers, it was stated that there was no adequate solution to the problem of effectively sealing joints in bridges. In all three papers, a succession of solutions was offered, which covered the design of bridge joints and preformed sealers, their application in construction, and the thermal characteristics of bridge end movements. In 1969, an experiment was undertaken in which two bridge structures were built utilizing the suggested design and construction procedures; all joints were redesigned and constructed as recommended by the research. Armored-joint construction and sawed-joint construction were used for expansion joints and fixed joints respectively. The purpose of this paper is to present engineers with procedures for the design and construction of adequately sealed joints, based on the findings of New Jersey's previous subject research and the results of this experiment.

SUMMARY OF SUPPORTING RESEARCH

For a period of several years, continual field observations were made of 17 bridge structures scattered throughout the state of New Jersey. Based on the trends revealed by these observations, an analysis was made of current and proposed joint construction and sealing methods and practices, including those of other states and countries. The findings indicated that current sealing systems are malfunctioning primarily because of inadequate construction practices. Nevertheless, it appeared that one particular system, preformed elastomeric sealers, could be made to function properly, provided that the sealer material and bridge behavior were understood; new design and construction methods were offered (1).

Supported by up-to-date knowledge of sealer material, tentative qualification and identification specifications were developed. These specifications, being realistic and closely related to field application, are now furnishing producers and users with practical ways to develop and/or identify a reasonably adequate product (2).

Because field observations led to the conclusions that the bridge deck end movements could, to a great degree, be identified as thermal in character, an attempt was made to summarize the reliable theoretical background of the thermal characteristics of a concrete bridge deck (3).

The information gained in the investigation of elastomeric sealers and joint movements eventually led to the development of new procedures for bridge joint design and construction. Finally, two experimental bridges were constructed to test the new procedures.

To ensure the correlation between the sealer specification and its functional application and between the temperature and bridge end movements, we initiated an ongoing research program.

TEST INSTALLATION

The subject experiment was developed and executed by utilizing as a base the techniques outlined in the first two papers (1, 2). The specific procedures used are summarized in Appendixes A, B, and C. The appendixes describe the selection of the sealer, the construction procedures of an armored joint, and the design of the joint armor. The sawed-joint procedure is omitted because it proved ineffectual. As part of the experiment, the sealer material was evaluated in accordance with latest New Jersey Department of Transportation preformed sealer specifications (2).

As is frequently the case, there were deviations in design and especially in execution of construction because of unforeseen circumstances. In New Jersey, the actual design and construction of joints and the installation of sealers are accomplished through consultants and contractors. With guidance from the department's research division, the consultant designed the joint armor and supplied supplemental construction drawings. Unfortunately, the drawings specified an excessive anchor spacing (18 in.).

The anchorage was supplemented by welding every available reinforcement bar to the joint's armor. However, some construction deviations also occurred, such as in the forming and sawing of joints, which could not be corrected.

The two experimental bridges have now been open to traffic for 2 years. In the spring of both years, dye tests were performed on these bridges for the purpose of detecting joint leakage.

DYE TESTS

Various colors of dye were used to locate the origin and determine the cause of leaks in bridge joint sealers. The dyes were poured at carefully selected points and were traced by observation of their destination. Generally, the tests were performed during weather conditions that would be most conducive to joint leakage, i.e., freezing and thawing with precipitation. Observation continued until results were ascertained. The only leak that to date has occurred in a fixed joint is attributed to a fault in construction.

CONCLUSIONS

To date, the sawed and armored joints on both bridges do not leak. The results of this experiment appear to bear out the earlier suggestions made regarding proper design and construction procedures (1, 2).

It is essential to recognize the realities of joint design and construction. In the absence of adequate quality control in construction, no material and no method of application will succeed. Joint-sealing and construction should be carried out by specialists, and adequate construction supervision should be provided. In addition, the experiment leads to the following conclusions, which reflect the current state of the art regarding joint-design and construction practices and procedures.

1. The experimental design approach initiated on the bridges has proved its merit. Briefly, basic design principles are as follows. Deck joints shall be horizontally straight from outer edge to outer edge, and the sidewalk joints shall be directly above them in the same straight fashion; main sealers are placed out to out. Sidewalk sealers are also placed out to out, i.e., bottom of curb to outside, with only one vertical shallow bend (60 deg) at the curb (Appendix B, Figs. 3 and 5 through 7).

2. The sawed joints are functioning because they are fixed joints; i.e., they do not incur the degree of movement of an expansion joint. Also, they have the advantage of being designed in accordance with the specialized procedures shown in Appendix A.

The results of poor sawed-joint construction could have been improved if the sealer in a few of the experimental joints had been replaced. Replacement of sealers is ill-advised unless it is performed with great care; it is expensive, and also inconveniences motorists. For these reasons, no sealers were replaced in this experiment. If the sealers in fixed joints (sawed) are replaced, as they should have been in at least one bridge, care should be taken not to jeopardize the functional efficiency of the replacement sealers. Because the joints were sawed improperly, they would first need to be resawed and then thoroughly cleaned and/or adequately repaired and prepared. Immediately thereafter, a proper-size continuous sealer should be installed in accordance with the originally established procedures. Prior to installation, sealers must be tested and approved by the department's bureau of quality control laboratory. Continual and adequate supervision is most essential. Of course, the best way to replace sealers is to utilize the armored type of joint construction and the recommended procedures.

3. The armored type of joint design appears to be the most advantageous of existing solutions to the joint design problem.

RECOMMENDATIONS

The experimental construction discussed here refers to only two bridges, each having only one simple span; yet far-reaching conclusions and broad recommendations have been made in this paper because the experimental installations represent several years of research effort in this field. The following recommendations are offered as an interim solution until more scientific information becomes available.

1. Adoption of the bridge joint design approach as outlined elsewhere (1, 2) and summarized in Appendix A is advised. In both experimental bridges, design and development of joints was fashioned in accordance with suggestions made in the previous papers (1, 2, 3).

2. Also suggested is the adoption of the design and construction procedures for joint armor as given in Appendixes B and C. Further discussion of armored-joint design and development can be found elsewhere (4, 6). Holland's discussion (6) has been clarified by Deuce. The essence of this clarification is as follows: (a) ... soundly constructed joints designed in accordance with the instructions given in Clause 7e should be satisfactory; (b) ... it was not intended to limit the application of the rules from applying to the turned down angle type of armoring; and (c) ... the vertical loading is taken directly from BS 153 (7) and has not so far been substantiated by actual loading measurements on joints. The horizontal loading was recommended as a result of the survey of expansion joints. In the United States there seems to be no specification available that is directly involved in the design of armored joints. For this reason, as an interim measure I have, adopted the use of existing related AASHO specifications (8) as shown in Appendix C.

3. For bridges with spans larger than those given in Tables 1 and 2 in Appendix A, the experimental installation of a "modular sealing system" advocated by Watson (5) should be attempted. The design approach for the modular system is similar to Watson's method.

4. Although various types of armored joints are given, their design is often questionable from structural as well as functional points of view. There are basically two problems that may lead to overdesign or the structural failure of armored joints. The first problem is that of determining accurate load distribution factors and dynamic load and impact factors. The second problem is in the actual stress analysis of the structurally indeterminate armored joint. More research is needed to solve these problems.

5. The sealer selection should be guided by the realization of the fact that there are two completely different types of preformed sealers. One is a compression sealer identified by its ability to produce considerable pressure when compressed. The other type could be called a compression-extension sealer and is currently identified as being very pliable and exerting little pressure when compressed but capable of accommodating some elongation if properly installed. The preformed compression sealer, which already has proved itself in widespread application, is the one discussed here. The compression-extension sealer should be researched separately because the prerequisites for its use

are the positive means of its adhesion to the joint's sides. With the advent of prefabricated joint armament systems, this type of sealer could be used.

ACKNOWLEDGMENT

The author is grateful to the personnel of the New Jersey Department of Transportation for their assistance in gathering and evaluating the data presented in this paper.

REFERENCES

1. Kozlov, G. S. Preformed Elastomeric Bridge Joint Sealers. Highway Research Record 200, 1967, pp. 36-52.
2. Kozlov, G. S. Preformed Elastomeric Bridge Joint Sealers: Evaluation of the Material. Highway Research Record 287, 1969, pp. 50-75.
3. Kozlov, G. S. Preformed Elastomeric Bridge Joint Sealers: Thermal Characteristics of Bridge End Movements. Highway Research Record 302, 1970, pp. 38-48.
4. Koester, W. Expansion Joints in Bridges and Concrete Roads. C. van Amerongen, Translator, Transatlantic Arts, Inc., New York.
5. Watson, C. S. New Developments in Joint Sealing Practice for Longer Spans. Highway Research Record 287, 1969, pp. 76-80.
6. Holland, A. D. Expansion Joints for Use in Highway Bridge Decks. Engineering Division, Ministry of Transport, England, Tech. Memorandum (Bridges) BE6.
7. British Standard 153: Part 3A: 1954. Specification for Steel Girder Bridges, Part 3A. Loads, British Standards Institution, London, England.
8. Standard Specifications for Highway Bridges. American Association of State Highway Officials, 1969, 1.2.5, 1.2.12 (C), and 1.3.2 (H).
9. Grover, L. Manual of Design for ARC Welded Steel Structures. Air Reduction, New York, New York.
10. Reinforced Concrete Design Handbook, A. C. I., Committee 317, Detroit, Michigan.

APPENDIX A

SELECTION PROCEDURE FOR SEALERS

The selection procedure described here accomplishes basically two purposes. It establishes the size of sealer to be used in a joint, and it determines at what width the joint must be constructed to ensure the effectiveness of the sealer. To utilize these procedures, one must set forth ahead of time the capabilities of the sealer in terms of three parameters: X_{max}, Y_{avg}, and Z_{min}. Each of the parameters is the ratio of the width of the sealers at a certain level of compression to its original preformed width W_n, multiplied by 100. Z_{min} is the value of the ratio at the maximum permitted compression of the sealer. Y_{avg} is the desired value of the ratio at the time of sealer installation. X_{max} is the value of the ratio at the minimum permitted compression of the sealer (enough compression to prevent leakage between sealer and joint face).

For the type of sealers currently available, it would appear that X_{max} can be no more than 80 percent, Z_{min} should be 40 to 50 percent, and therefore Y_{avg} should be approximately 60 percent.

The design essentially consists of establishing from Figure 1 the maximum expansion and contraction movements to be experienced at the joint for expected differences between installation deck temperature and subsequent deck temperatures. By using these movements and by applying the X_{max}, Y_{avg}, and Z_{min} values to an estimated sealer size, the construction width of the joint is then determined through a trial-and-error process.

As an example of the application of the data shown in Figures 1 and 2, a solution for a bridge with a span L = 60 ft is given. For New Jersey, a concrete temperature range of 0 to 100 F is assumed as being realistic. The wide range of sealer installation and

Table 1. Guide to design of sealers.

W_n (in.)	At 100 F		Δ at Δt = 70 F	At 30 to 90 F		Δ at Δt = 90 F	At 0 F		Limits of Span (ft)
	$W_{J_{min}}$	Z		W_J (in.)	Y		$W_{J_{max}}$	X	
$1\frac{1}{2}$	0.875	0.58	0.00	$\frac{7}{8}$	0.58	0.00	0.875	0.58	Up to 40
	0.695	0.46	0.18			0.24	1.115	0.74	
$1\frac{3}{4}$	0.945	0.54	0.18	$1\frac{1}{8}$	0.64	0.24	1.365	0.78	40 to 45
	0.915	0.52	0.21			0.27	1.395	0.80	
2	1.04	0.52	0.21	$1\frac{1}{4}$	0.625	0.27	1.52	0.76	45 to 55
	1.00	0.50	0.25			0.33	1.58	0.79	
$2\frac{1}{2}$	1.25	0.50	0.25	$1\frac{1}{2}$	0.60	0.33	1.83	0.73	55 to 70
	1.18	0.47	0.32			0.42	1.92	0.77	
3	1.555	0.52	0.32	$1\frac{7}{8}$	0.625	0.42	2.295	0.765	70 to 90
	1.455	0.485	0.42			0.53	2.405	0.80	
4	2.08	0.52	0.42	$2\frac{1}{2}$	0.625	0.53	3.03	0.76	90 to 120
	1.95	0.49	0.55			0.71	3.21	0.80	
5	2.575	0.515	0.55	$3\frac{1}{8}$	0.625	0.71	3.835	0.77	120 to 150
	2.435	0.49	0.69			0.89	4.015	0.80	
6	3.06	0.51	0.69	$3\frac{3}{4}$	0.625	0.89	4.64	0.77	150 to 180
	2.92	0.49	0.83			1.07	4.82	0.80	

Note: All the temperatures given in the table are those of the concrete. Because these temperatures cannot readily be measured, the daily average temperature of the air with a tolerance of +5 to +10 F would be currently acceptable.

Temperature range: 0 to 100 F
Construction temperature: 30 to 90 F
Installation temperature: 30 to 90 F
Degrees of efficiency: $Z_{min} = \pm 0.50\ W_n$; $Y_{average} = \pm 0.60$ to $0.65\ W_n$; and $X_{max} = \pm 0.80\ W_n$.

Table 2. Sealer design guide.

W_n (in.)	At 100 F		Δ at Δt = 70 F	At 30 to 90 F		Δ at Δt = 90 F	At 0 F		Limits of Span (ft)
	$W_{J_{min}}$	Z		W_J (in.)	Y		$W_{J_{max}}$	X	
$1\frac{1}{2}$	0.875	0.58	0.0	$\frac{7}{8}$	0.58	0.0	0.875	0.58	Up to 55
	0.621	0.41	0.254			0.327	1.202	0.80	
$1\frac{3}{4}$	0.746	0.43	0.254	1	0.57	0.327	1.327	0.75	55 to 65
	0.700	0.40	0.300			0.386	1.386	0.79	
2	0.825	0.41	0.300	$1\frac{1}{8}$	0.56	0.386	1.511	0.76	65 to 75
	0.778	0.39	0.347			0.446	1.571	0.79	
$2\frac{1}{2}$	1.153	0.46	0.347	$1\frac{1}{2}$	0.60	0.446	1.946	0.78	75 to 90
	1.084	0.43	0.416			0.535	2.035	0.81	
3	1.334	0.44	0.416	$1\frac{3}{4}$	0.58	0.535	2.285	0.76	90 to 110
	1.242	0.41	0.508			0.653	2.403	0.80	
4	1.867	0.47	0.508	$2\frac{3}{8}$	0.59	0.653	3.028	0.75	110 to 150
	1.682	0.42	0.693			0.891	3.266	0.81	
5	2.182	0.44	0.693	$2\frac{7}{8}$	0.57	0.891	3.766	0.75	150 to 200
	1.951	0.39	0.924			1.188	4.063	0.81	
6	2.576	0.42	0.924	$3\frac{1}{2}$	0.58	1.188	4.688	0.78	200 to 220
	2.484	0.41	1.016			1.307	4.807	0.80	

Note: All the temperatures given in the table are those of the concrete. Because these temperatures cannot readily be measured, the daily average temperature of the air with a tolerance of +5 to +10 F would be currently acceptable.

Temperature range: 0 to 100 F
Construction temperature: 30 to 90 F
Installation temperature: 30 to 90 F
Degrees of efficiency: $Z_{min} = 0.40\ W_n \pm$; $Y_{average} = 0.60\ W_n \pm$; and $X_{max} = 0.80\ W_n \pm$.

74

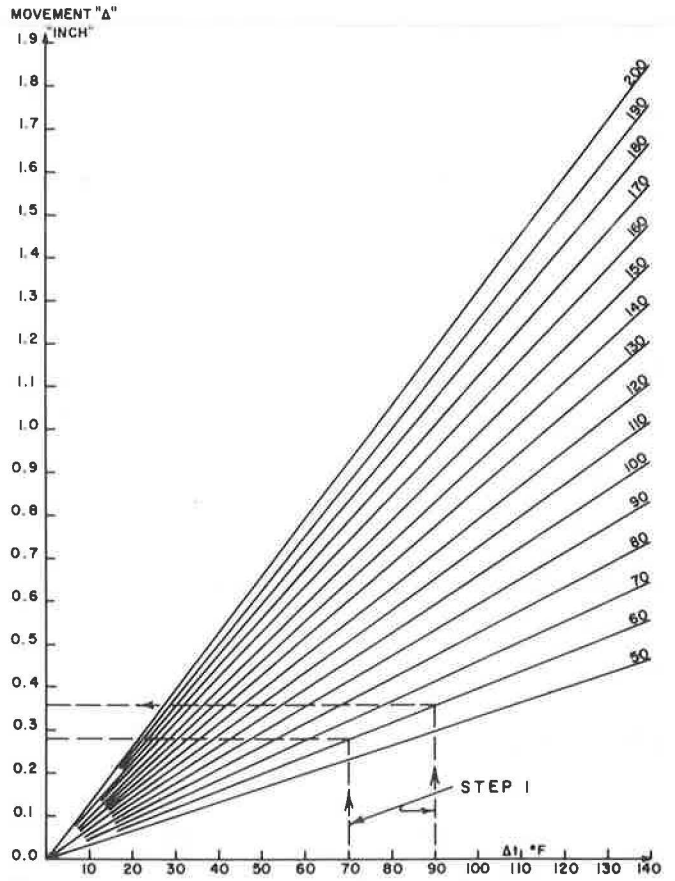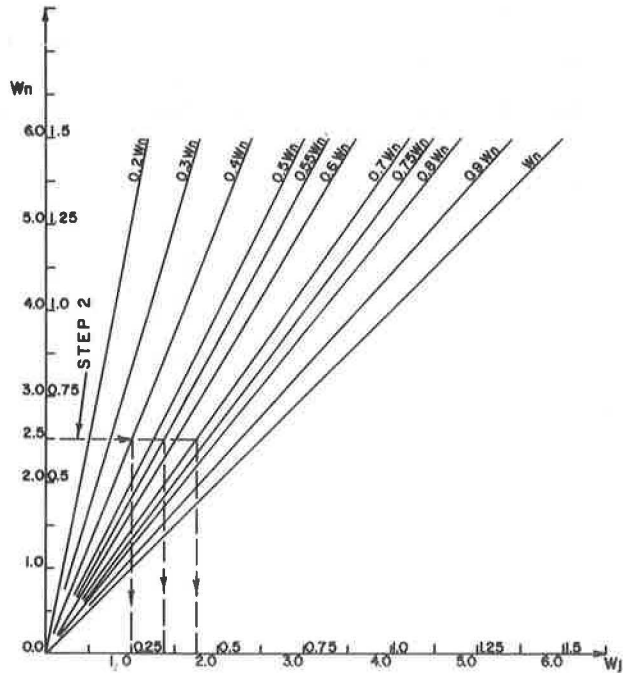Figure 1. "Δ" movement for S_L = 50 to 200 ft and t = -20 to 120 F.

Figure 2. Joint sealer efficiency chart.

construction temperatures of 30 to 90 F* is selected with required limits on efficiency coefficients taken as

Z_{min} = ± 50 percent at minimum width of joint ($W_{j_{min}}$) and 100 F,

Y_{avg} = ± 60 percent at installation width of joint ($W_{j_{inst}}$) and installation temperature from 30 to 90 F, and

X_{max} = ± 80 percent at maximum width of joint ($W_{j_{max}}$) and 0 F.

Step 1: From Figure 1, using maximum temperature differences between maximum and minimum concrete and installation temperature ranges of Δt = 70 F (100 - 30 F) and 90 F (90 - 0 F), we read off the bridge end movements of Δ = 0.28-in. expansion and 0.36-in. contraction.

Step 2: By estimating the sealer size W_n = 2.5 in. (Tables 1 and 2) and by using the limits Z = 0.5 W_n and X = 0.8 W_n, we find from Figure 2 that $W_{j_{min}}$ = 1.25 in. and $W_{j_{max}}$ = 2.00 in.

$(W_{j_{max}} - W_{j_{min}})/2$ = 0.75/2 = 0.375 in. > 0.36 in. (maximum joint movement).

Thus, the joint construction width should be

$$W_{j_{construction}} = 1\tfrac{1}{2} \text{ in. with } Y_{installation} = 0.60 \, W_n$$

The width of joint ($W_{j_{construction}}$) is measured at the upper portion of the joint where the sealer is located.

APPENDIX B

CONSTRUCTION PROCEDURE FOR ARMORED JOINTS

The concept of this method is that the entire system (armor plates with straps and seats welded to them and sealer properly precompressed between the plates and the supporting elements, such as clamps and attached bolts) is preassembled and then placed into the joint before the concrete is poured.

The procedure used should satisfy the design requirements and, at the same time, give the fullest possible consideration to construction practices.

On this basis, the best approach would be to have the elements of the system pre-assembled to the fullest practicable degree, delivered to the construction site, and assembled completely there. The deck should be poured so as to leave the necessary recess with deck reinforcement properly extended into it. After the concrete is set, the assembly can be placed into the recess, properly located, and the width of the joint between the armor plates adjusted in accordance with the design requirements; then the bar-straps should be welded to the main deck reinforcement. The recess should be filled to the level A (Fig. 3) with optimum-packed-up concrete of good quality. After the concrete in the recess is set, the supporting elements should be removed and the surfacing of the deck at the joint carefully completed.

This procedure, with a little care in construction, should give a satisfactorily sealed joint.

The armored deck joints should be continuous throughout the full width of the deck, and termination should be accomplished as shown in Figures 4 through 7. It is obvious that the armor is utilized for a dual purpose: to armor the joints where necessary and to form the best sealed joint possible.

The seal groove in the sidewalk should also be armored in the same manner, with the curb and outside ends installed as shown in Figures 3 through 7. A stay-in-place anchor seat could be added in the curb end at the bottom outside face of the armor shapes.

All steel of the armor network should be painted. In addition it is recommended that the armor be of ASTM A-242 steel. The stable rust characteristics of this mate-

Figure 3. Armored joint detail, section A-A.
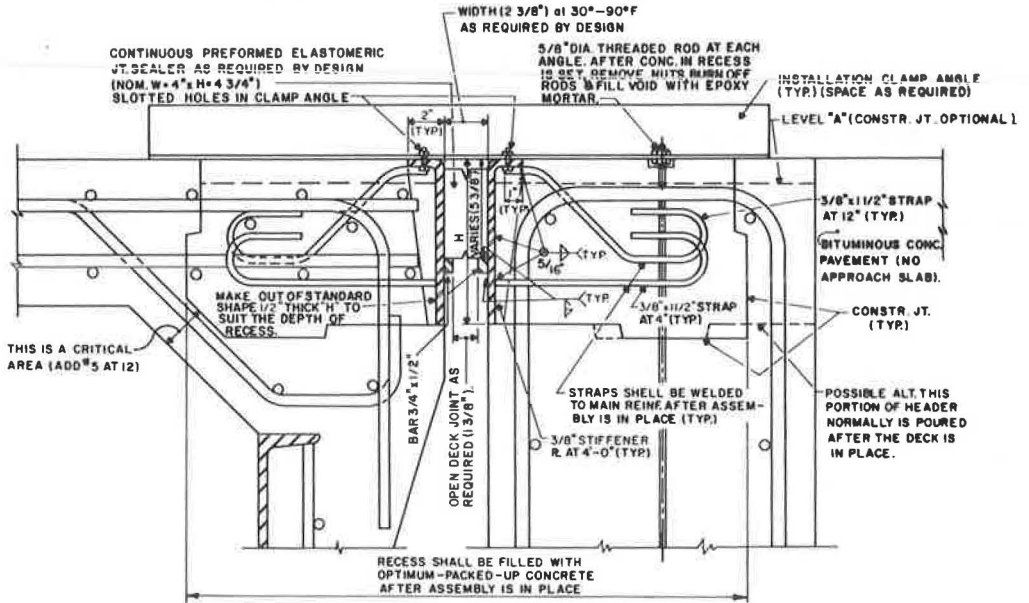
Figure 4. Proposed design of curb-sidewalk-parapet detail for bridges.
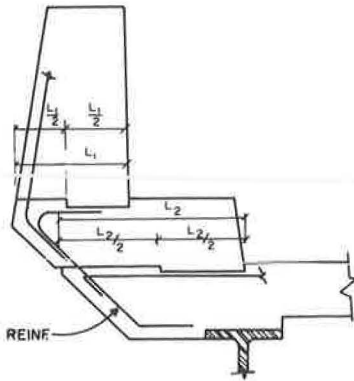
Figure 5. Typical joint detail at sidewalks and curbs.

Figure 6. Armored joint detail, safety walk and curb location.
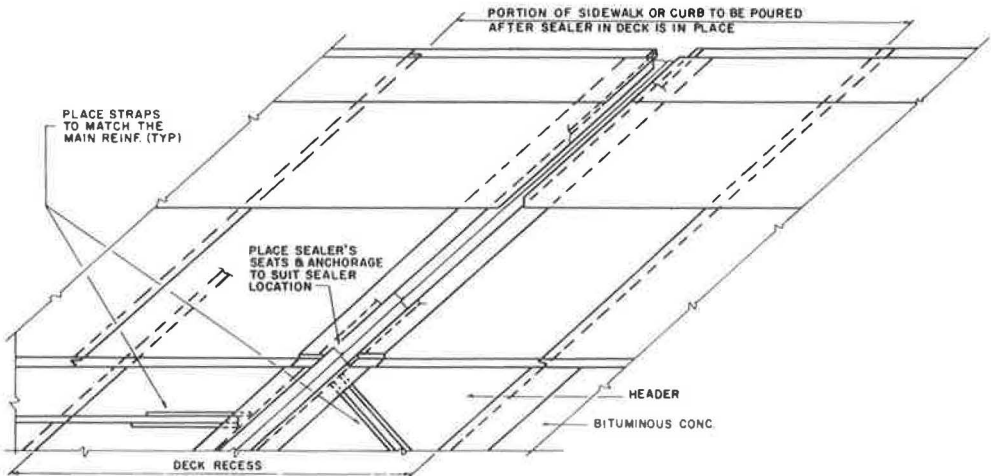
Figure 6. Armored joint detail, safety walk and curb location.

Figure 7. Armored joint detail, section B-B.
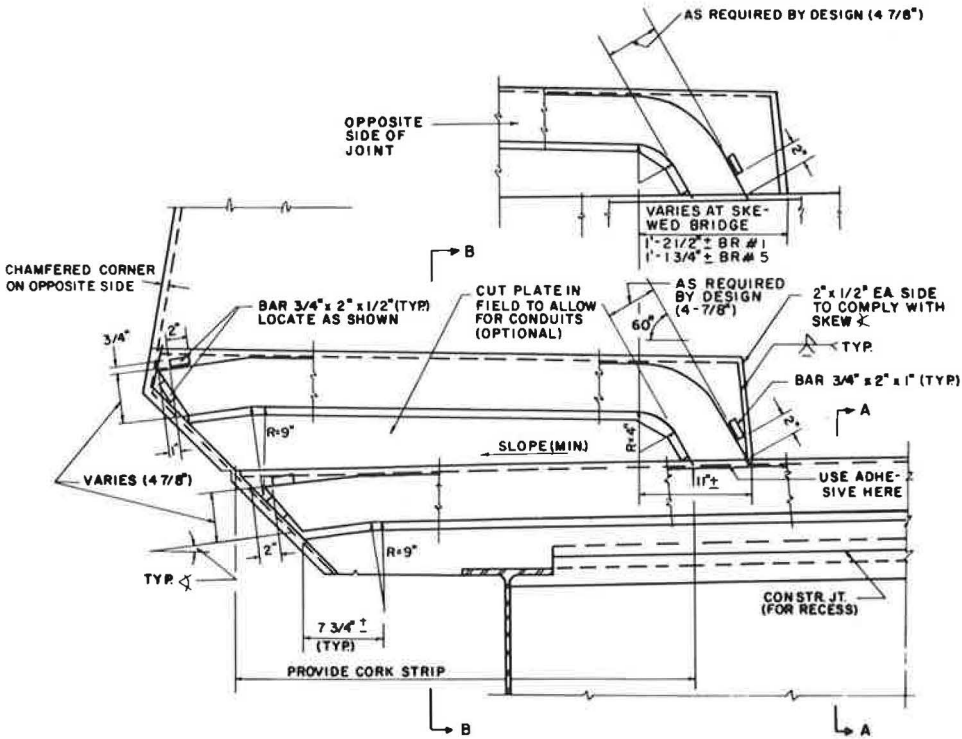
Figure 7. Armored joint detail, section B-B.
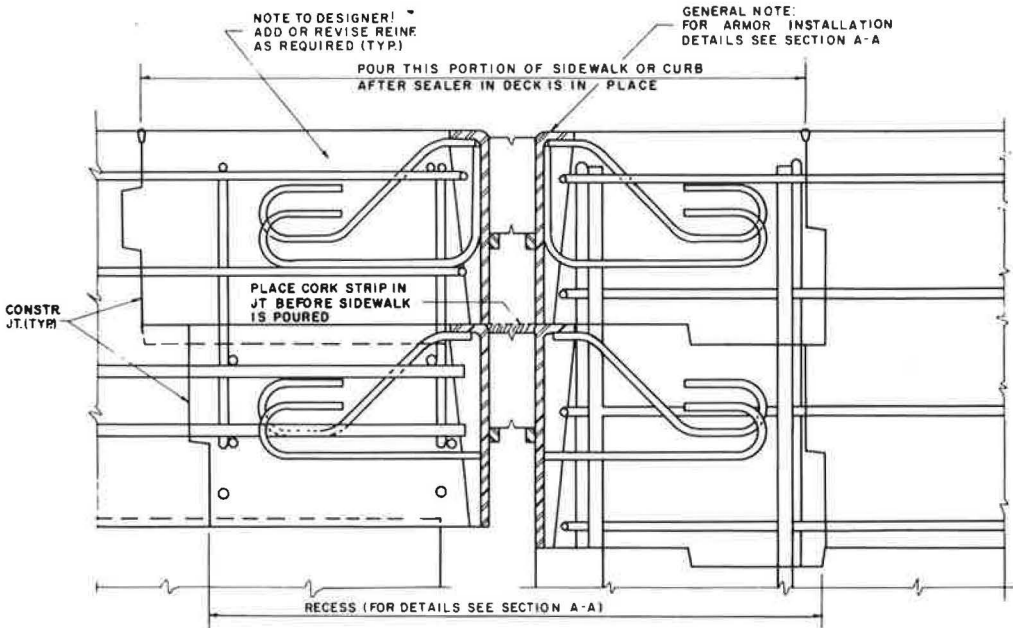
rial will serve advantageously in those areas where paint is likely to deteriorate rapidly with traffic.

Standard lubricant-adhesive shall be applied on both sides of the sealer when located in the armor.

APPENDIX C

DESIGN PROCEDURE FOR ARMORED JOINTS
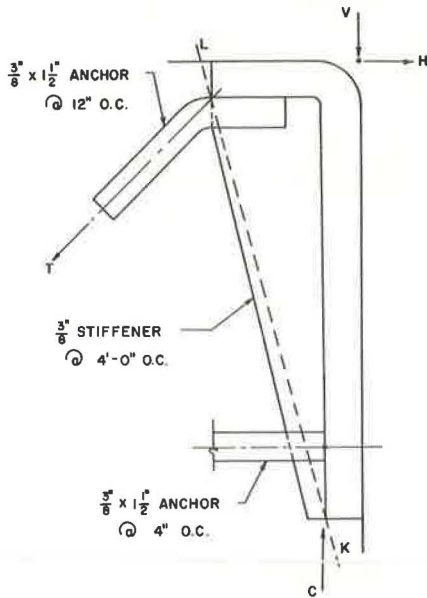
Loads

The accompanying figure is for design purposes only; assume that the concrete above line L-K gives no support to angle.

The following data are AASHO specifications (8) for HS 20-44 loading:

1. Concentrated loads (for shear), 26.0 kips;
2. Wheel load (for horizontal shear), 16.0 kips;
3. Impact fraction, 30 percent;
4. Friction factor for horizontal load, 0.75;
5. Moment per foot of cantilever slab = (P_x/E); and
6. Case B: $E = 0.35\,X + 3.2$.
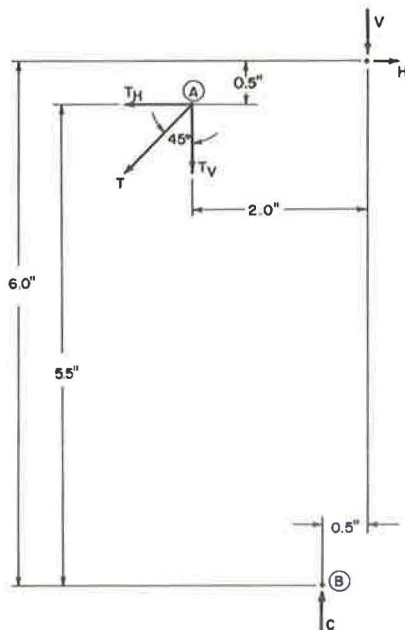
$$V = 26.0 + 0.3 \times 26.0 = 33.8 \text{ K/E}$$
$$H = 16.0 \times 0.75 = 12.0 \text{ K/E}$$

Load distribution:

$$E_1 = 0.35 \times 0.5 + 3.2 = 3.375 \text{ ft}$$
$$E_2 = 3.2 \text{ ft}$$
$$E_3 = 0.35 \times 0.17 + 3.2 = 3.26 \text{ ft}$$

In absence of definite guidelines, I am exercising my judgment in making reasonably severe assumptions. The following comment (4) is applicable.

> The severity of the forces acting on the edges of the joint increases with the gap width. This necessitates the provision of a steel edge-protection strip which must be so rigid and so closely anchored that it forms an indissoluble composite structure with the bridge deck. The prerequisite for this is that the steel components should be securely joined to the concrete at all contact surfaces.
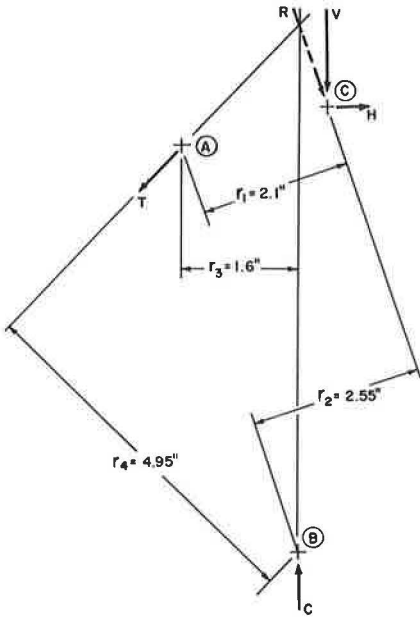
$$R = \sqrt{V^2 + H^2}$$

Moment about support A:

$$(R \times r_1) - (C \times r_3) = 0$$

$$C = (r_1/r_3) \times R = r_1/r_3 \times \sqrt{V^2 + H^2}$$

$$C = 2.1/1.6 \sqrt{(33.8/3.375)^2 + (12.0/3.20)^2}$$

$$C = 14.03 \text{ K/ft}$$

Moment about support B:

$$(R \times r_2) - (T \times r_4) = 0$$

$$T = (r_2/r_4) \times R = r_2/r_4 \sqrt{V^2 + H^2}$$

$$T = 2.55/4.95 \sqrt{(33.8/3.2)^2 + (12.0/3.26)^2}$$

$$T = 5.77 \text{ K/ft}$$

If $T = \sqrt{T_V^2 + T_H^2}$ and $T_V = T_H$ (at 45 deg), then $T_V = T_H = 0.707 \, T = 4.08 \text{ K/ft}$

Welding Stresses (9)

$$H_L = H_R = H = 5/12 \, f_h \, L$$

$$P_r = 0.707 \, f_{ALL} \, DL_1$$

$$(T_V - P_r) \times 17/18 \, L = H_L \times 2/3 \, L$$

Therefore,

$$f_h = 17/5 \, L \, (T_V - 0.707 \, f_{ALL} \, DL_1)$$

$$f_v = T_H/(2L + L_1)$$

$$f_r = \sqrt{f_h^2 + f_v^2}$$

Anchors at 12 in. O.C.: $T_V = 4.08_K$; $L_1 = 1.5$ in. (width of strap); $L = 1.0$ in.; $D = 5/16$ in. (size of weld); and $f_r = 0.707 \, f_{ALL} \, D$.

$$f_h = (17/5 \times 1.0) \, (4.08 - 0.331 \, f) = 13.85 - 1.13 \, f$$

$$f_v = (4.08/3.5) = 1.17$$

$$0.221 \, f = \sqrt{(13.85 - 1.13 \, f)^2 + 1.17^2}$$

$$f = 10.7 \text{ K/in.}^2 < f_{ALL}$$
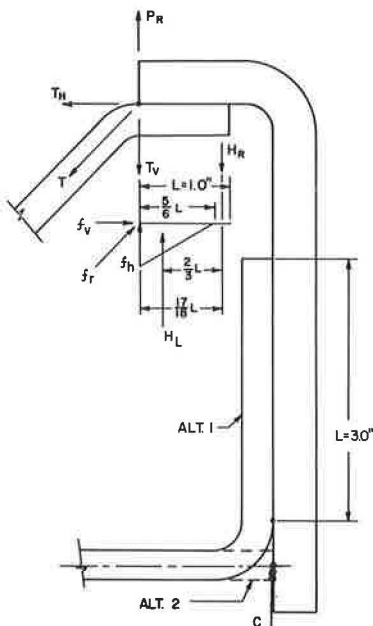
Alternate 1, anchors at 12 in. O.C.:

$$0.707 \times f \times D \times 2L = C$$
$$f = C/(1.41 \times D \times L) = 14.03/0.442L = 31.8/L$$

For $L = 3.0$ in. each side,

$$f = 31.8/3.0 = 10.6 \text{ K/in.}^2 < f_{ALL}$$

Bearing: Available $L = 9.0$ in. Assuming triangular bearing distribution, bearing stress shall be

$$f_{BEAR} = C/A = C/(1.5 \times L/2) = 2C/1.5L = (2 \times 14.03)/(1.5L) = 18.73/L$$
$$f_{BEAR} = 18.73/9.0 = 2.08 \text{ K/in.}^2 > f_{ALL}$$

Alternate 2, n anchors (welding stresses):

$$0.707\ f \times D \times 2(a+b) \times n = C$$
$$f = C/(0.707 \times D \times 3.75 \times n) = (14.03)/(0.83 \times n) = 16.95/n$$

For $n = 2$ or at 6 in. O. C.,

$$f = 16.95/2 = 8.5 \text{ K/in.}^2 < f_{ALL}$$

Shear stresses:

$$f_{SH} = C/(A \times n) = (14.03)/(0.375 \times 1.5 \times n) = 25.0/n$$

For $n = 2$,

$$f_{SH} = 25.0/2 = 12.5 \text{ K/in.}^2 < f_{ALL}$$

Bearing (alternate 2): Available $L = 10.5$ in.

$$f_{BEAR} = C/(1.5 \times L/2 \times n) = (2 \times C)/(1.5 \times L \times n) = (2 \times 14.03)/(1.5 \times 10.5 \times n) = 1.78/n$$

For $n = 3$ or at 4 in. O.C.,

$$f_{BEAR} = 1.78/3 = 0.593 \text{ K/in.}^2 < f_{ALL}$$

Therefore, use bottom anchors at 4 in. O. C.

Tension stresses in top anchors:

$$f_T = T/A = (5.77)/(0.375 \times 1.5) = 10.28 \text{ K/in.}^2 < f_{ALL}$$

Bond stresses: Assuming that hook shall develop 50 percent of the allowable stress in the strap, the bond stress shall be

$$f_{BOND} = T/[2(a + b) \, L \times 2] = (5.77)/(7.5 \times L) = 0.77/L$$

For L = 7 in.,

$$f_{BOND} = 0.77/7.0 = 0.11 \text{ K/in.}^2 < f_{ALL}$$

Headers

Failure of headers is not uncommon and has been observed personally by the researcher. It is believed that causes for their failure are as follows:

1. Loading, such as indicated in armor design;
2. Inadequate preparation of the backfill; and
3. Concrete approach slabs directly supported by headers.

For the second problem, only one remedy can be suggested—improvement of quality control in construction.

Design

The following are AASHO design specifications:

1. Concentrated loads, 26.0 kips;
2. Wheel loads for horizontal shear, 16.0 kips;
3. Impact fraction, 30 percent; and
4. Friction factor for tire against concrete, 1.0.
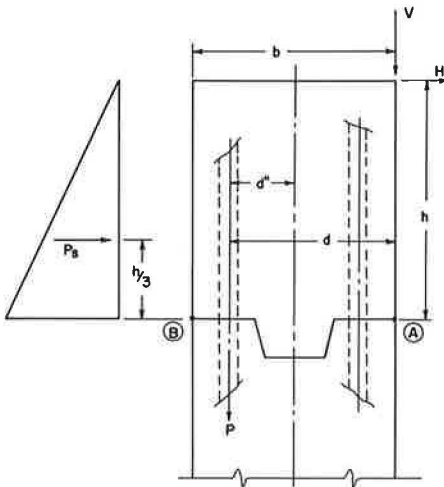
Cantilever slabs: Moment per foot of slab = P/E X, where E = (0.35 X) + (3.2). Thus, V = 33.8 K/E and H = 16.0 × 1.0 = 16.0 K/E.

Load distribution:

$$E = 0.35 \times 1.5 + 3.2 = 3.725 \text{ ft}$$

Moment about plane A-B:

$$M = (33.8)/(3.725) \times (b/2) + (16.0)/(3.725) \times h + P_s \times h/3$$

Total vertical load:

$$N = (33.8)/(3.725) + 0.15 \times 1.5^2 \times 1.0$$

Reinforcement design (10):

$$e = (12 \times M)/N + d \text{ (in.)}$$

$$P = N(e - jd)/jd \text{ (K/ft width)}$$

Although the stresses in the vicinity of point A are somewhat small because of moving loads, it is suggested that the same reinforcement be used on both sides of a header.

The problem of approach slabs is complex, especially if a rigid slab is supported on one end elastically and on the other end off a vertically rigid but horizontally flimsy support such as a header.

In such a case, the vertical effect on a header would be an eccentrically located static load and a distinctly possible substantial horizontal static force as well as other dynamic reactions.

A joint that is not permitted to function as designed cannot be sealed. Even a perfect solution of the joint sealing problem will be useless if a header failure disallows proper functioning of the joint.

In the experimental bridges, approach slabs were removed, and inadequate preparation of the backfill had to be overcome.

REPORT CONCERNING OBJECTS THROWN
FROM STRUCTURES ONTO FREEWAYS
IN MILWAUKEE COUNTY

Clayton A. Harley, Wisconsin Department of Transportation

ABRIDGMENT

•THIS paper presents a statistical compilation of reported occurrences of objects thrown onto freeways from structure overcrossings. All occurrences from January 1, 1967, to May 12, 1970, are categorized and analyzed with respect to location and time. A majority of occurrences took place on one relatively short section of the North-South Freeway. Most occurrences take place during after-school hours. Fencing on structures has almost, but not completely, eliminated the problem. The data can be used in making decisions to fence existing and future bridges over freeways located in similar neighborhoods or having similar pedestrian characteristics.

REPAIR OF SPALLING BRIDGE DECKS

John C. Kliethermes, Federal Highway Administration

Moisture, humidity, concrete cover, and age coupled with the increasing rate of chloride applications are causing embedded reinforcement steel to corrode and result in an alarming amount of bridge deck spalling. The spalling reduces the riding quality of the bridge and may have an effect on the structural integrity of the structure. The annual national cost associated with the repair is estimated to be approximately $40 million per year. The spalling problem is dealt with throughout the country by using various patching techniques. The permanency, i.e., time to replacement, of these patches has become critical especially in high traffic volume areas. Many patches are failing after relatively short service periods and cause numerous traffic interference problems. This paper discusses several patching techniques that will increase service life. The California Division of Highways through a highway planning and research project developed a nondestructive instrument that will detect corrosion in reinforced concrete structures. This paper also describes how this instrument may be put into operational use. Based on a bridge inventory using this equipment, a deck classification system is proposed that defines the type and extent of repairs that can be made. The classification also permits an administrative evaluation for maintenance and reconstruction scheduling.

•CONCRETE spalling and concrete delamination are generally recognized as the most serious and troublesome kinds of bridge deck deterioration. This deterioration results primarily from corrosion forces that radiate from the embedded steel. The forces normally produce cracks in the deck surface, which spall and ultimately expose the reinforcement. As a result, riding quality is impaired and structural integrity and safety may be severely reduced. It is now known that about 50 percent of the states are faced with a major deck repair or replacement program. The remaining states have not escaped the problem but are effected to a lesser degree.

In November 1971, the Federal Highway Administration (FHWA) completed its demonstration of a corrosion detection device in 46 states. As a result of the demonstration, we made some general observations and noted several trends in bridge deck repair. We have analyzed data collected during the demonstration program and found that the most serious deck spalling can be related to general geographical areas. A definite correlation was noted between salt usage and deck condition. In areas where little or no salt was used, spalling was not evident regardless of the age of the structure. Where structures had been exposed to heavy salting, deck spalling was found to be a serious maintenance problem. We also found that the method of repairing spalls varies from state to state and that numerous membranes and special deck treatments are being evaluated. It was apparent that there was considerable concern and interest in finding a way to control the effects of de-icing chemicals.

Much work has been done to analyze what happens when concrete is exposed to chemicals. Steel in concrete is protected from corrosion by the natural alkalinity of the concrete. This protection is related to the pH factor of the concrete, which is usually between 12 and 13. When sufficient amounts of chlorides are absorbed by the

concrete, the pH factor will eventually decrease until the concrete can no longer protect the steel. If moisture, oxygen, and chlorides (in sufficient quantities) are present at the level of the steel, corrosion will take place. The result is that as the metal corrodes it will expand and exert an outward force of approximately 4,000 psi, which causes delamination and spalling of concrete.

The corrosion of reinforcing steel is the result of an electrochemical process whereby corrosion cells are created by variable amounts of chloride, oxygen, and moisture along the length of the reinforcement. These cells produce a flow of electric current between two half-cells, the anode and the cathode. The corrosion cells may be minute with the anode and cathode microscopically spaced, such as seen when steel corrodes in air, or they may be spaced several feet, as frequently found in bridge decks. The steel corrosion detection device used in the FHWA demonstrations and developed by the California Division of Highways identified the location of the anode areas by measuring the potential difference between the reinforcement and a reference half-cell. The California laboratory work consisted of placing 200 concrete specimens in a salt solution and recording the voltage change as it occurred with time. From this experiment it was determined that the steel was in a passive stage and not likely to corrode as long as the voltage remained below a 0.3-V level. When the voltage was increased to a level above 0.3 V, the pH factor had been sufficiently reduced to where the reinforcement was no longer protected. This voltage level is considered active, and with proper conditions the corrosion cell will form.

It is of major significance that salt usage has increased approximately 400 percent in the past 5 years. It is anticipated that this trend will continue but at a diminishing rate. Those states that now use little or no salt, where icing or frosting occurs, are beginning to feel public pressures for a bare-pavement policy.

The time to deck deterioration can reasonably be correlated with the increased salt usage and the age of the structure. To date, we have found that, if de-icing salts are extensively used, some structures will spall in 4 to 6 years. Some severe spalling was observed on 8-year old structures. This spalling, however, was generally observed on decks with an early exposure to salt. Many structures in the 20- to 30-year category, which were not exposed to salt until several years after construction, were also observed as showing some deterioration but to a lesser degree.

With a high degree of confidence, it can now be said that most spalling results from the expansive forces associated with corrosion. It can also be said that the predominate cause of corrosion is the salt that is absorbed by the concrete. A cooperative study by the Portland Cement Association and several states identified some of these factors. The study concluded that the percentage of chloride ions in concrete varies with depth, and the deck condition can be related to the percentage of chloride ions at the level of reinforcement. Our work during the past 2 years supports their conclusions. One factor, however, has not been clearly documented: the extent and scope of the problem. In conjunction with our demonstrations we attempted to define the geographical areas that are affected and the cost that is involved. We reviewed research and maintenance reports, corresponded with various state highway departments, and made a geographical spot check to determine the current cost of deck repairs. From this exercise, several things become apparent.

1. Annual maintenance costs do not adequately indicate the scope of the problem. Most states that have a severe problem would spend more if funds were available.

2. Some states have areas of severe deterioration and areas of light or no deterioration. This complicates any attempt to show general affected locations.

3. The scope is changing rapidly. Many states indicate that both the cost and the number of bridges requiring maintenance are increasing.

After evaluating all conditions, we arrived at the following conclusions. The severe, moderate, and light problem locations fall into geographical areas (Fig. 1). There is, of course, no distinct division line, and some overlapping will occur. Based on spot checks within these areas, it was estimated that the national cost of repair for decks in 1971 was more than $40 million.

The challenge of what can be done to keep this cost at a minimum falls into two categories:

1. Establish an effective and permanent repair procedure for existing decks, and
2. Develop a technique that will prevent the problem from reoccurring by a change in new designs.

Extensive research is under way in both areas. This research includes the use of polymers in concrete, protective coatings for reinforcement, and cathodic protection. Many states use or are now considering the use of protective membrane treatments for both new and existing decks. We are, however, finding that the effectiveness of these waterproofing systems over concrete that has been contaminated with chlorides is highly speculative. We are especially concerned with overlays that are porous and that trap chlorides between the overlay and the deck. It is the opinion of many researchers that, once the corrosion cell has started, it will continue, and no corrective treatment, short of total removal, will be totally effective. They further contend that the membrane may provide additional service life, but it should not be considered a totally effective technique.

This paper is devoted primarily to what can be done on existing decks. I will offer some suggested techniques for patching spalled areas and also recommend a deck evaluation program by summarizing data collected with the corrosion detection device.

An informal survey conducted with the demonstrations indicated that a large variety of methods and techniques are being used to patch deteriorating decks. However, we have little confidence in any one method, and, without complete surface or total deck removal, no effective permanent repair method was found.

We found that many patching methods and/or patch materials do not protect the steel against corrosion and may accelerate the rate of deterioration. Because of this acceleration, an elaborate and costly patching procedure may only provide a temporary repair. Accelerated deterioration results from patching materials that are designed for rapid strength gain but that contain additives such as chlorides or other set accelerators that are highly corrosive to steel. The patching materials create strong anodes, and corrosion begins in the patch area soon after placement. The opposite is true when concrete is removed from a spalled area in a salt-contaminated deck and replaced with concrete that does not contain set accelerators. The new patch will be free of chlorides and will create a differential environment corrosion cell. The repaired area will take the position of a strong cathode and create a large potential difference between the patch and the remaining portion of the deck. This potential difference will cause a current flow resulting in accelerated deterioration.

As a result of observing and evaluating deck repairs during the demonstration program, in addition to work done by California State, we are now recommending a procedure for repairing deck spalls, which could produce a more permanent patch.

The first question to be answered is how much concrete area should be removed from around the spall. The maintenance engineer has four general choices: (a) remove only the concrete in the spalled or delaminated area, (b) remove the concrete to clean steel or just beyond the edge of visible corrosion, (c) remove all concrete considered active by an electrical potential survey, or (d) remove the entire deck surface. These limits will vary because of local conditions; however, several factors are now apparent.

1. The spalled area does not represent the total area of corrosion. We found that the corrosion extends beyond the immediate spall; therefore, a patch that merely replaces the spall is surrounded by corrosion and has a high probability of early failure.
2. The excavation, if extended from the spall to blue steel, does not represent the total active steel area. Active readings were found to extend beyond the corrosion limits. The active steel can be associated with the probability that the patch will accelerate corrosion in the remaining portion of the deck or that the patch itself will ultimately fail.

The probability of success can be increased by removing the concrete that surrounds active steel. In many situations, this will require total deck removal. Funding limitations and common practice often restrict this approach. In these situations and where the deck is of acceptable quality (even though active corrosion is suspected throughout

the deck), we believe that a method used by California state to repair bridge piers in a marine environment can be applied to deck patching. Theoretically, the reinforcement bar in the area of the patch can be eliminated from the corrosion circuit.

In order to accomplish this, we had to first remove all of the concrete surrounding the steel where the voltage level is greater than 0.3 V and then apply a uniform coating of epoxy to clean steel in the patch area. The epoxy will break the immediate electrical contact between the concrete and steel. The concrete should be removed to a depth below the steel, which permits uniform distribution of the maximum-sized aggregate. In this manner the epoxy environment electrically isolates the steel, and the remaining deck will act independently of the patch. We also recommend that a bonding agent be used when patching the interface with a concrete coat.

When the corrosion demonstration program was initiated, the principal objective was to explain the theory of the corrosion cell and its relation to concrete spalling and to demonstrate equipment that nondestructively could be used to analyze the corrosive condition of reinforced concrete.

We did not propose a formal operational procedure for the corrosion detection device. Some informal recommendations were made, but this challenge was generally left to the individual users. Based on our observations in some 46 states, we believe that corrosion detection equipment can be used as an operational tool; therefore, we are now recommending a general procedure that can be applied to a local or a statewide area. Little field work has been done based on these recommendations; however, I believe that the concept is sound and that it lays the foundation for further refinements.

We find that spalling bridge decks are in various stages of deterioration. I believe that, by categorizing these stages with readings obtained with the corrosion detection device, an efficient maintenance or rehabilitation program can be developed. By using a classification system, several decisions can be made.

1. The limits of concrete to be removed beyond the spalled area can be determined. As mentioned earlier, we recommend removing all concrete down to a passive level, i. e., less than 0.3 V. This will require an analysis of the readings obtained, which isolates the hot spots and calculates the area to be removed.

2. A decision can be made as to the type of patch and patch material to use. We believe that some patching methods are too elaborate to fit the corrosion condition of a deck; on some decks a more elaborate patching technique may guarantee adequate extended service life.

3. A decision can be made if a membrane is to be placed on the deck after patching. As mentioned earlier, placing an expensive membrane on a deck impregnated with salt and in the advanced stages of deterioration may be highly speculative.

4. An administrative decision can be made that reflects the number and types of decks that can be repaired or rehabilitated as related to the available resources. On some decks it may be economically sound to temporarily repair a deck with minimum traffic interference until resources become available for complete rehabilitation.

The decision to place a deck in a specific category will largely depend on the confidence placed in readings obtained with the corrosion detection device. We have analyzed the readings taken on 120 exposed concrete decks from 33 states. Data from the other states visited during the demonstration program were not included because in several states membranes are routinely used or the data had not been compiled at the time of this writing. The decks were objectively classified during the demonstration program as poor, fair, or good. After classification, readings were taken with the corrosion meter and recorded. We then grouped the maximum readings and established a frequency curve for the various classifications (Fig. 2).

All bridges classified as poor, i. e., spalled and cracked, contained readings that exceeded 0.4 V. For those decks classified as fair, i. e., cracked but not spalled, 90 percent of all readings were less than 0.45 V. For those bridges classified as good, 90 percent of all readings were less than 0.3 V.

This information confirms our original conclusions. Equipotential measurements do provide a good indication of the deck condition. It further signifies that, as the readings increase, the probability of deck spalling also increases.

When this information is considered in conjunction with several other variables, we believe three general condition classifications can be established. Of course, there will be some overlapping, but it does permit an objective approach to evaluating repair needs and methods.

The significant principle for classification should be the percentage of deck area considered active. The amount of cover and the chloride ion content can be used to assess priorities within any classification. These priorities should be subjective and can be coupled with local values, such as traffic, location, and highway classification.

It will be necessary to first take readings on the deck, draft the equipotential contours, and compute the percentage of deck area considered to be in an active stage. Second, sufficient concrete samples should be taken to establish the chloride ion content at the level of steel, and, third, sufficient measurements should be made to establish the depth of cover and the variation in cover.

The first classification should include all decks in an advance stage of deterioration with the following properties.

1. Corrosion readings indicate that active cells exist in from 50 to 100 percent of the deck area.
2. Concrete cover is variable.
3. Core samples indicate that chloride has impregnated a large percentage of the deck area.

A deck in this classification will normally require continual patching. Patching can be considered analogous to a cancer cell that has spread throughout a human body. Some types of corrective treatment may afford additional life, but they should be considered temporary. The common practice of sawing and patching with concrete is expensive, normally requires a traffic lane closure or detour, and, if the patch is incorrectly placed, fails in a short period of time. It is for this reason that we recommend a temporary patch—preferably a cold-mix bituminous patch or some other low-cost material that can be easily placed with a minimum delay to traffic. This type of maintenance will be satisfactory for surface spalls until a complete rehabilitation program can be scheduled. In those areas where spalling has progressed to the point that structural integrity is jeopardized, early patch failures have occasionally been associated with fatigue. In these areas, underbracing may be appropriate to significantly slow down the rate of failure.

We do not recommend placing a waterproof membrane on a deck in this category. An example of a deck in this classification is shown in Figure 3.

The second proposed classification indicates a reduction of active areas and could have the following properties.

1. Corrosion readings indicate that active cells are in 20 to 60 percent of the deck area. The cells can be isolated into hot spots and are surrounded by a substantial area of less than 0.3-V readings.
2. Concrete cover is reasonably uniform.
3. Core samples indicate that chloride is largely found only in spalling areas.

A deck in this classification can be considered appropriate for further evaluation. I recommend that the concrete be removed to a depth below the top mat, patched as recommended earlier, and thereafter periodically evaluated with the corrosion meter. In effect, an attempt should be made to remove the contaminated chloride areas and evaluate the results with the corrosion meter. To place a membrane at the time of patching would be speculative and is not recommended without the evaluation period. An example of a deck in this classification is shown in Figure 4.

The third proposed classification will indicate minor deterioration with properties as follows.

1. Corrosion detection readings indicate active areas ranging up to 25 percent of the deck area. These active hot spots can be isolated and are surrounded by a sizable area of less than 0.3-V readings.

Figure 1. Corrosion of reinforcing steel in highway structures.

MODERATE-SEVERE
LIGHT-MODERATE
NONE-LIGHT
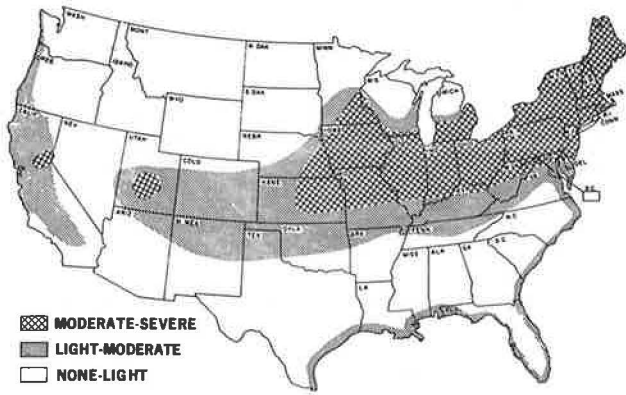
Figure 2. Bridge deck condition classification versus electrical potential.
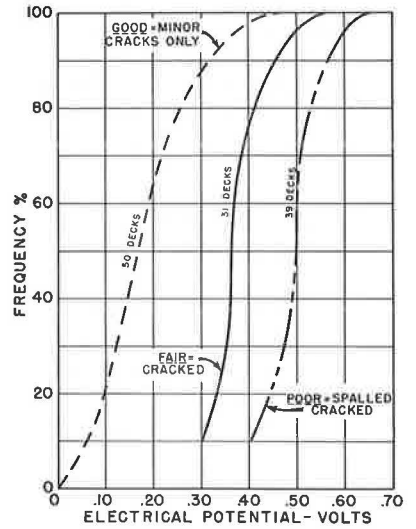
FHWA CORROSION DETECTION
DEMONSTRATION 1970-1971
120 EXPOSED DECKS, 33 STATES

Figure 3. Bridge deck condition classification 1.

Cover variable
Active area 94%
Chloride Ions - 2 #/cu. yd. at level of steel
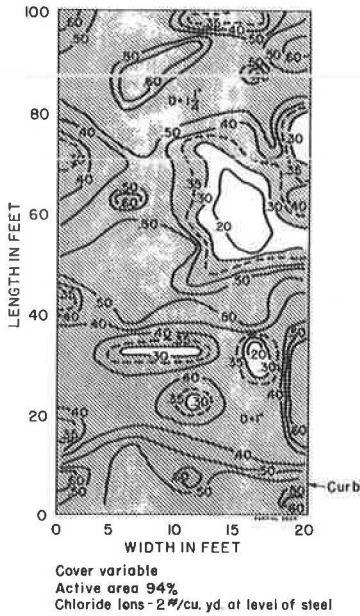
Figure 4. Bridge deck condition classification 2.

Cover variable
Active area 24%
Chloride Ions varies - 1 #/cu. yd. at level of steel
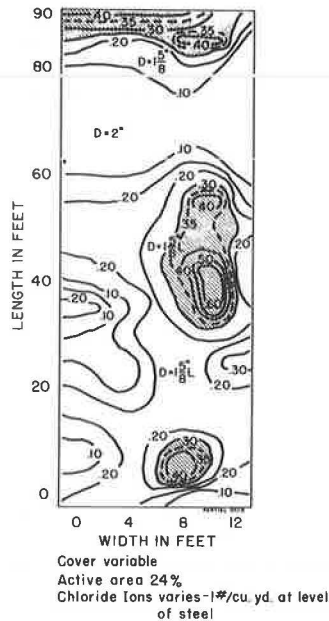
Figure 5. Bridge deck condition classification 3.

Cover adequate for present day design
Active area 5.0%
Chloride Ions - Trace
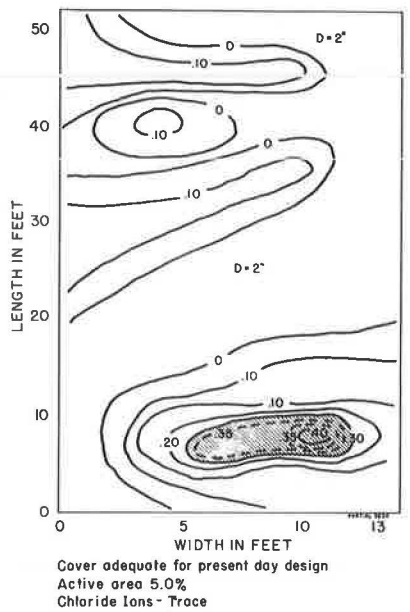
2. The cover is adequate for current design.
3. Deck core samples indicate a minor amount of chloride at isolated hot spots.

A deck in this classification is recommended for a more elaborate patching procedure. All concrete should be removed to a 0.3-V reading or to clean steel and to a depth below the steel, which is adequate to accommodate the maximum aggregate size. The concrete must be replaced with a chloride-free mix. The old concrete and the exposed steel should be coated as explained previously. We believe a membrane can be placed on this deck with satisfactory results. An example of a deck in this classification is shown in Figure 5.

At this time, it is standard practice to do little or no work on a deck in the type 3 classification. Generally, the deck condition is good, few if any spalls are evident, and usually there is no physical evidence of a major problem. However, it is this type of deck where proper patching and a protective membrane may greatly contribute to extending the service life. Most repair efforts are devoted to decks in the type 1 and type 2 categories. In general terms, the patching techniques recommended for categories 2 and 3 are being used for category 1 with unsatisfactory results. The combination of patching and placing a membrane may prove successful, but we do not believe this can be done with bridges in an advanced stage of deterioration.

No repair methods are considered to be foolproof and therefore should be tested under local conditions. For example, removing all concrete down to the 0.3-V level is an approximation of passive steel. Because of the complicated mechanism of the corrosion cell, no exact number will perfectly define the specific location.

In summary, the highway engineer is challenged to provide a transportation facility 24 hours per day, 365 days per year. De-icing salts have proved to be an effective maintenance tool in meeting this challenge. We are now challenged to find an economic solution to what appears to be a costly secondary effect. Bridge deck spalling is not a local problem. All indications are that the affected geographical area will increase in size with a corresponding increase in cost. We are hopeful that research can find preventive techniques.

ACKNOWLEDGMENT

REFERENCES

1. Stratful, R., and Spellman, D. An Electrical Method of Evaluating Bridge Deck Coatings. California Division of Highways, M and R 635116-5.
2. Stratful, R., and Spellman, D. Laboratory Corrosion Test of Steel in Concrete. California Division of Highways, M and R 635116-3.
3. Durability of Concrete Bridge Decks. U.S. Department of Transportation and the Portland Cement Association, Repts. 4 and 5.
4. Concrete Bridge Deck Durability. NCHRP, Synthesis of Highway Practice 4, Washington, D.C., 1970.
5. Concrete Structure Deterioration Due to Corrosion of Reinforcing Steel. Federal Highway Administration, June 7, 1971.

DISCUSSION

S. M. Cardone, Michigan Department of State Highways

The author has given us some excellent guidelines for the repair of spalling bridge decks, which are based primarily on the use of a detection device that in turn is based on the assumption that "deterioration results primarily from corrosion forces that radiate from the embedded steel."

The author is quick to caution, "The background support is admittedly weak, but we think the concept is sound and lays a good foundation to build on." We heartily agree with this statement and want to add that when sufficient empirical data are accumulated the corrosion detecting device can become an excellent tool to assist us in the repair of spalling bridge decks.

However, we should place the importance of this tool in proper perspective. We should realize that the tool merely allows us to predetermine the quantities of concrete that should be removed, which is of value for estimating purposes. It removes the guess in the estimating process for a repair project, but it does nothing to eliminate the causes.

The common practice at the present time is to program the removal of an estimated amount of concrete, with past experience as a guide, and then by mechanical and visual means remove and replace all concrete that appears to be unsound at the time. This is usually followed by the addition of either a water barrier or subseal with a flexible wearing course or a rigid impervious overlayment. This serves to protect both the old and new concrete from further attack.

We have used this technique as a standard procedure for the past 5 or 6 years with remarkable success. As a matter of fact, this procedure got its beginning in Michigan some 15 years ago. We used a structurally bonded overlayment of latex-modified portland cement mortar. This project (6) is in excellent condition to the present day.

I should like to comment on another point given prominence throughout the paper, that the real cause of deck deterioration is de-icing chemicals. Now, no one will deny that chlorides accelerate the corrosive action. But, when the writer states that, "if moisture, oxygen and chlorides (in sufficient quantities) are present at the level of the steel, corrosion will take place," does the writer mean to say that, if only moisture and oxygen are present, corrosion will not take place?

Further, in November 1967 a large bridge, 135 ft wide and 8,770 ft long, consisting of 27 acres of deck was opened to traffic in Detroit. In the nearly 3 years that the deck was under construction, extensive cracking occurred and spalling commenced within the first year of service. This spalling has been progressing at such an accelerated rate in the past 4 years that an extensive repair and overlayment project is being planned for this year estimated to cost in excess of $2 million. An overlayment of latex-modified mortar, which is the system that has given us by far the longest performance, will be used.

Several observations can be made from this special case: Was the spalling that started in less than a year of service due entirely to the action of salt, or did the corrosion start during the construction period when no salt was applied? One might also ask where does the salt come from to rust my garden hoe or the farmer's plow between periods of usage.

At times we are prone to conveniently single out chlorides as the villain in all our deck problems and at the same time assign a lesser role to important items such as water-cement ratio, cement factor, curing, finishing, placement technique, and use of concrete in tension.

In summary, I believe that we have the scientific knowledge today to produce an indestructible concrete bridge deck, but actually very little progress has been made in this direction in the past 15 to 20 years. The author seems to be carried away with his enthusiasm for the steel corrosion detection device, which is nothing more than a maintenance tool.

When we consider the expensive problem described on the Detroit project, it can scarcely be said that a solution to deck spalling is at hand.

Let's get to the heart of the problem. We know that steel rusts even without the presence of salt. We can build bridge decks to keep saltwater and air from hitting the steel. Why this is not done and why bridge steel continues to rust is not the fault of maintenance men or nature; it is the fault of the designers and builders.

Reference

6. Cardone, S. M., Brown, M. G., and Hill, A. A. Latex-Modified Mortar in the Restoration of Bridge Structures. HRB Bull. 260, 1960, pp. 1-13.

AUTHOR'S CLOSURE

Cardone has presented a large number of interesting questions about the theory of corrosion and offers several solutions to the spalling problem. I will first address myself to the questions that relate to the theory of corrosion and second to his proposed solutions.

One general statement should be clarified and put into proper perspective. I have made no assumptions about the theory of corrosion or the effects of chlorides on embedded steel. In those cases where spalling is properly identified, research (supported by field conditions) has associated chlorides with corrosion and in turn corrosion with spalling.

The answer is yes in reply to the question "does the writer mean to say that, if only moisture and oxygen are present, corrosion will not take place?" Both field experience and laboratory work show that steel will normally not corrode in concrete unless chloride ions are present. The basic theory is that concrete provides a film of calcium hydroxide that protects the steel from corrosion. This protection is destroyed in the presence of chloride ions. Although this theory is only briefly described in my paper, it is supported by much research and discussed in detail in various publications.

This condition is also closely related to the question, "Where does the salt come from to rust my garden hoe or the farmer's plow between period of usage?"

It is normal to find metals, particularly steel, corroding in air. This supports the fact that the plow and hoe will corrode in the atmosphere because they do not have the protection film provided by cement. In atmospheric corrosion, the cells are microscopically spaced and the corrosion appears as a continuous film. In chloride contaminated concrete, the steel corrodes in a manner that is commonly referred to as macroscopic corrosion, where the corroding area may be spaced several feet from the cathode or noncorroding area.

I am not inferring that steel exposed at a crack is protected by concrete. If cracks or honeycombing are present in the concrete, the atmosphere can penetrate to the exposed steel and normal atmospheric corrosion will occur. In this situation, corrosion will in all probability occur regardless of concrete chloride content. However, if chlorides are present, the corrosion rate loss is considerably higher.

The corrosion detection equipment is principally an application of the galvanic cell. The theory of the galvanic cell is not new, although application of this principle to bridge deck corrosion is relatively new. We now believe that research work has adequately verified the concept of the corrosion detection equipment, and on this basis we demonstrated its potential merit throughout the United States.

I agree that the corrosion cell is a complicated phenomenon. However, after reviewing some 422 bridge decks in 46 states, correlating salting practices with deck conditions, comparing actual deck chloride contents with deck conditions, correlating these facts with readings taken with the detection device, I am convinced that readings obtained with the corrosion detection do indicate the condition of spalling decks and see no merit in collecting additional data to support this conclusion.

I agree that the corrosion detection device does nothing to eliminate the cause of corrosion, and after another review of the paper I cannot visualize drawing that conclusion. It does, as was stated, permit predetermination of concrete quantities to be removed by evaluating both sound and deteriorated areas. It, therefore, follows that the entire deck condition can be evaluated. It is the value of this information that is not recognized in Cardone's discussion.

Comments on the solutions as proposed in Cardone's discussion are given below.

The commercial product referred to in the discussion can and will extend the service life of a deteriorating bridge deck. However, tests of this and numerous other products have resulted in the following observations.

1. Modified latex mortars are not impermeable as indicated in Cardone's discussion. Available information indicates that the performance of these mixes largely parallels the high cement and low water mixes. Laboratory tests now under way support this conclusion. In addition, we have tested nine modified latex mortar field installations in six states. Seven of these decks had active areas of steel corrosion as

indicated by the steel corrosion detection device. This means that sufficient chlorides have penetrated the latex mortar and activated the steel or that the initial cause was not eliminated and corrosion is continuing.

2. Many thin mortar treatments are now applied to scaling decks. Scaling does not result from corrosion. Therefore, we can expect that a good bonding overlay will perform satisfactorily with this type of deterioration.

3. The states of Iowa and Kansas, which use high cement contents in their overlays, are having good success. To date, these overlays have performed somewhat similarly to the latex mortars. This supports my earlier statement that cement is an excellent inhibitor of corrosion.

I interpret the article (6) Cardone discusses as referring to a scaling deck. Perhaps this is the key to his success. Scaling, as you know, is a surface mortar deterioration, commonly found in decks constructed with non-air-entrained concrete, and is not associated with the corrosion of steel. By removing the scaled surface and replacing it with good bonding overlay, the cause of deterioration has largely been eliminated, and the correction should prove successful.

Spalling decks, however, are not as easily corrected. The cause of the problem is the chloride content in the concrete at the depth of the steel, and, unless the concrete is removed to this depth, there is little chance for any overlay to perform satisfactorily.

Cardone also states that the problem with deck deterioration is poor design and construction and that bridges can be built to keep saltwater and air from hitting the steel. I cannot agree with this concept because to date, under the best controlled laboratory conditions, we have not been able to produce impermeable concrete. It is, therefore, impractical to expect that the quality of concrete will be better in construction projects than can be produced in the laboratory. We have, however, identified factors that will extend the time for chlorides to penetrate to the reinforcement. Low water-cement ratios and high cement contents decrease absorption of the concrete. When low-absorption concrete is combined with adequate cover and controls over the indiscriminate use of de-icing chemicals, the service life of a deck should be extended. In fact, in some cases, these extensions can be quite significant; however, oxygen, moisture, and chlorides will eventually penetrate even good-quality concrete. We are, therefore, confronted with time to corrosion, and, because of the many variables, the time factor has not been defined. As in many engineering designs and studies, we may never be able to assign a definite time.

In view of the preceding, it is recommended that our efforts be concentrated in areas where they can be of significant benefit. The following are examples of this type of approach.

1. Recognize construction tolerances; if the deck is located in a heavily salted area, spalling will occur. If the quality of construction is within reasonable limits, additional requirements may only be an exercise in human and equipment capabilities.

2. Recognize the importance of quality materials, mix design, and design cover. These factors may contribute significantly to an extension of service life.

3. Recognize that controls over the indiscriminate use of salt can extend the service life of a deck.

4. Correlate these factors, including salt usage, with the need for deck membranes.

CONCRETE OVERLAYS FOR BRIDGE DECK REPAIR

Howard Furr and Leonard Ingram, Texas Transportation Institute,
Texas A&M University

Tests were made on portland cement and resinous concrete overlays to determine their suitability as overlays for deteriorated concrete bridge decks. Direct shear strengths of overlays bonded with epoxy, portland cement grout, and latex-modified cement grout were compared with those applied with no bonding agent. Freeze-thaw tests were made to determine durability of bonding agents and of overlay concretes. Load tests were made on 8-ft span beams to determine the stiffening effect of overlays and the effect of repeated loadings on overlaid beams. Durability was studied further by gradually lowering laboratory temperature to 20 F during periods of repeated load applications. Low frequency and low amplitude vibrations were maintained on one beam by cyclic loading during placement and cure of a $1\frac{1}{2}$-in. overlay to simulate vibration due to traffic on a lane adjacent to the one being overlaid. Shear bond strengths ranged from 214 to 668 psi. Epoxy and portland cement grout bonding agents withstood the ASTM C 290 test without failure. Two of three overlays of latex-modified cement concrete came unbonded during the ASTM C 290 test. Latex-modified cement concrete overlay provided better freeze-thaw scale resistance than did other materials. No overlay failed in any way, except for tension cracks, in 2 million cycles of load.

•DEEP scaling and spalling in many concrete bridge decks have advanced to the point were major repairs are necessary to bring the decks back to acceptable levels of performance. The alternative to major repairs is the complete replacement of the deck. The choice between replacement and repair is normally dependent on the extent of deterioration, costs, and user consideration. There are many situations where repair holds a distinct advantage over replacement, and a number of repair methods have been reported (1, 5).

A study that was made to determine suitable overlays for repairing existing deteriorated concrete bridge decks is the subject of this report. The present report concerns materials, bonding methods, and flexural stiffness of relatively thin repair overlays to be applied on existing concrete bridge decks.

Four series of tests, series 1 through 4, were made to provide information from which repair methods might be developed. Information on the portland cement concrete mixes for the test specimens is given in Tables 1 and 2. All overlays, with the exception of F, were made of air-entrained concrete. No air entrainment was used in the grout.

The epoxy mortar overlay was a mixture of epoxy and concrete sand on 15 percent to 85 percent basis by weight. A proprietary product, a mixture of concrete sand and a polyester resin formulation, was used for overlay J.

In series 1, direct shear tests were made to determine the shear bond strength of bonding agents used to bond overlays to base concrete. Freeze-thaw tests were made in series 2 to determine the durability of bonding agents and overlay materials.

In series 3, beam tests were made to determine the effect of overlays and repeated loadings on the stiffness of a reinforced beam and to determine the effect of repeated loads on the bonding agents.

Repeated load tests were made in series 4 under cold temperature to determine the fatigue characteristics of overlaid beams in freezing environments.

TEST PROGRAM

Series 1

When the overlay was 7 days old, direct shear tests similar to those performed by Felt (5) in pavement overlays were made on the jig-mounted specimens. The shear bond strength was computed as the average shear stress over the interface area.

Series 2

The 3-in. by 3-in. by 16-in. specimens formed by sawing larger slabs were tested for freeze-thaw durability in accordance with ASTM C 290 (6). In this test, the specimens are alternately frozen and thawed in an automatic freeze-thaw cabinet. They are tested for fundamental traverse frequency at intervals not exceeding 30 freeze-thaw cycles.

In other freeze-thaw tests, 1-in. thick overlays were bonded to 10-in. square base slabs. Wells formed by metal rings fixed to the overlays were filled with a 5 percent saltwater solution. The overlays were under ponded saltwater continuously from 22 to $26\frac{1}{2}$ days. About one-half of that time was spent in a freezing chamber and the other half in a thaw chamber.

Series 3

Laboratory beams (Fig. 1) were tested under static and cyclic loads applied at midspan. Load and midspan deflection data were collected just before and just after overlays were placed and cured and at intervals during the cyclic load phase. These data (Table 3) were used to determine the stiffness effect of the overlay and to determine if there was any loss in stiffness brought about by th repeated loadings.

One cyclic load test was made to determine if low amplitude, slow vibration would be harmful to the setting up, bonding, and strength of the overlay concrete that was cast and cured on the vibrating beam. Details of all of the beam tests are as follows.

Static Load-Deflection Tests—The simply supported beam was loaded at midspan to 400 lb in increments of 100 lb after cracking and before the overlay was applied. Midspan deflections were read for each load increment. After the overlay was applied and cured, another load-deflection test was made in the frame used for cyclic loading. The test was identical to the pre-overlay test except that the load was carried to approximately 500 lb, and readings were taken at smaller load increments. A typical plot of the pre-overlay and post-overlay data is shown in Figure 2.

Cyclic Load Tests—The same types of static load-deflection tests were made at intervals of 500,000 load cycles during the repeated load tests. Typical load-deflection plots are shown in Figure 2 at 0 and 2 million cycles for overlay in compression. Cyclic loads were applied by a machine with rotating eccentric weights. The loading device was fixed to the beams at midspan by lugs cast in the beams during fabrication. Power was delivered from an electric motor through flexible shafting to the machine. The loader was operated at the cyclic rate necessary to produce a deflection that, calculated by elastic analysis, would produce 20-ksi tensile stress in the bottom steel of the cracked overlaid beam. The resulting rotational velocity of the eccentric weights, producing the same load on the lifting stroke as on the depressing stroke, was sufficient to overcome the dead weight of the beam and the loader and produce a net upward force.

Overlays Cast and Cured on Vibrating Beams—A 2-in. thick overlay, overlay type D, was cast on a beam while the beam was subjected to 400 load cycles per min by the cyclic loader. The loading was maintained continuously for 48 hours during which time about 1,100,000 load cycles had been applied. It was designed to approximately simulate vibration caused by traffic in one lane while the overlay was placed and partially cured in an adjacent lane. There are situations in which an overlay might be placed under conditions similar to this one (7).

Table 1. Base specimen designs and aggregate gradation.

Specimen (in.)	Coarse Aggregate Gradation	Mix Properties, lb/yd³				Concrete Properties				Sieve Size	Percent Retained on Each Sieve			
		Gravel	Sand	Cement	Water	Percent Air	Slump (in.)	Cement Factor (sk/yd³)	Water-Cement (gal/sk)		Grade 1	Grade 2	Grade 3	Grade 4
7 by 7 cubes	4	1,942	1,272	518	273	0.0	3	5.50	6.0	¾ in.	0	Steel fiber	0	20
10 by 16 by 2 slabs	3	1,761	1,323	518	269	5.5	3	5.50	6.0	½ in.	15	Steel wire*	5	30
10 by 10 by 2 slabs	3	1,761	1,323	518	269	5.5	3	5.50	6.0	⅜ in.	25	Steel wire*	38	30
7 by 8½ by 5 beams	4	1,942	1,272	518	273	0.0	3	5.50	6.0	No. 4	58	Steel wire*	57	20
										No. 8	2	Steel wire*	0	0

*Cut in short lengths (¾ in. by 0.010 in. by 0.022 in.).

Table 2. Overlay designs.

Overlay	Coarse Aggregate Grade*	Mix Properties, lb/yd³				Concrete Properties				Comment
		Gravel	Sand	Cement	Water	Percent Air	Slump (in.)	Cement Factor (sk/yd³)	Water-Cement (gal/sk)	
A	1	1,821	1,128	663	301	4.5	2½	7.04	5.13	Plain concrete
B	1	1,846	1,142	664	285	5.0	2½	7.06	5.00	4-gauge welded wire, 3 in. by 3 in., placed on bonding agent
C	2	0	2,390	748	394	9.3	0	7.95	5.95	Coarse aggregate replaced by 261 lb of steel fiber, ¾ in. by 0.010 in. by 0.022 in.
D	1	1,827	1,132	665	309	5.0	4	7.06	5.25	Chem Comp cement used with 4-gauge welded wire, 4 in. by 4 in., at mid height of overlay
E	3	1,531	1,350	607	124	9.2	7	6.45	4.05	Concrete modified with latex additives, 3½ gal per sk, latex was 48 percent solids by weight
F	1	1,846	1,142	664	279	0.0	1¾	7.16	4.75	Not air entrained
G	1	1,846	1,142	664	270	5.0	2	7.04	4.60	Air entrained
H-1	3	1,254	1,568	627	131	5.5	4½	6.67	4.04	Cement A latex-modified grout
H-2	3	1,254	1,568	627	131	6.0	5	6.67	4.04	Cement B latex-modified grout
Iᵇ										Epoxy, no primer, 15 percent epoxy, 85 percent sand by weight
Jᶜ										Polyester, primer, 4 lb of resin, 12 ml of catalyst

*See Table 1.
ᵇType I consists of 7½ lb of epoxy and 50 lb of concrete sand.
ᶜType J consists of 8¼ lb of resin, 33 ml of catalyst, and 40 lb of sand.

Figure 1. Beam details.
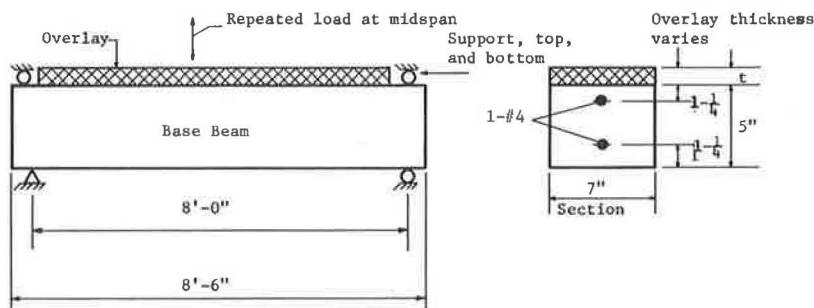
Beam concrete: See Table I

Nominal strength of cylinder at 28 days = 3000 psi

Nominal secant modulus at 1/2 f'_c = 6,000,000 psi

Table 3. Beam schedule and stiffness ratios.

| Beam Designation[a]	Overlay Type[b]	Overlay Bonding Agent	Overlay Thickness (in.)	Age of Test (days)	Without Overlay A	With Overlay No Cycles B	With Overlay 2 Million Cycles C	$\frac{B}{A}$	$\frac{C}{A}$
AG-12	A	Grout	2	38	3,810	41,100	37,800	10.7	9.9
AE-12	A	Epoxy	2	38	3,740	25,000	23,500	6.7	6.3
BG-12	B	Grout	2	39	4,450	34,200	29,200	7.7	6.6
BE-12	B	Epoxy	2	32	4,210	18,600	–	4.4	–
CG-12-1	C	Grout	2	10	5,200	36,900	29,200	7.1	5.6
CG-12-2	C	Grout	2	11	4,600	15,800	15,300	3.4	3.3
CE-12	C	Epoxy	2	9	3,150	12,400	11,600	3.9	3.7
DG-12	D	Grout	2	34	5,000	18,800	18,400	3.8	3.7
DE-12	D	Epoxy	2	9	4,700	19,500	16,400	4.1	3.5
EG-12-1	E	LM[d]	2	–	4,550	17,800	16,300	3.9	3.6
EG-12-2	E	LM	2	–	3,980	12,400	11,800	3.1	3.0
AG-11	C	Grout	$1\frac{1}{2}$	39	3,880	22,200	20,000	5.7	5.2
AE-11	C	Epoxy	$1\frac{1}{2}$	20	5,000	13,300	18,200	2.7	3.6
CG-11	C	Grout	$1\frac{1}{2}$	11	3,850	14,400	16,700	3.7	4.3
BG-11-1	B	Grout	$1\frac{1}{2}$	9	3,960	7,870	8,450	2.0	2.1
BG-11-2	B	Grout	$1\frac{1}{2}$	9	4,080	12,700	10,800	3.1	2.6
CG-11-1	C	Grout	$1\frac{1}{2}$	10	3,920	8,640	8,330	2.2	2.1
CG-11-2	C	Grout	$1\frac{1}{2}$	10	4,000	9,520	10,100	2.4	2.5
DG-11-1	D	Grout	$1\frac{1}{2}$	13	4,830	12,100	12,600	2.5	2.6
DG-11-2	D	Grout	$1\frac{1}{2}$	13	3,450	8,930	9,500	2.6	2.7
EG-11-1	E	LM	$1\frac{1}{2}$	10	3,670	8,350	8,430	2.3	2.3
DG-11-3	D	Grout	1	10	3,640	9,490	8,090	2.6	2.2
DG-11-4	D	Grout	1	10	3,840	11,100	9,100	2.9	2.4
EP-1	I	None	$\frac{1}{2}$	7	4,040	4,430	4,250	1.1	1.1
EP-2	I	None	$\frac{1}{2}$	7	5,080	5,650	4,800	1.1	1.0
EP-3	I	None	$\frac{1}{2}$	6	4,130	4,590	4,720	1.1	1.1
EP-4	I	None	$\frac{1}{2}$	6	3,960	4,380	4,410	1.1	1.1
PL-1	J	Polyester	$\frac{1}{2}$	7	3,840	5,150	5,370	1.3	1.4
PL-2	J	Polyester	$\frac{1}{2}$	7	3,750	4,090	4,090	1.1	1.1
PL-3	J	Polyester	2	2	2,860	4,680	5,000	1.6	1.8
PL-4	J	Polyester	$\frac{1}{2}$	2	2,960	4,190	4,360	1.4	1.5

Header row spanning note: P/Δ^c (lb/in.)

[a]See Figure 1 for beam dimensions.
[b]See Table 2 for description of overlay materials.
[c]Midspan load/midspan deflection.
[d]Latex-modified cement concrete.

Figure 2. Typical static load-deflection curves.

MIDSPAN DEFLECTION (10^{-3} in.)
(From Deadload Position)
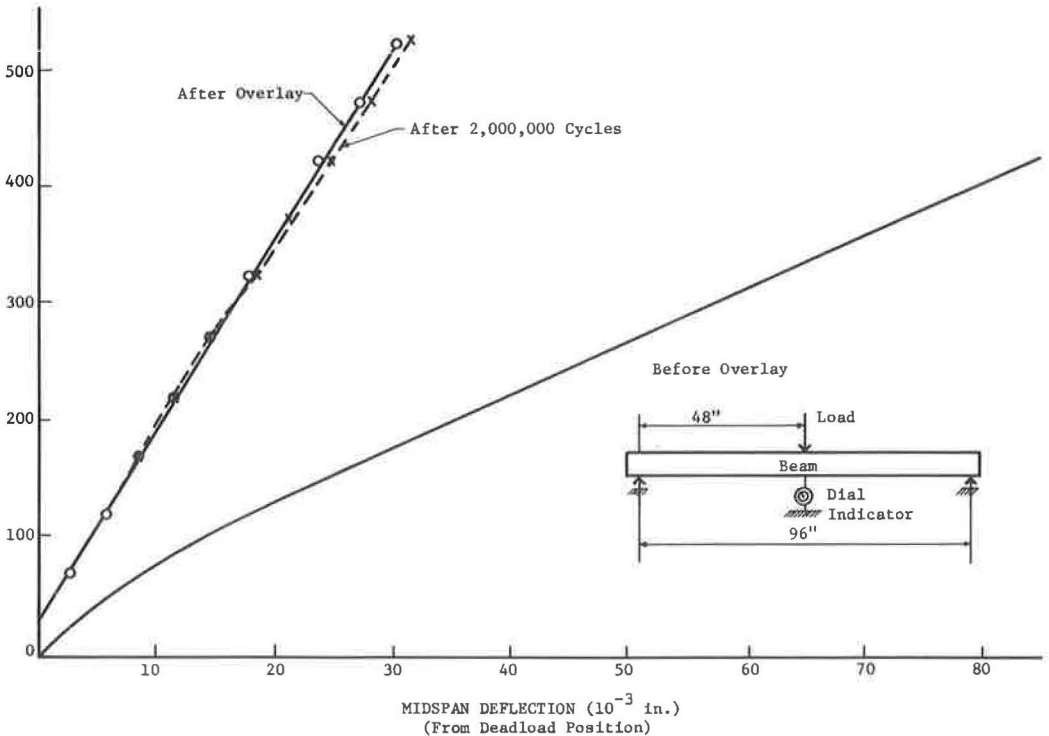
Series 4

The temperature was gradually lowered in the test chamber from 70 to 20 F during which period the beam underwent cyclic loading. The time-temperature-loading cycle schedule is shown in Figure 3.

A static load-deflection test was made before the overlay was applied and then again after it was applied and cured before cyclic load and temperature cycling began. Room temperature was gradually lowered from 70 to 20 F while load cycling was maintained at approximately 11 cycles per sec. After 500,000 cycles, loading was stopped and the temperature was increased to 70 F. Then, 12 hours after stopping, a static load-deflection test was made.

No continuous record of room temperature was kept of either the descending or the ascending curves, nor were temperatures within the beam measured. The freezing cycle required essentially a 12-hour day to draw the temperature from 70 to 20 F.

The pattern established on the run from 70 to 20 F for the first 500,000 cycles was maintained throughout the 2 million load cycle test. A total of 5 days were required for testing each beam subsequent to application of the overlay. Four of those days were spent in repetitive loading.

RESULTS

Series 1

Bond strengths of concrete overlays applied to sandblasted surfaces of 7-in. cubes using grout, epoxy, latex-modified cement, and polyester were tested. The base concrete mix and cure were constant (although several batches were made), and all batches were not cured at the same time. The failure surface generally followed the interface of overlay and cube with minor migrations, in some cases, into the base material and the overlay. The bond strengths are given in Table 4 as averages of either three or six tests.

A concrete bridge deck carrying service loads is stressed in horizontal shear that varies in intensity with distance from the surface to about middepth of the slab. When the slab carries an overlay, the shear stress at the interface of the overlay and the base slab is dependent on shear at the section and the relative thicknesses of the overlay and slab. A slab supported by beams is considered by AASHO (8) to be adequate in shear if it is designed for moment in accordance with AASHO specifications. A wheel would be carried by a slab strip about 4 ft wide on a bridge with stringers spaced about 8 ft apart. If the wheel were shifted to the edge of the stringer for maximum shear, an H 20 wheel plus impact (about 20 kips, spread over, for example, 3 ft) would cause a shear of 3.9 kips on a 7-in. wide section. By applying the horizontal shear formula $v = VQ/Ib$, to the interface of a 7-in. uncracked slab with a 2-in. overlay for a 3.9-kip load, we find the interface shear to be

$$v = 3,900 \times (14 \times 3.5)/(425 \times 7) = 64.2 \text{ psi}$$

This stress, which is only 30 percent of the minimum strength (214 psi) given in Table 4, would be safe for any of the bonds developed in the tests. Earlier overlays having no special bonding agent (9) developed 129 psi, two times the 64.2 psi previously computed.

Results of shear bond tests on overlays applied to concrete that had been treated earlier with waterproofing materials have been reported (10). These tests showed that a concrete overlay applied directly to a surface treated with a linseed oil-kerosene mixture developed a 61-psi bond; after the surface had been sandblasted, the bond was 367 psi. Corresponding values for a surface treated with a tung oil-kerosene mixture were 88 psi and 597 psi.

Specimens F and G were fabricated in the same manner as the earlier group, A through D, to determine if air entrainment affects the shear bond strength of portland cement concrete overlays. The values, the average of six tests, indicate that the air-entrained overlays, specimens G, have essentially the same strength as the concrete without air, specimens F. Both values are lower than the earlier ones in air-entrained specimens A through D, which is attributed to an unknown, and unintentional, difference in material or fabrication.

These tests, and previous ones (9), show consistently that portland cement grout provides superior bonding. It produced higher strength, an average of 541 psi in the 12 specimens (A through D, Table 4), considerably higher than the average bond from other materials in the same test series. Grouted specimens F and G given in Table 4 show that bond strength is not affected by the air entrainment used.

The load cycling of test series 3 and 4 had no noticeable effect on any bonding agent used in the tests. Every bonding agent tested provided far more shear than the 64.2 psi computed for a theoretical shear from a 20-kip truck wheel, but one of them failed the freeze-thaw tests.

Both epoxy and cement grout have been popular as bonding agents for applying concrete overlays to concrete pavements and bridge decks. The tests carried out here show that both of these perform well in the laboratory. The cement grout provided the highest bond strength, and it is easy to apply.

Series 2

All specimens, except two of the overlays E, completed 300 freeze-thaw cycles. Overlay E separated from the base at 183 cycles for one of the exceptions and at 246 cycles for the other one. At 300 cycles, the remaining four specimens of that overlay had deteriorated to the point where the overlay could be pulled away from the slab by hand.

No distress was noted in any other overlay during this test. Table 5 gives the properties and durability of the overlay material. Overlays C, both grout and epoxy bonded, showed no loss in durability factor after the 300 freeze-thaw cycles. The overlay material of these specimens contained 9.2 percent air (Table 2); high air content is characteristic of that material. If the high percentage of air benefited the bond durability of this overlay, it does not appear to have behaved in the same way for the E overlay, which contained essentially the same amount of air as the C overlay. From Table 5, it is evident that all base slab material had almost the same percentage of air.

The 10-in. square specimens with bonded overlays were subjected to two freeze-thaw cycles daily. The appearance of the overlay surfaces at approximately 50 freeze-thaw cycles is shown in Figure 4. The test showed that the bonding agent had no influence on surface deterioration. Figure 4 shows overlay E (with 9.2 percent air) to have much less surface scaling than the 9.3 percent concrete with wire fibers of overlay C.

Although the plain concrete of overlay A shows a little greater durability factor than overlay B, which contained welded wire fabric, no difference could be observed visually. It is evident from Table 5 that neither the grout nor epoxy bonding agent will be troublesome because of freeze-thaw action provided that both are properly placed. All other surfaces, A, B, and D, that contain from $4\frac{1}{2}$ to 5 percent air show moderate surface scaling. Based on results of similar freeze-thaw tests (11, 12), the performances of all specimens in resisting freeze-thaw scaling were satisfactory.

Series 3 and 4

The stiffness tests of series 3 and 4 show that a bonded overlay of 1 to 2 in. of concrete increases the stiffness of 5-in. thick beams from about two to five times prior to overlay. Overlays of $\frac{1}{2}$ in. add little to stiffness, but they would provide protection for the concrete deck and would make the surface smooth for traffic. The cost of resins would permit them to be used for added stiffness only in very limited volume. Therefore, the tests were not designed to provide extensive information on the stiffness of resin materials.

The beam that was overlaid while it was vibrated had a double vibrational amplitude (peak to peak) of 0.044 in. after the overlay was first cast. At an age of 24 hours under continuous vibration, the amplitude had reduced to 0.008 in. under the same load. The test was discontinued after 48 hours, and an inspection showed three tensile cracks near midspan in the overlay. These cracks were formed by the upward load part of the load cycle, which placed the overlay in tension. The concrete at the base of the cracks was inspected by chipping out cracked material, and the overlay was found to be fully and firmly bonded in the area.
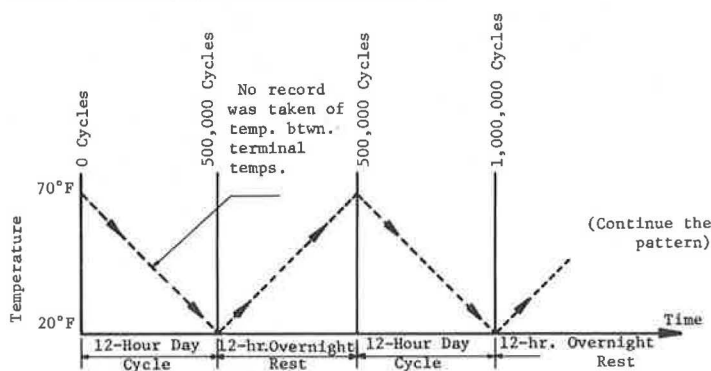
Figure 3. Loading cycle temperature and time.

Table 4. Shear strength of overlay bonds.

Overlay[a]	Base Surface Preparation	No Bonding Agent	Grout Bonding Agent	Epoxy Bonding Agent	Other	Comment
		Average Bond Shearing Stress, psi				
A	Sandblast	—	420	462	—	Air-entrained overlay
B	Sandblast	—	555	362	—	Air-entrained overlay
C	Sandblast	—	668	565	—	Air-entrained overlay
D	Sandblast	—	521	402	—	Air-entrained overlay
E	Sandblast	—			382	Latex-modified grout and overlay
F	Sandblast	—	393		—	No air-entrained overlay
G	Sandblast	—	388		—	Air-entrained overlay
H-1	Sandblast	—	—		458	Cement A, latex-modified grout and overlay
H-2	Sandblast	—	—		382	Cement B, latex-modified grout and overlay
I	Sandblast	214	—		—	Epoxy overlay
J	Sandblast	344	—		—	Polyester overlay

Note: The values shown represent the averages of three specimens for each overlay, A through D; six specimens for each of E through I; and four specimens for J. The average bond shearing stresses for overlays A through E were 541 psi with the grout bonding agent and 448 psi with the epoxy bonding agent.

[a]See Table 2 for description of overlay materials.

Table 5. Properties and durability factors of overlay concretes.

Overlay[a]	10- by 16- by 2-in. Slabs			1-in. Overlays			Durability Factor (ASTM C 290) of Overlayed System (average of 3)
	Percent Air	Cement Factor (sk/yd³)	Water-Cement (gal/sk)	Percent Air	Cement Factor (sk/yd³)	Water-Cement (gal/sk)	
AG	5.0	5.55	6.13	5.0	7.06	5.0	84.0
AE	5.0	5.55	6.13	5.0	7.06	5.0	85.5
BG	5.0	5.55	6.13	5.0	7.06	5.0	80.0
BE	5.0	5.55	6.13	5.0	7.06	5.0	82.5
CG	5.3	5.55	5.84	9.3	7.95	5.95	100.0
CE	5.3	5.55	5.84	9.3	7.95	5.95	100.0
DG	5.5	5.46	6.17	5.0	7.06	5.25	96.5
DE	5.5	5.46	6.17	5.0	7.06	5.25	87.8
EN	5.8	5.51	5.86	9.2	6.45	4.05	74.5[b]

[a]In the designation, the first letter refers to the overlay type given in Table 2; the second letters are G for grout, E for epoxy, and N for none.
[b]Total of six specimens cast. Because two overlays separated from specimens during freeze-thaw tests, durability factor is average of remaining four specimens.

100

Figure 4. Typical overlays after
freeze-thaw action under ponded
saltwater.

a) Overlay A - 53 Cycles (4-1/2% Air).

b) Overlay B - 53 Cycles (5% Air).

c) Overlay C - 50 Cycles (9.3% Air).

d) Overlay D - 44 Cycles (5.0% Air).

e) Overlay E - 51 Cycles (9.2% Air).
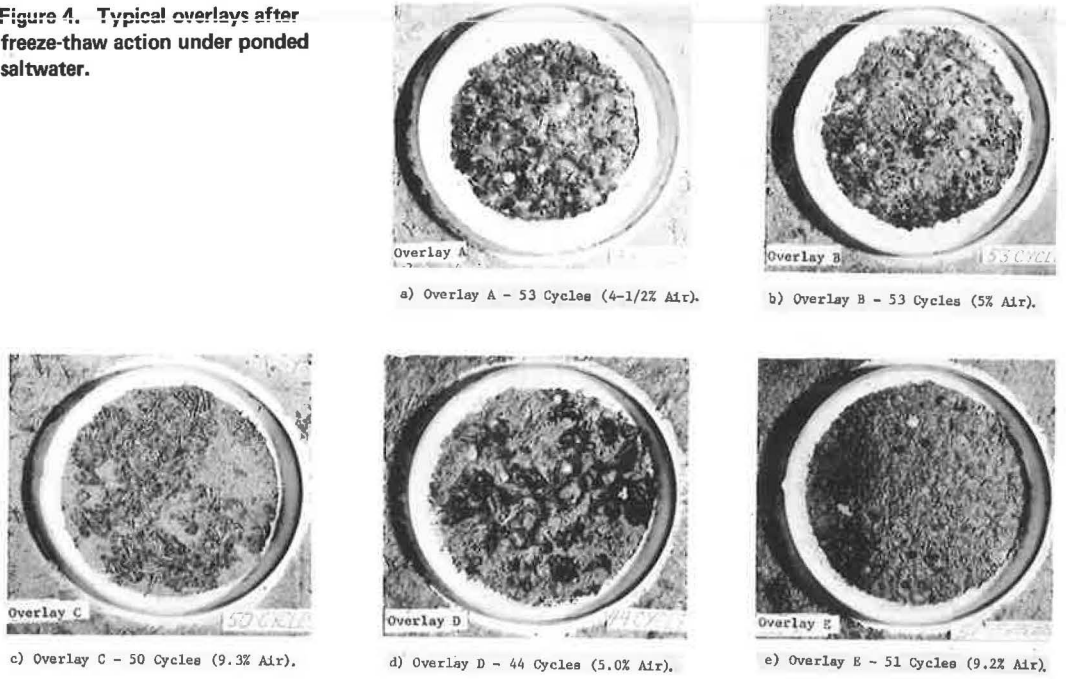
Table 6. Cold beam test.

Beam	Overlay Type	Thickness (in.)	S_w/S_D	S_f/S_w
FT-1	$1\frac{1}{2}$	Grout	3.4	1.0
FT-2	$1\frac{1}{2}$	Grout	3.1	0.9
FT-3	$1\frac{1}{2}$	Grout	2.4	0.9
FT-4	$1\frac{1}{2}$	Grout	3.5	0.9

Notes: Beam dimensions are given in Figure 1. Each beam was sub-
jected to 2 million load repetitions. S = stiffness and deflection of
midspan/load at midspan; S_D = S prior to overlay; S_w = S subsequent
to overlay prior to cycling; and S_f = S subsequent to overlay and
cycling.

Vibrational amplitudes before and after the overlay material (beam DG12) was cured are as follows.

	Amplitude (in.)		Amplitude/Span	
Initial	Final	Initial	Final
0.044	0.008	0.00046	0.0000835

The ratio of final amplitude to initial (plastic overlay) amplitude is 5.5. The ratio of amplitude to span, 0.00046 before the overlay stiffened, corresponds to a deflection of 0.33 in. for a beam spanning 60 ft. Under controlled traffic, it is not likely that this much deflection would occur in a lane being overlayed.

Two 6-in. diameter cylinder molds mounted on the vibrating beam were filled with the overlay concrete and vibrated with the beam as the cylinders cured. Two similar cylinders were made by standard procedures and cured on the floor near the vibrating materials. The cylinders were tested after 48 hours, and those that were mounted on the vibrating beam showed considerably higher strength than those cast and cured in the normal way.

Beams were tested to determine if the cycling of both load and temperature would adversely affect the overlay and its bonding agent. Careful visual inspection of each beam at the time of its static loading revealed no failure or distress of any kind. The load-deflection ratios given in Table 6 show that the beams were greatly stiffened by the addition of the overlay and that subsequent cycling of load and temperature reduced the stiffness by about 10 percent.

Good performance of the concrete overlay bonded with grout is shown in all four of the test series. The materials require proper treatment if good results are to be expected. But the treatment required is not difficult, and workmen are familiar with the materials and the treatment.

CONCLUSIONS

The following can be concluded from the tests discussed in this paper.

1. Portland cement concrete overlays from 1 to 2 in. thick bonded to a base concrete slab with either portland cement grout or epoxy resin are capable of developing shear bond strength far in excess of that normally required in service. The base material must be properly prepared to receive the bonding material.

2. Properly bonded concrete overlays of 1-to 2-in. thickness will undergo at least 2 million load cycles without bond failure.

3. Thin concrete overlays can be placed and cured on a vibrating base similar to a bridge deck under controlled traffic loads. Such an overlay will bond firmly to the base material when bonded with portland cement grout.

4. Portland cement grout and epoxy bonded concrete overlays will undergo ASTM C 290 durability test without failure.

5. Air entrainment provides excellent resistance to freeze-thaw scaling.

RECOMMENDATIONS

It is recommended that strong consideration be given to portland cement concrete overlays for bridge decks requiring surface repair. An overlay cannot solve the problem of a deck that is deteriorated from top to bottom, but it can be used to repair decks with deep scaling and delamination. Such an overlay repair installation must be carefully designed and properly placed. It should be sealed with a waterproof membrane if it is to be subjected to de-icing salts.

REFERENCES

1. Grace, W. A. Kentucky Bridge Decks Repaired With Latex Mortar Overlays. Better Roads, May 1969, pp. 19-21.

2. Hilton, N. A Two-Inch Bonded Concrete Overlay for the Port Man Bridge. Engineering Journal, May 1964, pp. 39-44.
3. Gillette, R. W. Performance of Bonded Concrete Overlays. Jour. ACI, Jan. 1963, pp. 39-49.
4. Tuthill, L. H. Conventional Methods of Repairing Concrete. Jour. ACI, Aug. 1960, pp. 129-138.
5. Felt, E. J. Repair of Concrete Pavement. Jour. ACI, Aug. 1960, pp. 139-153.
6. ASTM Standards. American Society for Testing and Materials, Part 10, Philadelphia, Pennsylvania, 1964.
7. Wies, C. O. Special Reports on Use of Equipment and Methods of Maintenance. U. S. Dept. of Transportation, Feb. 1969, p. 19.
8. Standard Specifications for Highway Bridges. American Association of State Highway Officials, Section 1.3.2 F, 10th Ed., 1969.
9. Sinno, R., and Furr, H. L. Bonded Concrete Overlays. Proc. ASCE, Aug. 1970, pp. 1627-1638.
10. Ingram, L. L., and Furr, H. L. The Effect of Surface Coatings and Bonded Overlays on Moisture Migration. Texas Transportation Institute, Texas A&M Univ., College Station, Res. Rept. 130-6, June 1971.
11. Meyer, A. H., and Furr, H. L. Reinforced Concrete Bridge Deck Deterioration: Diagnosis, Treatment, and Repair—Part II, Treatment. Texas Transportation Institute, Texas A&M Univ., College Station, Res. Rept. 130-2, Sept. 1968.
12. Furr, H. L., Ingram, L. L., and Winegar, G. Freeze-Thaw and Skid Resistance Performance of Surface Coatings on Concrete. Texas Transportation Institute, Texas A&M Univ., College Station, Res. Rept. 130-3, Oct. 1969.

DISCUSSION

Jerry Shackelford and Harvey Shafer, Dow Chemical Company

The authors have presented a convincing case for bonded, cement-rich, air-entrained concrete deck overlays. And yet, the results of the freeze-thaw scale durability tests suggest that the material used for repair causes the problem.

We at Dow have been working on latex modification of portland cement compositions, both in the laboratory and in the field, for many years. The depth of these investigations was manifested in 1969 when J. E. Isenburg reported on his research of both modified and unmodified materials by way of the scanning electron microscope.

Among the things we have learned is this: When you include a film-forming latex in a portland cement composition mix, you have an entirely different material with different handling characteristics and, more importantly, different curing requirements.

Curing needs for these materials are not unique and likely are more easily met under actual construction conditions. These needs are simply a short moist-cure followed by air-cure, which is necessary to allow the polymer to harden.

Synthetic latices, suitable for cement modification, contain air-entraining materials and so must not be used with additional air-entraining agents in the mix. Excessive air in the bonding matrix prevents proper bonding and allows infiltration of liquids to the bond interface.

When we relate these two variables to the Furr and Ingram paper, particularly to series 1 tests (shear bond) and series 2 tests (freeze-thaw durability), we may understand the relatively poor performance of the latex-modified specimens.

Both wet curing and use of air entrainment considerably reduce the effectiveness of the system. Because it appears that one or both were present in these tests and that therefore the properties of the system were not optimized, the validity of the evaluation may be questioned.

LaRue Delp, State Highway Commission of Kansas

Kansas is in the middle of a rather extensive program of repairing 5 to 10 percent of all bridges in the state, many with extensive deck deterioration. The scaled and spalled areas vary in magnitude and frequency. They range from the initial stage to full-depth deterioration. Temporary repairs are generally made on a day-to-day basis until about 30 to 40 percent of the deck reaches some degree of damage. Another criterion is the rate of deterioration. A contract is then let for the covering of the entire deck with a combination of full deck repair and/or a 2-in. bonded overlay.

We are currently programmed to advertise bridge repair contracts throughout the state for about $1 million annually, much of which is this type of work. We believe, at least for the present, that the program will be one of a continuing nature; however, there is no indication of any type of failure to date in the completed work on deck overlays. Some bridges are now more than 6 years old.

The report by Furr and Ingram, showing factual data of the various tests on this type of work, is of tremendous value for programming. It could furnish some sound guidelines.

For many years my role has been exclusively that of programming the repairs on all facets of the highway system. It is a constant process of weighing the economics of repair versus replacement. I mention this to point out the necessity for knowing the types of concrete (lightweight or conventional) and aggregate (limestone versus sand gravel, etc.). In many locations, the concrete in situ continued to deteriorate after the initial repairs were made, even though it appeared to be sound. This may eventually prove to be true on some of the bonded overlays covering the entire deck.

This is mentioned to point out the necessity of further comprehensive research that will develop guidelines oriented toward the aggregate of the in situ concrete as well as the bonding agent.

Although Kansas follows, for the most part, a rather rigid plan of repair and has been very successful with its use of bonding agents, difficulty is experienced in determining the strength of the in situ concrete. More work should be done to provide adequate data for determining the feasibility or practicality of a concrete deck overlay and the methods of measurement used for both the area and depth of deteriorated concrete.

The Furr and Ingram report covers the bonding agents very effectively and is a useful tool for programming bridge repair.

AUTHORS' CLOSURE

The State Highway Commission of Kansas has the most extensive experience in concrete bridge deck overlays known to the authors. The comments of Delp are particularly valuable because of that experience.

The maintenance engineer is always faced with the problem of deciding when a temporary repair program should be replaced with a major repair job. The practice of Kansas in overlaying when 30 to 40 percent of the deck shows damage might be helpful to others in deciding when a major repair job is warranted. Case histories are needed in developing information that is necessary for maintenance programming. Pieces of information on costs, installation, and performance are available here and there in literature, but a coordinated program is needed. An agency that would collect such information from highway departments throughout the country, classify it, and send it to interested parties would be very helpful in maintenance planning.

A number of state highway departments have used latex-modified portland cement concrete in bridge deck overlays and in other concrete repairs on bridges. Shackelford and Shafer of the Dow Chemical Company have been very helpful in providing assistance in the use of such material. Our test program showed laboratory freeze-thaw scaling to be almost negligible in the latex-modified material and in air-entrained portland cement concrete. The consensus now seems to be that spalling can be combatted best

by keeping water out of the concrete. If this is correct, an impervious cover over the new concrete deck would solve the spalling problem provided that such a cover is feasible.

The latex-modified concrete specimens used in series 2 freeze-thaw durability tests were moist-cured according to ASTM C 290. At the time of those tests, it was not known that the moist cure normally given ordinary portland cement concrete would be detrimental to bonding of this material. The latex-modified concrete specimens used in series 1 shear bond tests were moist-cured 1 day and then air-cured for 6 days. No air-entraining agent was used in either of these test series.

SPONSORSHIP OF THIS RECORD

GROUP 2—DESIGN AND CONSTRUCTION OF TRANSPORTATION FACILITIES
John L. Beaton, California Division of Highways, chairman

BRIDGE SECTION
Arthur L. Elliott, California Division of Highways, chairman

Committee on Bridge Design
Richard J. Posthauer, New York State Department of Transportation, chairman
William L. Armstrong, N. H. Bettigole, Louis M. Bjorn, J. N. Clary, Daniel E.
Czernik, A. L. Elliott, Frede Gloersen, George G. Goble, Theodore R. Higgins,
Nelson C. Jones, William A. Kline, Robert J. McDonagh, Robert M. Olson, Adrian
Pauw, Donald A. Recchio

Committee on Steel Superstructures
Gerard F. Fox, Howard, Needles, Tammen and Bergendoff, chairman
B. R. Davis, A. L. Elliott, John W. Fisher, Richard S. Fountain, C. H. Gronquist,
Theodore R. Higgins, William A. Kline, W. H. Munse, Frank D. Sears, A. A. Toprac,
I. M. Viest

Committee on Concrete Superstructures
Cornie L. Hulsbos, University of New Mexico, chairman
W. E. Baumann, Russell L. Chapman, Jr., Hotten A. Elleby, John M. Hanson, Norris
L. Hickerson, Francis J. Jacques, Daniel P. Jenny, Alan H. Mattock, J. L. Norris,
Robert A. Norton, Paul F. Rice, Dominick L. Somma, David A. Van Horn, Earle E.
Wilkinson

CONSTRUCTION SECTION
Robert D. Schmidt, Illinois Department of Transportation, chairman

Committee on Construction of Bridges and Structures
C. E. Klamm, Missouri State Highway Commission, chairman
Randle B. Alexander, W. E. Crum, Richard M. Dowalter, Dale F. Downing, Albert
L. Grubb, George A. Harper, Wayne Henneberger, M. H. Hilton, Bruce F. McCollom,
J. C. McGrew, G. I. Sawyer, Philo Howard Schultz, Kenneth R. Scurr, Samuel B.
Usry, H. R. J. Walsh, Harry N. Wenke

GENERAL MATERIALS SECTION
F. E. Legg, Jr., University of Michigan, chairman

Committee on Sealants and Fillers for Joints and Cracks
John P. Cook, University of Cincinnati, chairman
J. N. Clary, Donald Dreher, Frank W. Eschmann, Willian T. Helm, Harry W. John-
son, John C. Killian, W. H. Larson, R. V. LeClerc, Leonard T. Norling, Edward R.
Oglio, Dale E. Peterson, C. K. Preus, William G. Prince, Jr., Bernard A. Ross,
John J. Schmitt, Raymond J. Schutz, Chris Seibel, Jr., Egons Tons, Stewart C. Watson

GROUP 3—OPERATION AND MAINTENANCE OF TRANSPORTATION FACILITIES
Harold L. Michael, Purdue University, chairman

Committee on Structures Maintenance
Orrin Riley, Howard, Needles, Tammen and Bergendoff, chairman
S. M. Cardone, Willian M. Cheatham, D. L. Hawkins, Roy A. Maltby, John F.
McGovern, Ian B. Packman, Stephen E. Roberts, Harvey H. Shafer, Abel R. Sirois,
Vernon W. Smith, Jr., John C. Volk, Jr., H. R. J. Walsh, Alden Louis West

Committee on Roadside Maintenance
James F. Kelley, Massachusetts Department of Public Works, chairman
James Beard, Brian E. Cox, Vern L. Dorsey, Robert H. Ellis, Wesley L. Hottenstein,
Malcolm W. Kirby, James O. Kyser, Irvin C. Lloyd, Charles R. Miller, Thomas J.
Mracek, Charles F. Riebe, Robert S. Ross, James A. Saunders, Alred C. Scheer,
Glenn O. Schwab, C. A. Tottori, Ronald L. Zook

Lawrence F. Spaine, William G. Gunderman, R. Ian Kingham, and Adrian G. Clary,
Highway Research Board staff

The sponsoring committee is identified by a footnote on the first page of each report.